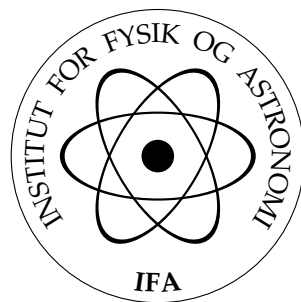

STRANGELETS

Effects of Finite Size and Exact Color Singletness

Dan Mønster Jensen

Institute of Physics and Astronomy
University of Aarhus



July 1996

Preface

The present volume has been submitted to the Faculty of Natural Science at the University of Aarhus, in order to fulfill the requirements for the Ph.D. degree in physics.

The work presented here has been done in collaboration with my supervisor, Jes Madsen, during my time as a Ph.D student at the Institute of Physics and Astronomy, University of Aarhus, and during a stay at the Physics Department, Brookhaven National Laboratory. I have also had the pleasure of working with another Ph.D. student, Michael B. Christiansen, here at the Institute of Physics and Astronomy.

List of Publications

The work presented here has been described in part in the following publications:

1. Dan Mønster Jensen and Jes Madsen, *Strangelets at Non-Zero Temperature*, in *Strangeness and Quark Matter*, edited by G. Vassiliadis, A. D. Panagiotou, S. Kumar, and J. Madsen (World Scientific, Singapore, 1995), pp. 220–229.
2. Jes Madsen, Dan M. Jensen, and Michael B. Christiansen, *Color Singlet Suppression of Quark-Gluon Plasma Formation*, *Phys. Rev. C* **53**, 1883 (1996).
3. Dan M. Jensen and Jes Madsen, *Strangelets with Finite Entropy*, *Phys. Rev. D* **53**, R4719 (1996).
4. Dan Mønster Jensen, Jes Madsen, and Michael B. Christiansen, *Color Singlet Strangelets*, to appear in *Heavy Ion Phys.* (1996).

The contents of Paper 1 has been described in Chapter 3 and Chapter 4, with some additional details not included in the paper.

The subject of Paper 2 is described in Chapter 7, but some new material has been added, as discussed in that chapter.

Chapter 6 discusses the same problem that is treated in Paper 3, but again some additional aspects are discussed, some of them also presented in Paper 4.

Notation

I use the Einstein summation convention, where implicit summation is understood whenever an index is repeated, as in

$$\mu_q N_q \equiv \sum_q \mu_q N_q,$$

but not if one of the indexed quantities appear as an argument

$$N_q(\mu_q) \neq \sum_q N_q(\mu_q).$$

Relativistic convention:

$$\begin{aligned} x^\mu &= (t, \mathbf{x}) & x_\mu &= (t, -\mathbf{x}) \\ \partial_\mu &= \left(\frac{\partial}{\partial t}, \nabla\right) & \partial^\mu &= \left(\frac{\partial}{\partial t}, -\nabla\right) \end{aligned}$$

Minkowski metric:

$$\eta^{\mu\nu} = \eta_{\mu\nu} = \begin{pmatrix} 1 & 0 & 0 & 0 \\ 0 & -1 & 0 & 0 \\ 0 & 0 & -1 & 0 \\ 0 & 0 & 0 & -1 \end{pmatrix}$$

Unless otherwise noted I have used so-called natural units, in which the Planck constant, the Boltzmann constant, and the speed of light are unity

$$\hbar = k_B = c = 1.$$

Acknowledgements

First and foremost I would like to thank my supervisor, Jes Madsen. During all of my Ph.D. study he has provided me with constant inspiration, and guidance.

Many thanks to Carl Dover for making my visit at the Physics Department, Brookhaven National Laboratory possible. I was sad to learn that Prof. Dover passed away recently.

I would also like to thank my office mates Michael B. Christiansen and Georg Bergeton Larsen for many interesting discussions, and for being great company. At Brookhaven I shared office, a single computer terminal, and many good times with Raffaele Mattiello.

My Ph.D. study has been financed by a scholarship from the University of Aarhus. I also appreciate the generosity and hospitality of Brookhaven National Laboratory who funded part of my stay.

A very special thanks goes to my girlfriend Rikke Fürsterling, for putting up with me for all these years, especially during the writing of this thesis. Thanks for all your love and support!

Last, but not least, I wish to thank my parents, Inge Mønster Jensen and Carl M. Jensen, who have always backed me up in what I did. Thanks!

Contents

Preface	iii
List of Publications	iii
Notation	iv
Acknowledgements	iv
1 Introduction	1
1.1 Basic Ideas	1
1.2 Phase Diagram of Strongly Interacting Matter	4
1.3 The Cosmological Quark-Hadron Phase Transition	6
1.4 Ultrarelativistic Heavy-Ion Collisions	6
1.5 Strange Stars	7
1.6 Thesis Outline	9
2 Quark Matter in the MIT Bag	11
2.1 The MIT Bag Model	11
2.2 Shell Model	14
2.3 Liquid Drop Model	16
2.3.1 Density of States	16
2.3.2 Partition Function	20
2.3.3 Mass Formula	25
2.4 Summary and Discussion	26
3 Strangelets at Finite Temperature	31
3.1 Equilibrium Conditions	31
3.2 Mass Formula	32
3.2.1 Fixed Temperature	34
3.2.2 Fixed Entropy	34
3.3 Phase Diagram	35
3.4 Summary and Discussion	37
4 Quark Matter – Hadronic Matter Equilibrium	39
4.1 Scenario	39
4.2 Description of the Model	40
4.2.1 The Quark Phase	40

4.2.2	The Hadronic Phase	41
4.2.3	Equilibrium Criteria	42
4.3	Results	42
4.3.1	The Phase Diagram at $T = 0$	43
4.3.2	The Phase Diagram for $T \neq 0$	44
4.4	Conclusion and Discussion	46
5	The Color Singlet Projection	49
5.1	Some Results from Group Theory	49
5.1.1	Lie Groups	50
5.1.2	Representations	50
5.2	The Group Theoretical Projection Method	52
5.3	A Simple Example: $U(1)$	54
5.4	The Color Singlet Partition Function	55
5.4.1	Background	56
5.4.2	The Partition Function	58
5.5	Evaluation of the Partition Function	62
5.5.1	Massless Quarks and Gluons	62
5.5.2	Saddle-Point Approximation	64
5.5.3	Numerical Evaluation	66
5.6	Summary and Discussion	67
6	Color Singlet Strangelets	69
6.1	Massless Quarks	69
6.1.1	Saddle-Point Approximation	69
6.1.2	Numerical Calculation	72
6.2	Massive Quarks	74
6.3	Conclusion and Discussion	76
7	Color Singlet Suppressed Nucleation	77
7.1	Nucleation Rate	77
7.1.1	Free Energy Barrier	77
7.2	Rate Suppression	79
7.3	Conclusion and Discussion	81
8	Finale	85
8.1	Thesis Conclusion and Summary	85
8.2	Outlook	87
A	The Multiple Reflection Expansion	89
A.1	Trace Formula for the Density of States	89
A.2	Density of States for a Free Field	92
A.3	Expansion of the Green's function	94
A.4	Expansion of the Density of States	98

B Fermi-Dirac and Bose-Einstein Integrals	99
B.1 Fermions	99
B.2 Bosons	100
B.3 Complex Chemical Potential	100
C The SHELL Program	103
C.1 The Main Loop	103
C.2 Minimizing the Energy	103
C.2.1 MinimumEnergy	104
C.2.2 Energy	104
C.2.3 Find_chempot	105
C.2.4 Number	105
C.3 The Optimal Composition	106
C.3.1 Find_composition	106
C.3.2 Sort_levels	108
C.4 The Eigenvalues	109
C.4.1 Find_levels	109
C.4.2 Get_eigenvalues	110
C.4.3 Dirac	111
C.4.4 f_kx	112
Bibliography	119
Index	121

Chapter I

Introduction

This thesis deals with quark matter, in particular, strange quark matter with the focus being on very small systems, the so-called *strangelets*. Quarks are fundamental particles, just like the electron, but they are a sort of ghosts, who never show themselves. A free quark has thus never been seen, and it is believed to be a law of nature that quarks may not be observed directly. They always come either as three quarks, making up what we call baryons, of which the familiar proton and neutron are the most well-known, or as a pair of quark and antiquark, called a meson, of which the π -meson is an example. The complicated rules stating what combinations of quarks are allowed (the so-called color singlet states) do not limit the spectrum to the baryons and the mesons, but also allow for the existence of conglomerates of an integer multiple of three quarks. The lightest of these are the baryons, whereas a six quark state is sometimes called a dibaryon. All of these heavier states are collectively called quark matter, and unlike nuclei which cease to exist at a baryon number of ~ 240 , strange quark matter, if stable, could span a range in baryon number all the way from light nuclei to stars, as heavy as or heavier than our own sun.

The purpose of this chapter is to give an introduction to strange quark matter for the benefit of the non-specialist reader, as well as to give an overview of the properties of this exotic phase of matter, and where it might play a role.

1.1 Basic Ideas

Quark matter is best explained by contrasting it with ordinary nuclear matter. Whereas the quarks in a nucleus are confined within the nucleons (protons, neutrons) the quarks in quark matter are free to roam the entire phase (see Fig. 1.1). Thus one can imagine quark matter as a nucleus made up of quarks that are not correlated in such a way as to form nucleons. From nuclear physics we know that in fact quarks *do* lump together to form nucleons which in turn make up the nucleus.

So what makes contemplations on quark matter more than a purely academic exercise? The answer is *strangeness*. Nature has supplied us with three so-called



Figure 1.1: A nucleus (left) consisting of 7 nucleons (*e.g.*, ${}^7\text{Li}$), with each nucleon made up of three quarks; and a strangelet (right) composed of $3 \times 7 = 21$ quarks.

families of the fermionic constituents of matter. Each family consists of two quarks and two leptons, each with a corresponding antiparticle. The particle members of a family are grouped together in columns below

$$\begin{array}{ccc}
 u & c & t \\
 d & s & b \\
 \nu_e & \nu_\mu & \nu_\tau \\
 e^- & \mu^- & \tau^-
 \end{array}$$

Corresponding members in different families are alike in all respects except for their masses. The first family consisting of the u and d quarks and the electron and its neutrino (along with their respective antiparticles) are lighter than their counterparts in the two other families. What makes the strange quark particularly interesting is that it is the lightest of the heavy quarks¹ (or the heaviest of the light quarks), and thus the one most easily produced.

If we think of quark matter in terms of a simple Fermi-gas model, the quarks are filled into single particle levels up to a maximum energy, the Fermi energy, ϵ_F . As long as the strange quark mass is less than the Fermi energy, it is favorable to have strange quarks in the system in addition to up and down quarks. This is illustrated schematically in Fig. 1.2. Thus it is possible that the energy per baryon of 3 flavor quark matter, in addition to being smaller than that of 2 flavor quark matter, is also smaller than the energy per baryon of nuclear matter, making it the true ground state of strongly interacting matter.

We therefore have the following situation: 2 flavor quark matter must have a higher energy per baryon than nuclear matter, which would otherwise decay into u , d quark matter. Strange quark matter, on the other hand, has a lower energy per baryon than non-strange quark matter, and it could possibly be lower than that of nuclear matter. The latter case is obviously the more exciting since it should then be possible to produce, and observe, strange quark matter.

But wouldn't nuclei immediately decay into small lumps of strange quark matter if that were to be the state of lower energy? For such a decay to happen

¹The current-quark mass of the strange quark is estimated to be 100–300 MeV [1].

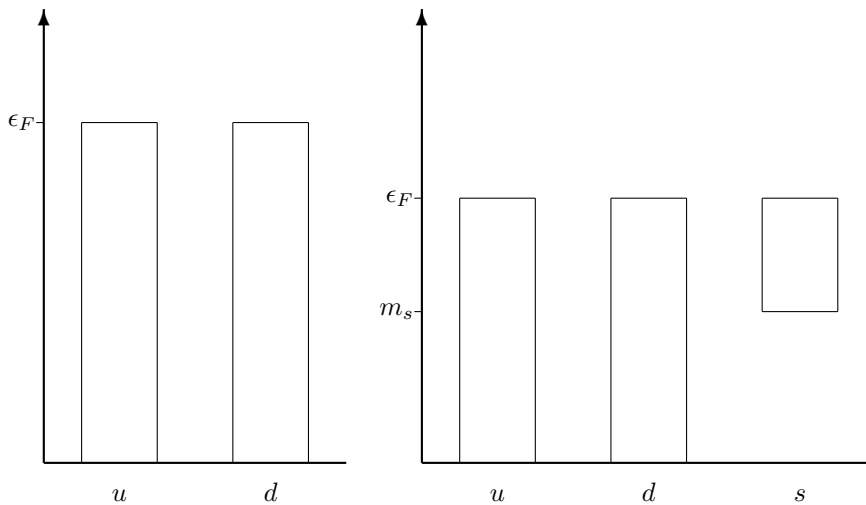


Figure 1.2: The distribution of quarks in 2 and 3 flavor quark matter. The addition of an extra flavor lowers the Fermi energy, and thus the total energy of the system.

to a nucleus with baryon number A , roughly one u or d quark per nucleon would need to be converted into s quarks *simultaneously*. This means that A simultaneous β -decays must take place, which is a highly unlikely event as soon as A exceeds a few. An estimate of the probability of such a process can be made using the Fermi theory of weak interactions, where each β -decay has an amplitude proportional to the Fermi constant G_F , giving a total amplitude

$$\mathcal{A}(^A X \rightarrow ^A \{uds\}) \propto G_F^A. \quad (1.1)$$

Since G_F is very small² the amplitude (and thus the probability) is *very* small.

So even if strange quark matter turns out to be absolutely stable relative to nuclear matter, we need not worry that our surroundings will suddenly turn strange.

The first to entertain the idea that strange quark matter might be stable, was Bodmer [2], who in 1971 pointed out that the existence of “collapsed nuclei”³ with lower energy than normal nuclei does not conflict with the fact that we observe normal nuclei, but not their collapsed counterparts, since nuclei would simply be very long-lived with respect to “collapse”. Bodmer also suggested that strange quark matter might have been produced in the early hot stages of the universe, and might still be found in cosmic rays or even in the interior of stars or planets, possibly slowly converting ordinary matter into strange quark matter.

² G_F is approximately $10^{-5}m_p^{-2}$, where m_p is the proton mass.

³Bodmer used the phrase collapsed nuclei to denote what we now call strange quark matter.

In 1979 Chin and Kerman [3] discussed the possible metastability of hyperstrange multiquark droplets, and suggested that such states could be produced in the collision of heavy ions at relativistic speed. Similar considerations were put forward by Terazawa [4] at about the same time.

The absolute stability of strange quark matter, as first suggested by Bodmer, was not considered again until 1984, when Witten [5] rehabilitated the idea, giving it new impetus that resulted in a series of articles by many authors trying to refine and explore the many ideas put forward by Witten (see Ref. [6] for an overview). Like Bodmer before him, Witten considered the production of strange quark matter in the very early universe, where lumps of strange quark matter—so-called quark nuggets—would emerge as survivors of a first order quark-hadron phase transition.

A thorough and comprehensive study of the properties of strange quark matter, following Witten’s conjecture, was performed by Farhi and Jaffe [7]. They considered both bulk systems, which contain electrons in addition to quarks, and small systems where the electrons required for overall charge neutrality form a cloud around the strange matter nucleus. For the latter systems, which correspond to a baryon number less than roughly 10^7 , they coined the term *strangelet*.

It was found by Witten, and confirmed by Farhi and Jaffe’s more detailed calculations, that there is a range of model parameters (see Chapter 2 for details) for which strange quark matter is stable in the bulk, and for the most optimistic choices also at even very low baryon number. The condition of stability of strange quark matter is that its energy per baryon should be lower than the proton (or neutron) mass which is approximately 938 MeV. Absolute stability would also require that the energy per baryon should be lower than that of the most stable nucleus with an energy per baryon around 930 MeV, but just as a nucleus would not readily decay into strange quark matter, so would the decay of strange quark matter into a nucleus be greatly inhibited.

For an energy per baryon greater than the nucleon mass (~ 938 MeV) but lower than the Λ mass (~ 1116 MeV), strange quark matter would be metastable, decaying via the emission of primarily neutrons, followed by the conversion (β -decay) of strange quarks into up and down quarks, to restore the most favorable flavor composition. If the energy per nucleon exceeds the Λ mass, strange quark matter will be unstable; immediately dissolving into a gas of Λ ’s.

1.2 Phase Diagram of Strongly Interacting Matter

If ordinary nuclear matter is compressed to very high densities, say 2–3 times normal nuclear matter densities, nucleons would overlap and lose their separate identities. This would bring about a transition into quark matter. Likewise at very high temperature, the energy density will be very high and the asymptotic freedom of quantum chromodynamics will allow quarks to move freely about, in

⁷This is not a footnote, it’s an exponent. $10^7 = 10000000$.

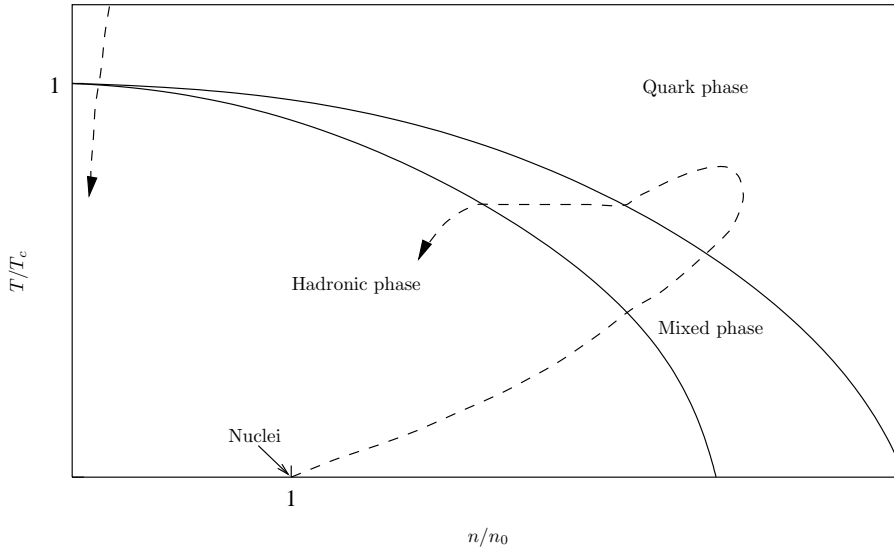


Figure 1.3: Schematic phase diagram of strongly interacting matter.

a hot quark-gluon plasma. The temperature at which this occurs in a baryon free environment has been estimated from lattice calculations to be around 150–200 MeV.

A schematic view of how the phase diagram of baryonic matter may look is shown in Fig. 1.3. The baryon number density n_B is in units of normal nuclear matter density n_0 , and the temperature T is in units of the critical temperature T_c . At low temperature and baryon number density the hadronic phase resides, while at high T or high n_B , matter is in the quark phase. There is also an area where both phases coexist. At fixed T these coexisting phases do not have the same baryon number density, so a point in the mixed phase is characterized by the mean baryon number density of the whole system, even though none of the two phases actually has this density. There are other transitions than the one shown here, *e.g.*, there is a transition from a nuclear liquid to a hadron gas, but here focus is entirely on the quark-hadron phase transition.

I have tacitly assumed that the phase transition is of first order, since otherwise there would be no mixed phase, as the energy density and baryon number density are continuous during a second order phase transition. The order of the phase transition is unknown, but lattice calculations [8] for pure gauge fields show a first order phase transition. Of course the quark fields cannot be neglected, but they are notoriously hard to incorporate in lattice gauge calculations. The order of the phase transition depends on the quark masses, where the pure gauge case corresponds to all quark masses being infinite. Two massless quark flavors seem to indicate a second order phase transition, whereas three

massless flavors give a first order phase transition. The real world with two approximately massless flavors (u and d) and one massive flavor (s) lies somewhere in between.

1.3 The Cosmological Quark-Hadron Phase Transition

It is very difficult indeed to probe this phase diagram, since the conditions needed to approach the phase boundary are so extreme. In astrophysical settings, however, we find conditions unattainable in any earthly laboratory. The hottest environment ever to exist is to be found in the early universe, where during some epoch matter was in the quark phase, until the universe expanded and cooled enough to reach the quark-hadron phase transition temperature⁴, where bubbles of hadronic matter started to nucleate. The path followed by matter in the early universe is shown as the arrow crossing the phase border from above at low baryon number density. The reason that the baryon number density was low in the early universe is that almost as much antimatter as matter was formed in the big bang. The small asymmetry between baryons and antibaryons is what provided us with the matter now present in the universe—matter of which we ourselves are made.

It was Wittens [5] original idea that quark matter might have survived the cosmological quark-hadron phase transition, still being around at present as a form of dark matter. The physical mechanism allowing strange quark matter to survive the phase transition is the concentration of strangeness in the quark phase. Notwithstanding their formation in the phase transition, quark nuggets may not survive the hostile environment following their creation, as they are prone to suffer from surface evaporation of neutrons and protons [9, 10, 11], making it unlikely that nuggets with an initial baryon number less than 10^{30} – 10^{40} have survived. The upper limit on the baryon number is set by the baryon number inside the particle horizon, which was around 10^{48} at the time of the quark-hadron phase transition.

But even if no nuggets survived, we may still be able to observe their “fossilized remains,” in that they would have produced inhomogeneities in the baryon number distribution, owing to their higher density than the surrounding phase, and their propensity to absorb neutrons. This baryon number inhomogeneity would in turn influence the primordial nucleosynthesis, *e.g.*, by causing less ${}^4\text{He}$ to be produced.

1.4 Ultrarelativistic Heavy-Ion Collisions

If strange quark matter is to be produced in a laboratory, the most likely source is the collision of two heavy nuclei at very high energy. Such ultrarelativistic heavy-ion collisions are taking place both at CERN and at Brookhaven National

⁴In fact the very pure plasma phase most likely experienced a significant amount of supercooling.

Lab., at present using fixed targets. The Brookhaven Alternating Gradient Synchrotron (AGS) is capable of accelerating nuclei as heavy as Au to a momentum of 14.5 GeV/ c per nucleon [12], while the Super Proton Synchrotron (SPS) at CERN can achieve a momentum of 158 GeV/ c per nucleon for a Pb beam [13]. The Relativistic Heavy Ion Collider (RHIC), which is under construction at Brookhaven, will ultimately accelerate beams of heavy ions to energies as high as 100 GeV per nucleon, using the AGS as an injector. Colliding the two beams of the RHIC will hopefully allow experimentalists to observe the creation of a quark-gluon plasma, the Holy Grail of heavy-ion physics. A possible path that the central region of the colliding nuclei could follow to enter the quark phase, and then cool and expand (much like the early universe scenario) ending up in the hadronic phase again, is shown in Fig. 1.3.

So far the creation of the quark-gluon plasma has not been established, mainly because most of the signals that would indicate the creation of a quark-gluon plasma phase in the early stages of a heavy-ion collision, can be mimicked by a hot and dense hadronic gas. The creation of a strangelet in a heavy-ion collision is one of the cleanest imaginable signals of the creation of a quark-gluon plasma.

A scenario for the production of strangelets in high-energy heavy-ion collisions, was proposed by Greiner *et al.* [14, 15, 16]. The proposed scenario builds on the mechanism of separation of strangeness and antistrangeness, where most of the strangeness is concentrated in the quark phase, while antistrangeness is carried by the antistrange mesons, mainly K^0 and K^+ .

1.5 Strange Stars

If strange quark matter is absolutely stable, all known neutron stars are not neutron stars at all, but most likely *strange stars*, *i.e.* stars composed of strange quark matter. In the event of metastable strange quark matter, a core of strange quark matter could still be present, in what would then be denoted a *hybrid star*. Both strange stars and hybrid stars would probably be surrounded by a nuclear crust composed of mainly ^{56}Fe nuclei, arranged in a Coulomb lattice, as well as electrons. Figure 1.4 shows a schematic cross section of a hybrid star (see Ref. [17] for details). The outermost layer is the nuclear crust, just mentioned, while deeper in the star neutron rich nuclei, and electrons coexist with superfluid neutrons. At greater depths the density becomes so high that electrons and protons are converted to neutrons and neutrinos, in the inverse β -decay reaction $p + e^- \rightarrow n + \nu_e$, and the predominant component is a superfluid neutron liquid. Finally, if the pressure becomes high enough, even neutrons dissolve into their constituent quarks, giving way to a core of strange quark matter.

A strange star is what results if strange quark matter is absolutely stable, in which case, the quark matter core would extend all the way out to the outer crust. For a review of strange stars see Alcock [18] or Weigel and Weber [19].

Unfortunately it is rather difficult to distinguish between a strange star and a

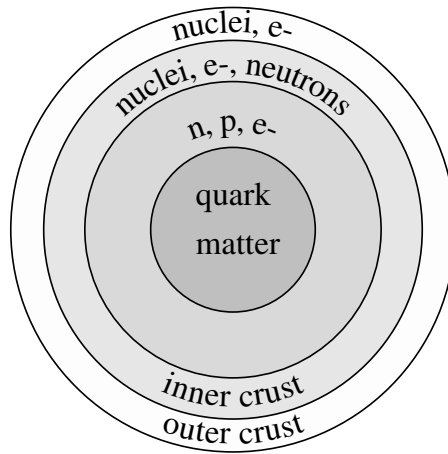


Figure 1.4: Cross section of a hybrid star. An inner core of quark matter is surrounded by a neutron liquid, also containing some protons and electrons. Further out nuclei are also present, along with neutrons that literally drip out of the nuclei, and e^- to keep charge neutrality. The outermost layer is a nuclear crust.

neutron star observationally. A strong indication of the existence strange stars, and thus the absolute stability of strange quark matter, would be the observation of a pulsar with a rotation period less than 1 ms. The reason is that a neutron star pulsar has an upper limit to its rotational speed of about 1000 rotations per second. If it were to rotate faster than this the centrifugal force at the surface of the star would exceed the gravitational force, resulting in mass loss, and slowing down of the stars rotation. This is the so-called Kepler limit. Another upper limit to a neutron stars rotation frequency is set by Einstein's theory of general relativity, which predicts that a neutron star spinning faster than around 1000 revolutions per second will radiate energy in the form of gravitational radiation due to its deviation from spherical symmetry.

A strange star, on the other hand, is not subject to this restriction since it is bound not by the gravitational force, but by the strong force, allowing it to rotate about twice as fast. So far no pulsars exceeding the limits for neutron stars have been observed—the fastest known pulsar rotates at 641 revolutions per second [19].

Strange quark matter may be present in the cosmos, arriving at Earth as a component of cosmic rays. Such a cosmic presence could be remains of nuggets formed in the early universe, as discussed in section 1.3, or it could originate from the collision of two compact objects, one of them being a strange star.

Very strict flux limits have been set on such a cosmic presence of strange quark matter, by Madsen [20, 21], using stars as detectors. The argument is that if a supernova progenitor is hit by a quark nugget that makes its way to

the interior of the star, it would still be around after the supernova explosion, in the collapsed core. Once there, it could initiate the conversion of a neutron star into a strange star. A neutron star could also absorb a quark nugget after its birth. By this argument all neutron stars should in reality be strange stars if strange quark matter is stable (and an initial cosmic abundance of nuggets was present). On the other hand if a single neutron star is identified as a neutron star, strange quark matter is likely not stable, or there are no nuggets left over from the big bang.

1.6 Thesis Outline

Concluding this introductory chapter, let me give a brief outline of the remainder of this thesis.

Chapter 2 gives an introduction to the MIT bag model, which I have used as the basis of all my work. Following this introduction, is a description of two alternative ways to treat strange quark matter in the MIT bag model: the shell model, in which quarks are filled into single particle states, and the liquid drop model, which is a more statistical approach. Both of these models are inspired by their well-known namesakes from nuclear physics. The main advantage of the liquid drop model, adopted for most of the remaining chapters, is that many quantities can be evaluated analytically, albeit not in the most general cases. In contrast, the shell model must be explored using numerical techniques, but is able to reveal features such as shell closures, which are not accessible in the liquid drop model.

Chapter 3 deals with strange quark matter at non-zero temperature. The basic methods developed in this chapter is used in several of the later chapters, where additional complications are added to the rather simple picture presented in Chapter 3.

In Chapter 4, I treat the equilibrium between strange quark matter and hadronic matter, at finite temperature—a situation of importance for the possible creation of strangelets in heavy-ion collisions. The emphasis is on the effect of strangeness on the equilibrium between the two phases, and the effect of finite size on the quark matter phase.

Chapter 5 develops the methods used in Chapter 6 and Chapter 7 to investigate the effect of demanding exact color singletness. Most of the material in Chapter 5 has appeared in the literature, but some of the more detailed calculations have been added, hopefully making it easier to read than the original papers.

In Chapter 6 I apply the color singlet projection, developed in Chapter 5, to describe color singlet strangelets at finite temperature. Most of the results are for massless quarks, but massive quarks are also treated.

Chapter 7 deals with the suppression of the rate of quark matter droplet formation, due to the color singlet constraint. This has important consequences for quark-gluon plasma formation in heavy-ion collisions, as well as the nucleation of quark matter in neutron stars.

Finally, I have included three appendices. Appendix A is an introduction to the multiple reflection expansion, on which the liquid drop model is based. Apart from reproducing some results from the literature in a slightly generalized form, I also show how to obtain the density of states, which is the quantity of interest in the liquid drop model.

Appendix B gives results of special cases of the Fermi-Dirac and Bose-Einstein integrals, which are used throughout the thesis, but which do not seem to be well known, and are somewhat inaccessible through the standard literature.

Since, as mentioned above, analytical solution of the shell model is not possible, a description of how to solve it is equivalent to providing an algorithm. Therefore I have given, in Appendix C, an implementation of a program to calculate strangelet masses in the shell model.

Chapter II

Quark Matter in the MIT Bag

The standard model of elementary particle physics describes the strong interaction in terms of a Yang-Mills gauge theory based on the internal symmetry of color $SU(3)$, in which the dynamical degrees of freedom are the quark and gluon fields. In principle the properties of quark matter should be derived on the basis of this theoretical foundation. However, the only analytical scheme of calculation available is perturbation theory, which is only applicable if the strong fine structure constant is sufficiently small, *i.e.* at high energy or equivalently at small scales. Hence all low-energy phenomena are inaccessible to analytical calculations, and at present the only alternative is to do lattice calculations, which is a numerical solution to the field equations of QCD in a discretized space-time.

Because of our inability to perform calculations, many so-called phenomenological models have been proposed. These are models which are believed to contain a large part of the relevant physics, and which are simpler to solve than the original equations. The MIT bag model—developed at the Massachusetts Institute of Technology, whence the name—is one such model. In the following a short introduction to this model will be given.

2.1 The MIT Bag Model

The basic idea of the MIT bag model [22, 23] is that quarks and gluons should be confined within a finite region of space. This region of space therefore acts as a container for the fields, and is somewhat colloquially referred to as a ‘bag’. By construction, the MIT bag model therefore reproduces one well known property of QCD, *viz.* confinement.

The region of space Ω inside the bag is endowed with a constant energy density which, as will be seen, acts as a source of confinement. This energy density B is an extra parameter of the model, which otherwise depends only on the usual parameters such as quark masses and coupling constants. All the non-perturbative effects are put into the structure of the so-called perturbative vacuum inside the bag, in which the quark and gluon fields propagate. This

means that perturbation theory is applicable to fields inside the bag as opposed to the field free region—the true vacuum—outside the bag. The constant energy density B of the perturbative vacuum is called the *bag constant*.

Since fields are only allowed inside the bag, we may summarize the model by saying that it is described by the Lagrangian

$$L = \int d^3\mathbf{r} (\mathcal{L}_{\text{QCD}} - B) \theta_{\Omega}(\mathbf{r}), \quad (2.1)$$

where $\theta_{\Omega}(\mathbf{r})$ is a function which is unity for $\mathbf{r} \in \Omega$ and zero otherwise, and \mathcal{L}_{QCD} is the ordinary QCD Lagrangian density. Applying the variational principle to this Lagrangian will give a set of field equations, valid in Ω , as well as accompanying boundary conditions to be satisfied on the bag surface $\partial\Omega$. The field equations are the ordinary field equations of QCD, and a careful treatment (see [22]) yields the appropriate boundary conditions.

I will only consider non-interacting fields, but perturbative corrections are possible, *e.g.* in the framework developed by Hansson and Jaffe [24]. Note that I do not use the terms ‘non-interacting’ and ‘free’ interchangeably. The latter term is taken to mean a quark (or gluon) which is not confined and non-interacting, whereas the former term is used for a non-interacting but confined particle. For non-interacting quarks the equation of motion and the boundary conditions are given by

$$\begin{aligned} (i\gamma^{\mu}\partial_{\mu} - m)\Psi(x) &= 0 & \mathbf{x} \in \Omega \\ in_{\mu}\gamma^{\mu}\Psi(x) &= \Psi(x) & \mathbf{x} \in \partial\Omega \\ n_{\mu}\partial^{\mu}\bar{\Psi}(x)\Psi(x) &= -2B & \mathbf{x} \in \partial\Omega. \end{aligned} \quad (2.2)$$

Here $n^{\mu} = (n_0, \mathbf{n})$, where \mathbf{n} is the outward unit normal to the bag surface $\partial\Omega$, and $n_0 = 0$ in the instantaneous rest frame, giving the normalisation $n_{\mu}n^{\mu} = -1$. The first equation is the Dirac equation for a non-interacting quark. The remaining two equations are the boundary conditions of the bag model.

The second equation is a boundary condition saying that there is no quark current across the bag surface. The 4-vector probability current of a Dirac field is $j^{\mu} = \bar{\Psi}\gamma^{\mu}\Psi$. To see that the first boundary condition is equivalent to zero quark current crossing the boundary consider the equivalent equation for the conjugate spinor $\bar{\Psi} = \Psi^{\dagger}\gamma^0$, which is easily obtained using the Clifford algebra $\{\gamma^{\mu}, \gamma^{\nu}\} = 2\eta^{\mu\nu}$, where $\eta^{\mu\nu} = \text{diag}(1, -1, -1, -1)$ is the Minkowski metric, giving

$$\bar{\Psi}(x)in_{\mu}\gamma^{\mu} = -\bar{\Psi}(x). \quad (2.3)$$

Next consider the contraction of n_{μ} with the probability current

$$in_{\mu}j^{\mu}(x) = \bar{\Psi}(x)in_{\mu}\gamma^{\mu}\Psi(x). \quad (2.4)$$

Using the first boundary condition in Eq. (2.2) to evaluate the right hand side gives $\bar{\Psi}\Psi$, whereas using Eq. (2.3) gives $-\bar{\Psi}\Psi$. This shows that $\bar{\Psi}\Psi = 0$ and

$$n_{\mu}j^{\mu}(x) = 0 \quad \mathbf{x} \in \partial\Omega, \quad (2.5)$$

which means that the component of the quark current perpendicular to the bag surface vanishes at the surface.

The second boundary condition in Eq. (2.2) expresses equality between the pressure exerted by the quarks on the surface and the bag constant which acts as an external pressure. Without the quark fields to counter this pressure the bag would not be stable. To see that the second boundary condition is equivalent to pressure equilibrium look at the energy momentum tensor

$$T^{\mu\nu}(x) = T_q^{\mu\nu}(x) + \eta^{\mu\nu} B \quad (2.6)$$

for a quark field in a bag. The energy momentum tensor for the quark field alone is [25]

$$T_q^{\mu\nu}(x) = -\frac{i}{2} \{ \bar{\Psi}(x) \gamma^\mu \partial^\nu \Psi(x) - [\partial^\nu \bar{\Psi}(x)] \gamma^\mu \Psi(x) \}. \quad (2.7)$$

The momentum flow through the surface, as given by $n_\mu T^{\mu\nu}$, should be zero. The contraction of n_μ with the energy momentum tensor is easily evaluated at the bag surface by using the first boundary condition in Eq. (2.2) and Eq. (2.3) to give

$$n_\mu T^{\mu\nu}(x) = -\frac{1}{2} \partial^\nu \bar{\Psi}(x) \Psi(x) + n^\nu B \quad \mathbf{x} \in \partial\Omega. \quad (2.8)$$

Contracting with n_ν and setting the result equal to zero, using $n_\nu n^\nu = -1$ then gives

$$0 = n_\nu n_\mu T^{\mu\nu}(x) = -\frac{1}{2} n_\nu \partial^\nu \bar{\Psi}(x) \Psi(x) - B \quad \mathbf{x} \in \partial\Omega, \quad (2.9)$$

which is recognized as the second boundary condition in Eq. (2.2). The interpretation is that the quark pressure $-\frac{1}{2} n_\nu \partial^\nu \bar{\Psi}(x) \Psi(x)$ balances the bag pressure B .

The ground state of an MIT bag only contains quarks, but if gluons are present (at finite temperature) they also contribute to the pressure through a term [25]

$$T_g^{\mu\nu} = -\frac{1}{4} \eta^{\mu\nu} F^{\alpha\beta} F_{\alpha\beta} + F^{\mu\lambda} F_\lambda{}^\nu, \quad (2.10)$$

in the energy momentum tensor, which, since the gluon field tensor $F^{\mu\nu}$ has to fulfill the boundary condition $n_\mu F^{\mu\nu} = 0$, gives a contribution to the pressure which is $\frac{1}{4} F^{\alpha\beta} F_{\alpha\beta}$.

This short discussion of the boundary conditions of the MIT bag shows that the idea of confining fields to a region of space naturally leads to boundary conditions for the quark and gluon fields which correspond to the fact that there is no probability current across the bag surface. A second boundary condition is interpreted as pressure equilibrium, between the dynamical pressure generated by quarks and gluons inside the bag on the one side and the pressure exerted by the physical vacuum outside the bag on the perturbative vacuum inside the bag on the other side.

l	$j = l \mp 1/2$	$\kappa = \pm(j + 1/2)$	d_κ	$x_{1,\kappa}$
0	1/2	-1	6	2.04279
1	1/2	1	6	3.81135
1	3/2	-2	12	3.20394
2	3/2	2	12	5.12302
2	5/2	-3	18	4.32726
3	5/2	3	18	6.37010

Table 2.1: The quantum number systematics and degeneracies of the solutions to Eq. (2.11). The solutions listed in the last column are for a massless quark species.

2.2 Shell Model

The description of quark matter (or ordinary hadrons) in the framework of the MIT bag model is a question of solving the Dirac equation with the appropriate boundary conditions, as given by Eq. (2.2). Given the single quark energy levels, it is a matter of filling quarks into these levels using the *Aufbau principle*.

For a static spherical bag with radius R the Dirac equation can be split into an angular part and a radial part. The radial equation is [26, 27]

$$f_\kappa(x_{\nu\kappa}) = \frac{-x_{\nu\kappa}}{(x_{\nu\kappa}^2 + m^2 R^2)^{1/2} + mR} f_{\kappa-1}(x_{\nu\kappa}), \quad (2.11)$$

where $x_\kappa = k_\kappa R$ is the momentum k_κ in units of the inverse radius, and m is the quark mass. The function $f_\kappa(x)$ is given by

$$f_\kappa(x) = \begin{cases} j_\kappa(x) & \kappa \geq 0 \\ y_\kappa(x) = (-1)^{\kappa+1} j_{-\kappa-1}(x) & \kappa < 0 \end{cases}, \quad (2.12)$$

where $j_\kappa(x)$ and $y_\kappa(x)$ are spherical Bessel functions [28] of order κ . The quantum number κ is the eigenvalue of the operator $K = \beta(\boldsymbol{\sigma} \cdot \boldsymbol{\ell} + 1)$ where β is the Dirac β -matrix, $\boldsymbol{\sigma}$ the Pauli matrices, and $\boldsymbol{\ell}$ the angular momentum operator. The possible values of κ are [29]

$$\kappa = \pm \left(j + \frac{1}{2} \right), \quad \text{for } j = l \mp \frac{1}{2}, \quad (2.13)$$

where $j(j+1)$ is the eigenvalue of the square of the total angular momentum $\mathbf{j} = \boldsymbol{\ell} + \mathbf{s}$.

The quantum number $\nu = 1, 2, \dots$ in Eq. (2.11) is a principal quantum number which labels the different solutions to the equation for fixed κ . The degeneracy of a multiplet $|\nu\kappa\rangle$ is $d_\kappa = 3(2j+1)$, where the factor 3 is due to the color degree of freedom. The solutions to Eq. (2.11) for a massless quarks species (in which case $x_{\nu\kappa}$ is independent of R) is shown along with the degeneracies for the first few values of κ , l , and j in Table 2.1.

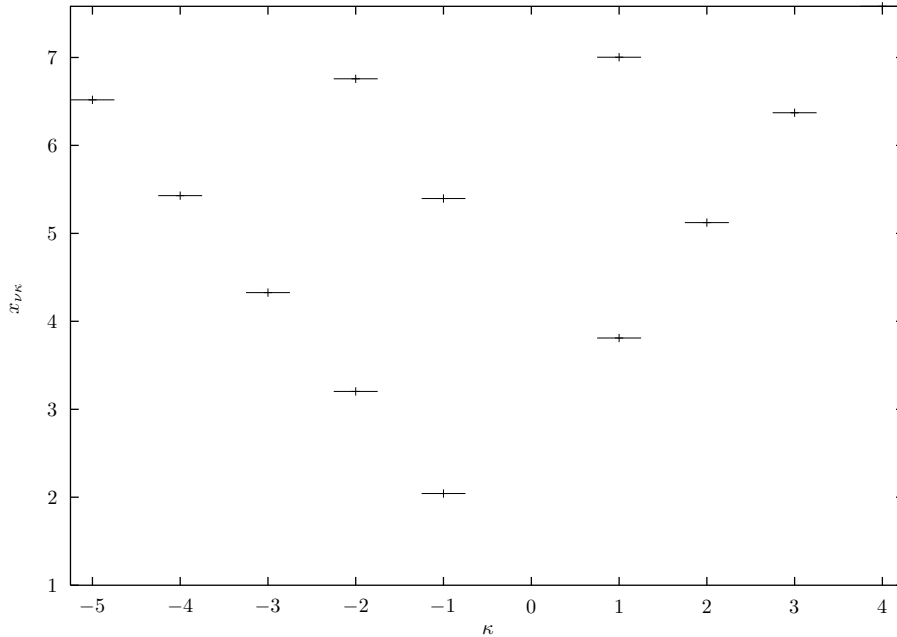


Figure 2.1: The lowest lying solutions $x_{\nu\kappa}$ to Eq. (2.11), for a massless quark species. Some of these levels are tabulated in Table 2.1.

The first few solutions are also shown in Fig. (2.1), where the order of the levels is more clearly seen. Since this is again for a massless quark species, the ordinate is readily converted to an energy (momentum) by dividing by the radius (in units of MeV^{-1}) of the spherical cavity. For a given value of j the level with negative κ is observed to lie below the level with positive κ . The lowest lying $\nu = 2$ level is $\nu = 2, \kappa = -1$, which is lower in energy than the $\nu = 1, \kappa = 3$ level listed in Table 2.1.

With the solutions $x_{\nu\kappa}$ to the radial equation (2.11) given, the total energy for a lump of quark matter in a bag with radius R is

$$E = \sum_{q,\nu,\kappa,j} \epsilon_{q,\nu,\kappa}(R) + \frac{4}{3}\pi R^3 B, \quad (2.14)$$

where $q = u, d, s$ is a flavor index, and the single particle energies are given by

$$\epsilon_{q,\nu,\kappa}(R) = \sqrt{x_{\nu\kappa}^2 R^{-2} + m_q^2}. \quad (2.15)$$

The energy arising from the non-zero vacuum energy density, as given by the bag constant B , has been added to the energy of the quarks to obtain the total

energy. To construct a strangelet with a fixed baryon number A the constraint

$$3A = \sum_q N_q, \quad (2.16)$$

must be satisfied, where N_q is the number of quarks of species q . The lowest energy for a given baryon number is then obtained by minimizing the energy with respect to radius, flavor composition, and the distribution among the different levels.

Such calculations have been performed by Vasak, Greiner, and Neise [30] for two flavor quark matter, and by Greiner, Rischke, Stöcker, and Koch [15], Gilson and Jaffe [31] and Madsen [32] for strangelets. In Appendix C I have provided a program which implements the solution of Eq. (2.11). The resulting plot of the energy per baryon as a function of baryon number for 3 quark flavors can be seen in Fig. (2.2), where results of liquid drop model calculations are also shown. Conspicuous shell effects are seen—most notably the shell closure that occurs at $A = 6$ (except for the highest value of m_s) which corresponds to 6 quarks of each flavor in the lowest energy level $\nu = 1$, $\kappa = -1$. The next three quarks added at $A = 7$ must go into the level with the next to lowest energy resulting in a sharp increase in the energy per baryon. Shell closures also occur at higher baryon numbers, but the locations of these “magic numbers” are seen to depend on the strange quark mass (u and d are assumed massless). For moderate strange quark masses the next shell closure occurs at $A = 18$ which corresponds to three flavors filling the level $\nu = 1$, $\kappa = -2$. For $m_s > m_u, m_d$ (which is certainly the case in reality) the lighter u and d quarks fill the $\nu = 1$, $\kappa = -1$ level before the s quarks, with the result that the shell model calculations for different values of m_s yield identical results for $A \leq 4$, since these systems consist entirely of u and d quarks.

2.3 Liquid Drop Model

The Liquid drop model of strange quark matter in the MIT bag is essentially a Fermi gas model, where each quark flavor $q = u, d, s$ is ascribed a chemical potential μ_q , and the energy levels are filled according to the Fermi-Dirac distribution. At finite temperature there are also antiquarks and gluons.

2.3.1 Density of States

In the case of bulk quark matter the boundary conditions have no effect—one may as well choose periodic boundary conditions as is often done when quantizing fields in a large volume. The allowed momenta are then

$$\mathbf{k} = \frac{2\pi\mathbf{n}}{L} \quad n_i \in \mathbb{Z}, \quad (2.17)$$

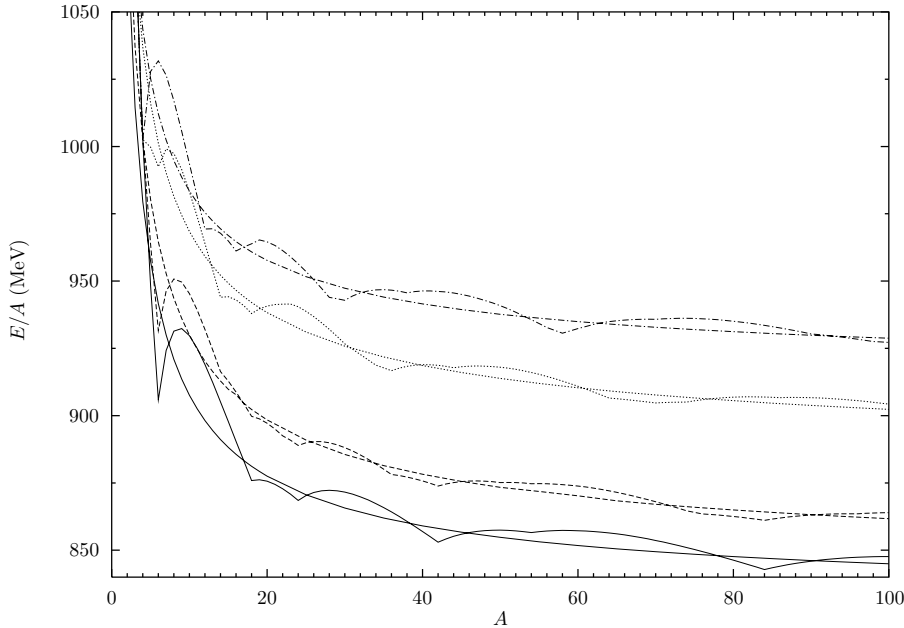


Figure 2.2: The energy per baryon as a function of baryon number for three flavor quark matter, with $B^{1/4} = 145$ MeV and $m_u = m_d = 0$. Full curves are for $m_s = 0$, dashed curves for $m_s = 50$ MeV, dotted curves for $m_s = 150$ MeV, and dot-dashed curves for $m_s = 250$ MeV. For each value of m_s both liquid drop and shell model results are shown.

where L is the linear dimension of the box. Sums over \mathbf{k} can be replaced by integrals in the large volume limit

$$\sum_{\mathbf{k}} \rightarrow \frac{V}{(2\pi)^3} \int d^3\mathbf{k}, \quad (2.18)$$

where $V = L^3$ is the volume of the box, and $V/(2\pi)^3$ is the number of states per volume in momentum space. The density of states $\rho(k)$ is introduced as

$$\frac{V}{(2\pi)^3} \int d^3\mathbf{k} = \int_0^\infty dk \rho(k) \implies \rho(k) = \frac{Vk^2}{2\pi^2}, \quad (2.19)$$

For small system size there are important corrections to this density of states, which depend on the boundary conditions imposed, as well as on the detailed geometry of the confining surface. These finite size corrections to the density of states can be calculated by using the *multiple reflection expansion* method developed by Balian and Bloch [33, 34, 35]. I have given a detailed description of the multiple reflection expansion in Appendix A, with emphasis on the case of

a spinor field satisfying the Dirac equation with MIT bag boundary conditions. The multiple reflection expansion density of states has the form

$$\rho(k) = \frac{Vk^2}{2\pi^2} + f_S\left(\frac{m}{k}\right)kS + f_C\left(\frac{m}{k}\right)C + \dots, \quad (2.20)$$

where S is the surface area of the confining boundary, and C is the extrinsic curvature given by the surface integral

$$C = \oint_{\partial\Omega} d^2\sigma \left(\frac{1}{R_1(\sigma)} + \frac{1}{R_2(\sigma)} \right). \quad (2.21)$$

R_1 and R_2 are the principal radii of curvature. For a spherical system $V = 4/3\pi R^3$, $S = 4\pi R^2$, and $C = 8\pi R$, and Eq. (2.20) is seen to be an expansion in powers of $(kR)^{-1}$.

The multiple reflection expansion is valid whenever the surface is smooth (on the scale set by the momentum), which is why the surface $\partial\Omega$ can be represented by just two invariants, *viz.* the surface area and the extrinsic curvature. Another well known invariant quantity, the Gaussian curvature

$$K = \oint_{\partial\Omega} d^2\sigma \frac{1}{R_1(\sigma)R_2(\sigma)}, \quad (2.22)$$

is of higher order in the inverse of the principal radii of curvature, and is therefore among the left out terms, indicated by ‘...’ in Eq. (2.20).

The volume term is seen to be universal in the sense that it is independent of the nature of the field (*i.e.* the field equation) and the boundary condition. The coefficient functions f_S and f_C depend on the momentum and the mass as indicated, but also on the type of field (scalar, spinor, vector,...) as well as on the boundary condition.

Quarks and Antiquarks

The density of states is the same for antiquarks as for quarks, so all the results in this section, although stated for quarks, are also valid for antiquarks.

The detailed calculation of the surface and curvature terms in the multiple reflection expansion of the density of states for quarks has never appeared in the literature, but Berger and Jaffe reported the result of a calculation of the surface term in Ref. [36, 37], which was later pointed out by Mardor and Svetitsky [38] to be wrong by a factor of 2. The (corrected) result obtained by Berger and Jaffe is

$$f_S\left(\frac{m}{k}\right) = -\frac{1}{8\pi} \left(1 - \frac{2}{\pi} \tan^{-1} \frac{k}{m} \right). \quad (2.23)$$

It is interesting to note that in the limit of zero mass this expression vanishes. This has the important consequence that for massless quarks the leading order correction to the bulk approximation to the density of states is the curvature term.

The curvature coefficient f_C has not been calculated using the multiple reflection expansion in the general case of massive quarks, but for massless quarks with MIT bag boundary conditions the result is [7, 38] $f_C = -1/24\pi^2$. In the limit of infinite mass the quark can be considered non-relativistic and the field equation reduces to the wave equation. In this case the boundary condition of the MIT bag is the well known Dirichlet boundary condition [22] studied by Balian and Bloch [33] who derived the result $f_C = 1/12\pi^2$. The limits $m \rightarrow 0$ and $m \rightarrow \infty$ are thus known, and it was shown by Madsen [32] that the expression

$$f_C\left(\frac{m}{k}\right) = \frac{1}{12\pi^2} \left[1 - \frac{3k}{2m} \left(\frac{\pi}{2} - \tan^{-1} \frac{k}{m} \right) \right], \quad (2.24)$$

has the right limiting values and furthermore is in exceedingly good agreement with shell model calculation (see also Fig. 2.2 and Fig. 2.3). In view of the very good agreement both with the known analytic limits and with shell model calculations it seems more than reasonable to adopt Eq. (2.24) as the curvature term for quarks.

Gluons

The surface term for gluons is zero, as it is for massless quarks. The MIT bag boundary condition $n_\mu F^{\mu\nu} = 0$ is equivalent to the boundary condition studied by Balian and Bloch [34] for the electromagnetic field, and it gives the curvature term [38]

$$f_C = -\frac{1}{6\pi^2}. \quad (2.25)$$

Comparison to Shell Model

The expression for the density of states of quarks as given by Eqs. (2.20), (2.23), and (2.24) can be compared to the spectrum obtained by solving the Dirac equation (2.11) numerically. Since this exact density of states is a sum of delta functions

$$\rho(k) = \sum_{\nu, \kappa} d_\nu \delta(k - k_{\nu\kappa}), \quad (2.26)$$

it is more convenient to compare the integrated density of states

$$N(k) = \int_0^k dk' \rho(k'), \quad (2.27)$$

which is the number of states with momentum less than k . This will be a step function in the shell model. In the liquid drop model the volume, surface, and curvature terms can immediately be integrated to give

$$N(k) = VN_V(k) + SN_S(k) + CN_C(k) \quad (2.28)$$

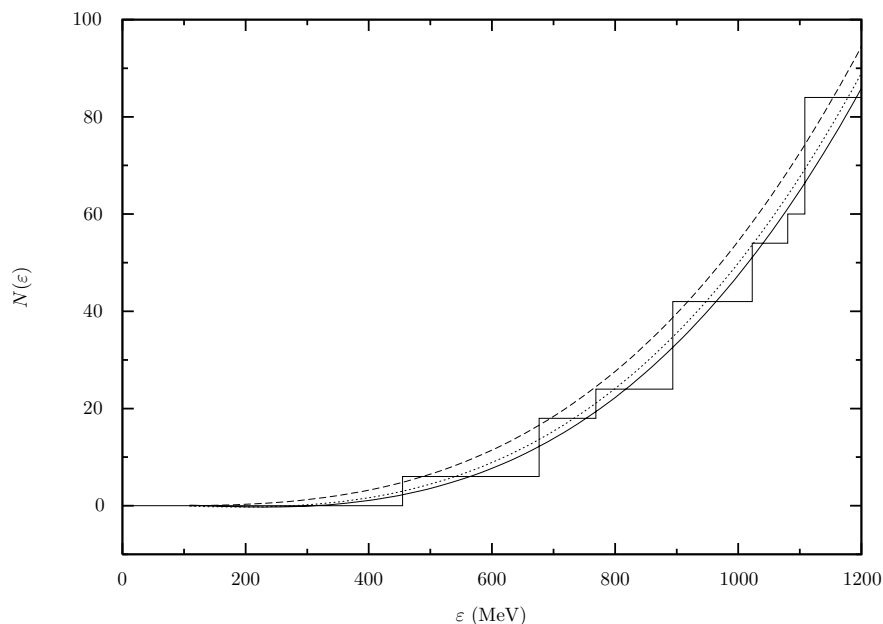


Figure 2.3: Plot of the number of states $N(\varepsilon)$ with energy less than ε for shell model and liquid drop model. Parameters chosen are: $m = 100$ MeV and $R = 1$ fm. The smooth solid line includes both volume, surface, and curvature terms, the dotted line is for volume and surface terms, and the dashed curve is the volume term only.

$$N_V(k) = \frac{k^3}{\pi^2} \quad (2.29)$$

$$N_S(k) = -\frac{3m^2}{4\pi^2} \left\{ \frac{k}{m} + \frac{\pi}{2} \left(\frac{k}{m} \right)^2 - \left[1 + \left(\frac{k}{m} \right)^2 \right] \tan^{-1} \frac{k}{m} \right\} \quad (2.30)$$

$$N_C(k) = \frac{m}{8\pi^2} \left\{ \frac{k}{m} - \frac{3\pi}{2} \left(\frac{k}{m} \right)^2 + 3 \left[1 + \left(\frac{k}{m} \right)^2 \right] \tan^{-1} \frac{k}{m} \right\}. \quad (2.31)$$

In Fig. 2.3 a plot of the number of states $N(\varepsilon)$ with energy less than ε , has been plotted using the above expressions for the liquid drop model, and a numerical calculation for the shell model. The plot shown is for a single quark species, and it is seen that the inclusion of the surface and curvature terms in the liquid drop calculation give a much better agreement with the shell model result.

2.3.2 Partition Function

In order to calculate the energy of a strangelet in the liquid drop model to get a result that parallels Eq. (2.14) in the shell model it is convenient to go through

the grand canonical partition function, since it at once generalizes the liquid drop model to finite temperature.

The grand canonical partition function \mathcal{Z} is defined as the trace over all states

$$\mathcal{Z} = \text{Tr} e^{-\beta(\mathcal{H} - \mu_i \mathcal{N}_i)}, \quad (2.32)$$

where β is the inverse temperature, \mathcal{H} is the Hamiltonian, and \mathcal{N}_i is the number operator for particles of species i , with μ_i being the corresponding chemical potential. For a system of non-interacting particles, as is the case here, the Hamiltonian splits up into a sum of single particle Hamiltonians, and the partition function factorizes. So for a collection of quarks, antiquarks, and gluons in an MIT bag, the logarithm of the partition function may be written as the sum

$$\ln \mathcal{Z} = \sum_i \ln \mathcal{Z}_i - \beta BV, \quad (2.33)$$

in which the summation index i runs over all species present, and the last term is the contribution from the bag constant. The contribution from each species is of the form

$$\ln \mathcal{Z}_i = \pm g_i \int_0^\infty dk \rho_i(k) \ln \left[1 \pm e^{-\beta(\epsilon_i(k) - \mu_i)} \right], \quad (2.34)$$

where the upper sign is for fermions, and the lower for bosons. Here the sum over discrete momentum eigenvalues has been supplanted by an integral over k weighted by the density of states $\rho_i(k)$. g_i is a statistical weight, taking into account the degeneracy due to *e.g.* spin and color. The energy $\epsilon_i(k)$ for a particle with mass m_i is given by the relativistic dispersion relation $\epsilon_i(k) = \sqrt{k^2 + m_i^2}$. μ_i is the chemical potential of the species, which is zero for gluons, since the number of gluons is not a conserved quantity.

To obtain the total energy, baryon number, and other characteristics of the system one goes through the thermodynamic potential Ω defined by

$$\Omega = -T \ln \mathcal{Z}, \quad (2.35)$$

with the differential

$$d\Omega = -SdT - N_i d\mu_i - pdV + \sigma dS + \gamma dC, \quad (2.36)$$

where S is the entropy, N_i is the number of particles of species i (where a sum over i is implied), σ is the surface tension, and γ is the generalized force conjugate to the curvature, which is an external parameter on the same footing as temperature, volume and surface area. The thermodynamic potential introduced above should not be confused with the set of points comprising the bag, which was denoted by the same symbol in section 2.1, but the distinction should always be clear.

Because of the simple dependence of the density of states Eq. (2.20) on the geometry, the thermodynamic potential for a single species has the form

$$\Omega_i(T, \mu_i, V, S, C) = \Omega_{i,V}(T, \mu_i)V + \Omega_{i,S}(T, \mu_i)S + \Omega_{i,C}(T, \mu_i)C, \quad (2.37)$$

which makes it possible to identify the pressure, surface tension, and curvature coefficient in Eq. (2.36), as

$$p = - \left(\frac{\partial \Omega}{\partial V} \right)_{T, \mu, S, C} = -\Omega_V(\mu, T) \quad (2.38)$$

$$\sigma = \left(\frac{\partial \Omega}{\partial S} \right)_{T, \mu, V, C} = \Omega_S(\mu, T) \quad (2.39)$$

$$\gamma = \left(\frac{\partial \Omega}{\partial C} \right)_{T, \mu, V, S} = \Omega_C(\mu, T). \quad (2.40)$$

The free energy F is obtained from the Ω potential, by the Legendre transformation $F = \Omega + \mu_i N_i$, which gives the differential

$$dF = -SdT + \mu_i dN_i - pdV + \sigma dS + \gamma dC, \quad (2.41)$$

exchanging the natural variable μ_i of Ω_i with N_i , where N_i is obtained from Ω by differentiation

$$\begin{aligned} N_i &= - \left(\frac{\partial \Omega_i}{\partial \mu_i} \right)_{T, V, S, C} \\ &= N_{i,V}(T, \mu_i)V + N_{i,S}(T, \mu_i)S + N_{i,C}(T, \mu_i)C, \end{aligned} \quad (2.42)$$

so that F is also a sum of volume, surface, and curvature terms. This is a feature shared by all those quantities, which in the bulk limit are extensive thermodynamic variables. With the inclusion of finite size effects these quantities receive contributions from the surface and curvature terms in addition to the volume term.

Finally the energy is given by $E = F + TS$, with the differential

$$dE = -TdS + \mu_i dN_i - pdV + \sigma dS + \gamma dC, \quad (2.43)$$

which allows us calculate the mass of a strangelet.

Gluons

Gluons have a statistical weight of $g = 16$, since they can be in either of 2 helicity states, and form an octet in color space.

The thermodynamic potential $\Omega_g = -T \ln \mathcal{Z}_g$ for gluons can be expressed in terms of the integrals given in Appendix B, after performing a partial integration to get rid of the logarithm. Using the results Eq. (B.12) and Eq. (B.14) immediately gives

$$\Omega_{g,V} = -\frac{8}{45} \pi^2 T^4, \quad (2.44)$$

for the volume term, and

$$\Omega_{g,C} = \frac{4}{9} T^2, \quad (2.45)$$

for the curvature term. Both of these terms vanish in the limit of zero temperature, since gluons are only present as ‘thermal radiation’.

Quarks

The thermodynamic potential for quarks $\Omega_q = -T \ln \mathcal{Z}_q$ can be evaluated analytically in the limit of zero temperature. In the limit of zero quark mass the sum of thermodynamic potentials for a quark and its corresponding antiquark can be evaluated provided that $\mu_{\bar{q}} = -\mu_q$, which is the case if quarks and antiquarks are in equilibrium through processes such as $q\bar{q} \leftrightarrow gg$ and $q\bar{q} \leftrightarrow \gamma\gamma$.

The statistical weight g for quarks and antiquarks receives contributions from spin (a factor 2) and color (a factor 3), totalling $g = 6$.

Massless Quarks The thermodynamic potential for massless quarks can be written as an infinite sum in powers of μ_q/T [39, 40], but the combination with positive and negative chemical potential treated in Appendix B gives only a finite number of terms. This is exactly the combination relevant when a quark and its antiquark are both present as noted above. At zero temperature the antiquark contributions disappear and only the quark terms are left. Using the results Eq. (B.5) and Eq. (B.7) gives the quark-antiquark volume term

$$\Omega_{q\bar{q},V} \equiv \Omega_{q,V} + \Omega_{\bar{q},V} = -\frac{7\pi^2}{60}T^4 - \frac{1}{2}\mu_q^2T^2 - \frac{1}{4\pi^2}\mu_q^4, \quad (2.46)$$

and the quark-antiquark curvature term

$$\Omega_{q\bar{q},C} \equiv \Omega_{q,C} + \Omega_{\bar{q},C} = \frac{1}{24}T^2 + \frac{1}{8\pi^2}\mu_q^2. \quad (2.47)$$

The *net number* of quarks of species q , *i.e.*, the number of quarks *minus* the number of antiquarks is then given by

$$N_q = -\left(\frac{\partial\Omega_{q\bar{q}}}{\partial\mu_q}\right)_{T,V,C}, \quad (2.48)$$

with the volume and curvature contributions given by

$$N_{q,V} = \mu_q T^2 + \frac{1}{\pi^2}\mu_q^3 \quad (2.49)$$

$$N_{q,C} = \frac{1}{4\pi^2}\mu_q \quad (2.50)$$

Zero Temperature At $T = 0$ the thermodynamic potential is given in terms of known integrals [41], and the volume and surface terms were first calculated by Berger and Jaffe [36, 37], while the curvature term was calculated by Madsen [32]. Introducing $x = \mu_q/m_q$ as the chemical potential in units of the mass, the relevant expressions are

$$\Omega_{q,V} = \frac{1}{4\pi^2}m_q^4 \left[x(x^2 - 1)^{1/2}(x^2 - 5/2) + \frac{3}{2} \ln(x + (x^2 - 1)^{1/2}) \right] \quad (2.51)$$

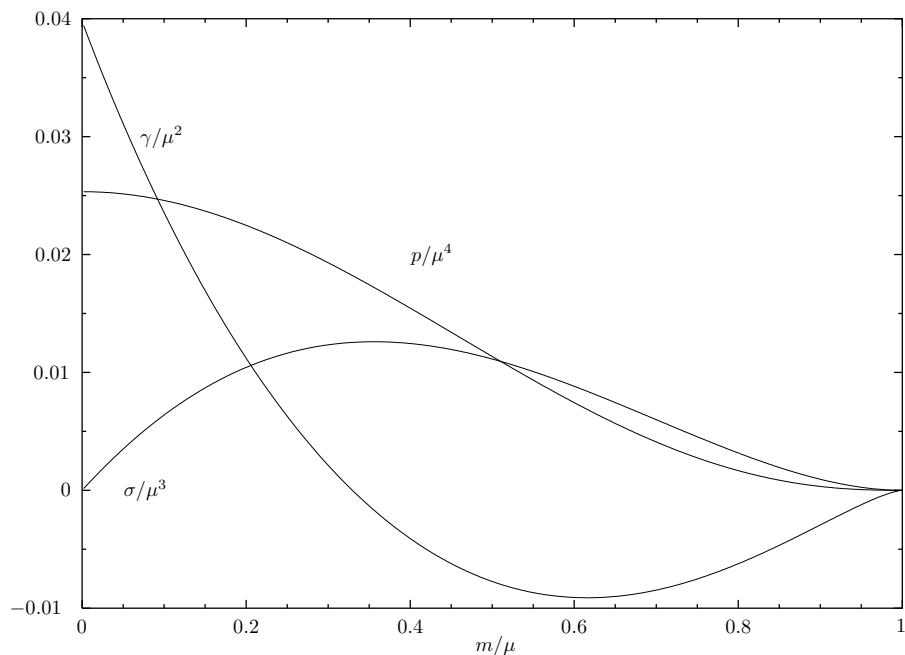


Figure 2.4: Plot of the pressure p , surface tension σ , and the curvature coefficient γ for a single quark species at zero temperature, as a function of mass m in units of the chemical potential μ .

$$\Omega_{q,S} = \frac{3}{4\pi} m^3 \left\{ \frac{1}{6} x(x^2 - 1) - \frac{1}{3}(x - 1) - \frac{1}{3\pi} \left[x^3 \tan^{-1}(x^2 - 1)^{1/2} - 2x(x^2 - 1)^{1/2} + \ln(x + (x^2 - 1)^{1/2}) \right] \right\} \quad (2.52)$$

$$\Omega_{q,C} = \frac{1}{8\pi^2} m^2 \left\{ \frac{\pi}{2} x(x^2 - 1) - \pi(x - 1) + \ln(x + (x^2 - 1)^{1/2}) - x^3 \tan^{-1}(x^2 - 1)^{1/2} \right\} \quad (2.53)$$

The pressure $p = -\Omega_{q,V}$, surface tension $\sigma = \Omega_{q,S}$, and the curvature coefficient $\gamma = \Omega_{q,C}$ for a single quarks species, as given by the above expressions, are plotted in dimensionless units as a function of x^{-1} in Fig. 2.4. Note that whereas the pressure and surface tension are always positive, the curvature term is negative for $1/3 \lesssim m/\mu < 1$. As m approaches μ all three quantities vanish; reflecting the disappearance of quarks of the given species.

The quark number densities are again found by differentiation of the ther-

modynamic potential with respect to chemical potential, and the result is

$$N_{q,V} = \frac{1}{\pi^2} m^3 (x^2 - 1)^{3/2} \quad (2.54)$$

$$N_{q,S} = -\frac{3}{4\pi} \left\{ \frac{1}{2}(x^2 - 1) - \frac{1}{\pi} \left[x^2 \tan^{-1}(x^2 - 1)^{1/2} - (x^2 - 1)^{1/2} \right] \right\} \quad (2.55)$$

$$N_{q,C} = \frac{3}{8\pi^2} m \left[-\frac{\pi}{2}(x^2 - 1) + \frac{1}{3}(x^2 - 1)^{1/2} + x^2 \tan^{-1}(x^2 - 1)^{1/2} \right] \quad (2.56)$$

2.3.3 Mass Formula

At zero temperature the liquid drop model can be used to construct a mass formula for strange quark matter, analogous to the well known liquid drop mass formula of nuclear physics. Such mass formulae have been studied extensively by Madsen [42, 43, 32, 27, 44].

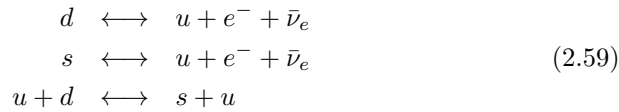
The energy for a strangelet at zero temperature is given by the expression

$$E = \sum_q (\Omega_q + \mu_q N_q) + BV. \quad (2.57)$$

Considering only spherical systems, we seek to minimize this expression with respect to V (S and C are now given in terms of V), and with respect to each of the chemical potentials μ_q , which govern the flavor composition of the strangelet. The minimization has to be done under the constraint that the number of quarks of all flavors add up to give a total number of quarks equal to three times the baryon number

$$A = \frac{1}{3} \sum_q N_q. \quad (2.58)$$

Flavor equilibrium is maintained by the weak interaction, through processes such as



Since the condition of optimal composition is

$$\mu_i dN_i = 0, \quad (2.60)$$

the chemical potentials are connected through

$$\mu_d = \mu_s = \mu_u + \mu_e + \mu_{\bar{\nu}_e}, \quad (2.61)$$

but neutrinos are never present¹ in the system so $\mu_{\bar{\nu}_e} = 0$. For bulk systems electrons would be present, but for the very small systems considered here, electrons, which are not confined, will escape, perhaps to form a surrounding electron cloud if the strangelet is positively charged. Thus for strangelets we may set $\mu_e = 0$, and we get a common quark chemical potential

$$\mu \equiv \mu_u = \mu_d = \mu_s. \quad (2.62)$$

Finding the minimum energy of a strangelet with baryon number A is thus reduced to the problem of simultaneously solving the equations

$$\sum_q \left(\Omega_{q,V}(\mu) + \frac{2}{R} \Omega_{q,S}(\mu) + \frac{2}{R^2} \Omega_{q,C}(\mu) \right) + B = 0, \quad (2.63)$$

and

$$A = \frac{1}{3} \sum_q N_q(\mu), \quad (2.64)$$

expressing respectively mechanical equilibrium, and baryon number conservation. In Eq. (2.63), I have used the fact that $dS/dV = 2R^{-1}$, and $dC/dV = 2R^{-2}$ for a sphere of radius R . The equation Eq. (2.63) without the surface and curvature terms would simply be pressure equilibrium, so it is equivalent to the second boundary condition of the MIT bag, given in Eq. (2.2).

These equations are easily solved on a computer, and the result of such a numerical solution can be seen in Fig. 2.2. The very good agreement with shell model calculations shows the success of the multiple reflection expansion, and the viability of the *Ansatz* Eq. (2.24), of Madsen, for the quark curvature term.

2.4 Summary and Discussion

This chapter has introduced the MIT bag model which *all* the results in the rest of this thesis build on. It must always be remembered that the bag model is exactly that—a model. If we know when a model can be applied we are not doing something new; hence there is always the chance that the model used is for some as yet unknown reason not suited to the problem to which it is applied. Even if the model is suited it can not be trusted to give exact results. In a way every theory should be considered a model eventually to be superseded by a better model. What we today call fundamental theories may turn out tomorrow to be approximations to some more elaborate theory. Theories are merely models that enjoy a rare longevity. There are many indications that the so-called standard model of physics is not *the* fundamental theory, and high-energy physicists are constantly inventing new ones.

Setting aside these more philosophical considerations, the MIT bag model is certainly known to have very specific shortcomings. The idea of a static

¹Except in supernova explosions, where matter densities are so high that neutrinos do not immediately escape.

bag surface is in conflict with basic quantum mechanics, since according to Heisenberg's uncertainty principle there should be a certain fuzzyness to the bag surface. The bag surface should in reality be a dynamic object whose degrees of freedom is governed by the fields inside the bag. Another disease of the bag model is that the boundary conditions of the MIT bag violate chiral symmetry, which is a symmetry of the QCD Lagrangian.

Notwithstanding these drawbacks, the bag model has been very successful in reproducing many hadronic properties. Most important in this context is the successful reproduction of the hadronic mass spectrum [45, 23] which gives a certain confidence when applying the model to the calculation of strangelet masses.

The MIT bag model is not the only phenomenological model that has been applied to the problem of hadron structure or quark matter. Some other contenders are the solitonic bag [46], the Budapest bag model [47], the Skyrmion [48, 49], and the chiral bag [50]. In addition to these relativistic models there have also been attempts to use non-relativistic potential models, with constituent quarks [51].

The liquid drop model and the shell model both assume that the ground-state configuration is that of a degenerate Fermi gas. The possibility of a superconducting ground-state has been investigated by Iwasaki and Iwado [52, 53]. This could be relevant for quark matter in neutron stars. Superconductivity in quark matter was also discussed by Bailin and Love [54, 55].

The liquid drop model of strangelets introduced in this chapter builds on the multiple reflection expansion explained in Appendix A. A very good agreement between liquid drop model results and shell model calculations performed using the program in Appendix C has been demonstrated in this chapter. The first comprehensive comparison including the curvature term for massive quarks was performed by Madsen [32] at zero temperature. It is reassuring to note the very different approach by De Francia [56] gives results identical to those obtained using the multiple reflection expansion, in the case of massless quarks and gluons at finite temperature. In the case of pure glue Kajantie, Kärkkäinen, and Rummukainen [57] find that lattice gauge calculations are in good agreement with the results obtained with the MIT bag model and the multiple reflection expansion, as regards the vanishing of the surface term and the magnitude of the curvature term. A similar study by Huang, Potvin, and Rebbi [58] finds that the curvature term agrees with the bag model results for hadronic bubbles, but not for purely gluonic bubbles for which they obtain the opposite sign relative to both Kajantie *et al.* [57] and the bag model results. There is a clear sign that the curvature term is the dominating contribution for massless species, but apparently there is no consensus among lattice studies regarding the exact value.

When the bag model is applied to hadrons one usually includes a term $-Z_0/R$ in the energy, where R is the radius of the bag which is normally considered spherical. Z_0 is a purely phenomenological parameter. The physical basis for such a term is twofold. One effect which gives such a dependence is a

spurious center of mass energy, which the above term serves to subtract. Another effect which contributes such a term is the zero-point energy of the fields in the bag. A fit to the hadron spectrum [23] gives a value² of $Z_0 = 1.84$.

We have seen that the multiple reflection expansion gives rise to surface and curvature terms in the energy. For a spherical bag of radius R these terms are proportional to R^2 and R respectively. The R^{-1} term discussed above will only be significant for very small systems, where the liquid drop model should not be applied anyway, so for strangelets such a term is not relevant.

I mentioned in section 2.1 that it is possible to do perturbation theory in the bag model. Hansson and Jaffe [24] have formulated Feynman rules for quantum chromodynamics in the bag model using the multiple reflection expansion for the bag propagator of quarks and gluons. It should therefore be possible to include both the effect of finite size and the strong interaction, but only for the volume term are the α_s -corrections known [59, 60, 61, 62, 63, 7, 64]. To first order α_s -corrections are repulsive, resulting in a higher energy per baryon for strange matter. However, it was shown by Farhi and Jaffe [7] that a non-zero value of the strong fine-structure constant α_s can be absorbed in a decrease in the bag constant B . This rescaling of the parameters does probably not hold exactly, especially when finite size effects are included, but for the moment there seems to be no alternative, so I will assume $\alpha_s = 0$ throughout this thesis.

Non-zero α_s corrections were taken into account in a shell model approach by Ishii and Tamagaki [65] using the MIT bag model, and the effect of α_s -corrections have also been studied by Ishii *et al.* [66, 67] in a constituent quark model of strange quark matter. In these studies the finite size effects *were* taken into account, but not in the liquid drop approach.

The Coulomb energy of a strangelet can be estimated as being that of a sphere with a uniform charge density Z/V , where $Z/e = \frac{2}{3}N_u - \frac{1}{3}(N_d + N_s)$, and $V = 4/3\pi R^3$ is the volume of the sphere, giving $E_{\text{Coulomb}} = \alpha Z^2/(10R)$, where α is the fine-structure constant. It was shown by Madsen [43] that the Coulomb energy is negligible for strangelets compared to the surface and curvature energies.

The criteria for the stability or metastability of strange quark matter was discussed in Chapter 1. Here I will briefly mention what this translates to in terms of the parameters $B^{1/4}$ and m_s of the MIT bag model, assuming $\alpha_s = 0$. First of all there is an important lower limit on $B^{1/4}$ set by the fact that two flavor quark matter must be unstable, *viz.*, $B^{1/4} \gtrsim 145$ MeV. This limit assumes $m_u = m_d = 0$ and *does* include Coulomb effects which are important when only two flavors are present.

Absolute stability relative to nuclei such as ^{56}Fe means that the energy per baryon for strange quark matter must not exceed 930 MeV, and whether strangelets are absolutely stable can be learned from Fig. 2.2. But even if strange quark matter has a higher energy per baryon, it could be very long lived. The next decay mode which comes into play is neutron (and to a lesser extent

²The values of all parameters in the fit mentioned are: $B^{1/4} = 146$ MeV, $Z_0 = 1.84$, $\alpha_c = 0.55$, $m_s = 279$ MeV, $m_u = m_d = 0$.

proton) emission. As soon as the energy per baryon for a bulk system becomes larger than the neutron mass $m_n \approx 940$ MeV it is favorable to emit neutrons. For $m_s = 0$ this corresponds to $B^{1/4} \gtrsim 165$ MeV, and for $m_s = 150$ MeV it corresponds to $B^{1/4} \gtrsim 157$ MeV. If the energy per baryon of strange quark matter is larger than the Λ mass $m_\Lambda \approx 1116$ MeV it would rapidly emit Λ particles, quickly to be totally dissolved. This happens for $B^{1/4} \gtrsim 195$ MeV at $m_s = 0$ and for $B^{1/4} \gtrsim 188$ MeV at $m_s = 150$ MeV. For small systems the change in energy per baryon due to particle emission becomes important, and also shell effects cannot be neglected. Berger and Jaffe [36] discussed the various decay modes of strange quark matter in detail.

Chapter III

Strangelets at Finite Temperature

In this chapter I briefly discuss how to treat strange quark matter at non-zero temperature in the liquid drop model. The results are an application of the formalism set up in section 2.3, and serve as a link between Chapter 2 and Chapter 4 in which a hadronic phase is also present. The important effect of color singletness is not taken into account here—it is the subject of Chapter 5 and Chapter 6.

Strangelets at finite temperature (without the color singlet constraint) have been studied in the liquid drop model by Mustafa and Ansari [68], Jensen and Madsen [69], and by He *et al.* [70] who present results for a large range of parameters. Shell model calculations at finite temperature have been performed by Mustafa and Ansari [71], but unfortunately—even though the approach is sound—the results displayed in Ref. [71] contain an error.

3.1 Equilibrium Conditions

At finite temperature, it is the free energy $F = \Omega + \mu_q N_q$, rather than the energy that must attain a minimum, for the system to be in equilibrium.

Quarks and their antiquarks are assumed to be in equilibrium through the processes $q\bar{q} \leftrightarrow gg$ and $q\bar{q} \leftrightarrow \gamma\gamma$, so that the antiquark chemical potential is given by

$$\mu_{\bar{q}} = -\mu_q. \quad (3.1)$$

The optimal composition is still governed by the weak equilibrium processes Eq. (2.59), but depending on the physical conditions, these processes may not be fast enough to keep (or attain) equilibrium between flavors. Hence if weak equilibrium is reached, the chemical potentials for the different quark flavors will be equal just as at zero temperature. In the quark-gluon plasma, thought to be produced in high-energy heavy-ion collisions, flavor equilibrium is not likely to be reached, and so each flavor is described by a separate chemical potential. This situation is dealt with in Chapter 4, while in this chapter flavor equilibrium will be assumed.

Gluons are not subject to number conservation and are ascribed zero chemical potential. Photons will be present at $T > 0$, but since, unlike gluons, they are not confined to the bag volume, photons will be present not only in the quark matter phase, but also in the surrounding phase. Accordingly the photon contribution to the free energy is left out, since it will be countered by a like term in the surrounding phase.

In flavor equilibrium the thermodynamic potential for a gas of \mathcal{N}_q massless quark flavors, their antiquarks, and gluons in an MIT bag is given by (see Eqs. (2.44)–(2.47))

$$\begin{aligned} \Omega(T, \mu, V, C) = & - \left[\left(\frac{7\mathcal{N}_q}{60} + \frac{8}{45} \right) \pi^2 T^4 + \frac{\mathcal{N}_q}{2} \left(\mu^2 T^2 + \frac{\mu^4}{2\pi^2} \right) - B \right] V \\ & + \left[\left(\frac{\mathcal{N}_q}{24} + \frac{4}{9} \right) T^2 + \frac{\mathcal{N}_q}{8\pi^2} \mu^2 \right] C, \end{aligned} \quad (3.2)$$

where μ is the common quark chemical potential. If massive quarks are present they contribute not only volume and curvature terms, but also a surface term, and at $T > 0$ these must be evaluated numerically.

The net quark number derived from the above thermodynamic potential is

$$N(T, \mu, V, C) = \mathcal{N}_q \left[\left(\mu T^2 + \frac{1}{\pi^2} \mu^3 \right) V - \frac{1}{4\pi^2} \mu C \right] \quad (3.3)$$

At fixed temperature and baryon number, the condition for a minimum in the free energy is

$$-pdV + \gamma dC + \sigma dS = 0, \quad (3.4)$$

which for a *spherical* MIT bag leads to

$$\Omega_V(T, \mu) + \frac{2}{R} \Omega_S(T, \mu) + \frac{2}{R^2} \Omega_C(T, \mu) = 0. \quad (3.5)$$

This equation expresses mechanical equilibrium, between quarks and gluons on the one hand, and the bag pressure B on the other hand. At fixed T this has to be solved for R and μ along with the equation expressing fixed baryon number A , *viz.*,

$$3A = N(T, \mu, R). \quad (3.6)$$

This is a cubic equation in R , which can be solved by use of Cardano's formula, to give an expression in terms of μ (and T and A) which can then be substituted into the mechanical equilibrium condition, which may then be solved numerically for μ at fixed T and A . In the more general case where massive quarks are present, a wholly numerical approach is necessitated.

3.2 Mass Formula

Solving the equations Eq. (3.5) and Eq. (3.6), enables us to calculate the mass of a strangelet at finite temperature, by inserting the found values for μ and R

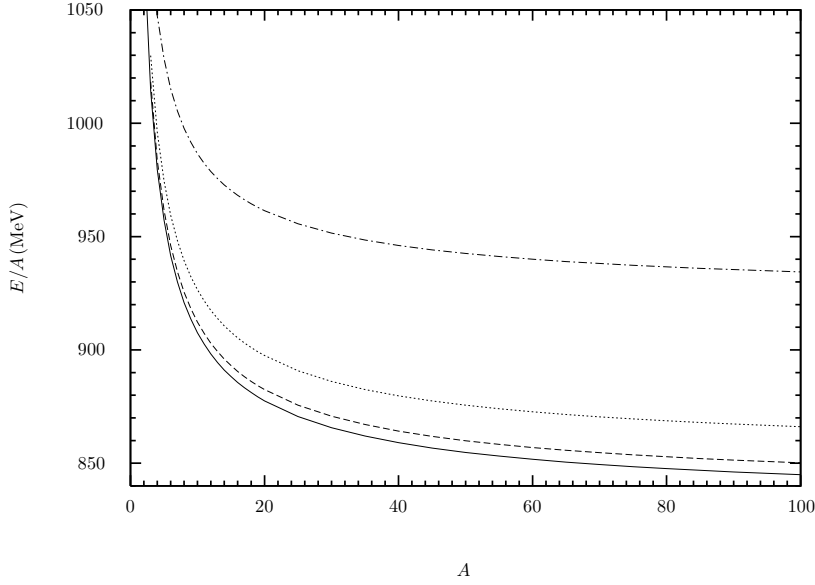


Figure 3.1: Energy per baryon for three massless quark flavors ($\mathcal{N}_q = 3$). From bottom to top: $T = 0$ MeV, 10 MeV, 20 MeV, and 40 MeV. $B^{1/4} = 145$ MeV, but results for other values can easily be obtained, since E/A scales proportionally to $B^{1/4}$.

into the expression for the energy

$$E = \Omega + \mu N + TS, \quad (3.7)$$

where the entropy is obtained from Ω as $\mathcal{S} = -\partial\Omega/\partial T$. For \mathcal{N}_q massless quark flavors the entropy is

$$\mathcal{S} = \left[\left(\frac{7\mathcal{N}_q}{15} + \frac{32}{45} \right) \pi^2 T^3 + \mathcal{N}_q \mu^2 T \right] V - \left(\frac{\mathcal{N}_q}{12} + \frac{8}{9} \right) TC, \quad (3.8)$$

giving an expression for the energy which is

$$E = \left[\left(\frac{7\mathcal{N}_q}{20} + \frac{8}{15} \right) \pi^2 T^4 - \frac{3\mathcal{N}_q}{2} \left(\mu^2 T^2 + \frac{1}{2\pi^2} \mu^4 \right) + B \right] V - \left[\left(\frac{\mathcal{N}_q}{24} + \frac{4}{9} \right) T^2 + \frac{\mathcal{N}_q}{8\pi^2} \mu^2 \right] C \quad (3.9)$$

Notice that with the expressions given for massless quarks and gluons $E_V - B = -3(\Omega_V - B)$, which is the usual equation of state ($\varepsilon = 3p$) valid for massless relativistic particles. In addition $E_C = -\Omega_C$, and the condition of mechanical equilibrium is $\Omega_C C = -3\Omega_V V$. Using these three equations gives [72]

$$E = E_V V + E_C C = (4B - 3\Omega_V) V + 3\Omega_V V = 4BV, \quad (3.10)$$

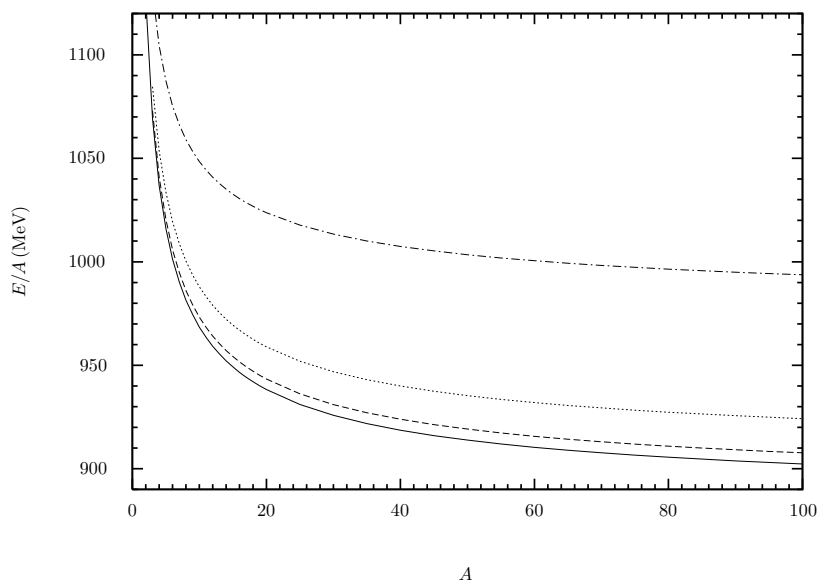


Figure 3.2: Energy per baryon for strangelets, with a strange-quark mass of 150 MeV. From bottom to top: $T = 0$ MeV, 10 MeV, 20 MeV, and 40 MeV. $B^{1/4} = 145$ MeV.

for the energy *in equilibrium*. It is stressed that this result is valid *only for massless quarks*, since for massive quarks the equation of state $\varepsilon = 3p$ no longer holds.

3.2.1 Fixed Temperature

A plot of the energy per baryon at fixed temperature and baryon number, as a function of baryon number is seen in Fig. 3.1 for massless quarks. The energy per baryon is seen to increase rapidly with temperature, reflecting the T^4 dependence of the energy. For massless quarks the only energy scale in the equations is $B^{1/4}$, so all quantities scale with $B^{1/4}$ according to their energy dimension. For instance the energy per baryon scales proportionally to $B^{1/4}$, while the radius scales inversely proportional to $B^{1/4}$.

An equivalent plot for a strange-quark mass $m_s = 150$ MeV is shown in Fig. 3.2, and the curves resemble those in the $m_s = 0$ case—the major difference being the shift in energy scale.

3.2.2 Fixed Entropy

Instead of fixing the temperature, one may consider the case where the entropy and the baryon number (and thus also the entropy per baryon) are fixed. The equilibrium state of the system is then found by solving $dE = 0$, since the energy

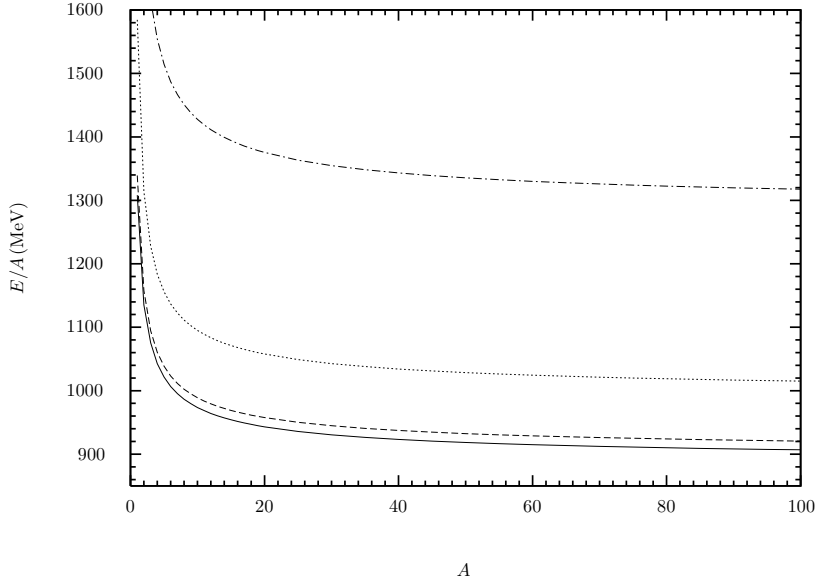


Figure 3.3: Energy per baryon for a strangelet with fixed entropy per baryon. From bottom to top: $S/A = 1, 2, 5,$ and 10 . $B^{1/4} = 145$ MeV and $m_s = 150$ MeV.

has natural variable \mathcal{S} rather than T . The condition of mechanical equilibrium Eq. (3.5), and Eq. (3.6) expressing fixed baryon number are unchanged, but must be accompanied by the supplementary equation

$$\frac{1}{A} \left(\frac{\partial \Omega}{\partial T} \right)_{V, C, \mu} = \frac{\mathcal{S}}{A}, \quad (3.11)$$

which is to be solved in conjunction with Eq. (3.5) and Eq. (3.6) for T , μ and R .

Numerical solutions to these three equations are displayed in Fig. 3.3, for the same set of parameters ($m_s = 150$ MeV, $B^{1/4} = 145$ MeV) as in Fig. 3.2.

3.3 Phase Diagram

By solving Eq. (3.5) and Eq. (3.6) at fixed temperature the chemical potential μ and the radius R , so found, can be used to calculate the baryon number density

$$n_B \equiv \frac{A}{V}. \quad (3.12)$$

Doing this for all possible temperatures, it is possible to construct a phase diagram for quark matter, *i.e.*, a plot of T vs. n_B . Such a phase diagram is

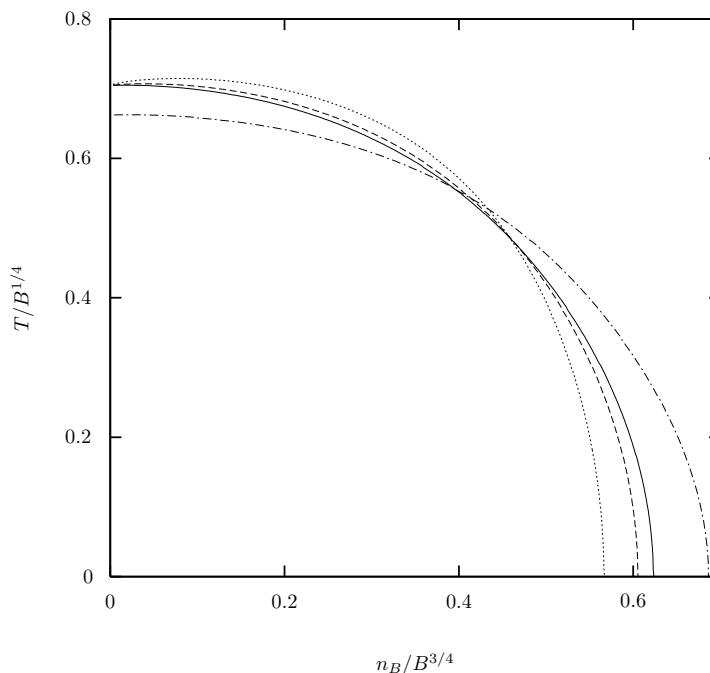


Figure 3.4: The phase diagram for quark matter in the MIT bag model, with massless quarks. The solid line is for $A = 100$, the dashed line for $A = 20$, and the dotted line for $A = 5$; all for $\mathcal{N}_q = 2$. The dotted-dashed line is for $\mathcal{N}_q = 3$ and $A = 100$.

shown in Fig. 3.4, for both 2 and 3 massless flavors, and a range in baryon number.

All curves with the same value of \mathcal{N}_q intersect the T -axis at the same temperature, *viz.* the critical temperature T_c . This is because at zero baryon density $\mu = 0$, and the solution to Eq. (3.5) is

$$T_c = \left(\frac{\pi^2}{90} g_\star \right)^{-1/4} B^{1/4}, \quad (3.13)$$

where g_\star is the effective number of degrees of freedom, defined as

$$\frac{\pi^2}{90} g_\star = \left(\frac{7\mathcal{N}_q}{60} + \frac{8}{45} \right) \pi^2. \quad (3.14)$$

In the bulk limit the critical temperature is also the highest attainable temperature, but when finite size effects are taken into account, the maximum T occurs for a finite baryon number, as noted by Mustafa and Ansari [68].

Comparing the curves for $A = 100$ and $\mathcal{N}_q = 2, 3$ it is seen that adding an extra flavor decreases the critical temperature. This is because the critical

temperature is determined by the effective number of degrees of freedom g_* . Adding an extra flavor increases the effective number of degrees of freedom, so that pressure equilibrium is obtained at a lower temperature. On the other hand the baryon number density at $T = 0$ increases when an extra flavor is added. This is because the baryon number can be packed closer with three flavors than with two flavors, due to the Pauli exclusion principle.

The effect of finite baryon number is also clearly seen in Fig. 3.4 as a decrease in baryon number density at low T with decreasing baryon number. This is a consequence of the finite size effects which cause a decrease in the density of states, as seen in Fig. 2.3, and a therefore a larger volume is required to hold the same baryon number, resulting in a smaller density.

Quark matter is in equilibrium along the curves shown in Fig. 3.4, whereas outside the region delimited by such a curve the combined pressure of the quarks and gluons exceeds the bag pressure, and matter in this part of the phase diagram will be in the form of a deconfined quark-gluon plasma. The region lying within the confines of a particular curve does not correspond to a physical system unless there is a hadronic phase present. This case will be treated in Chapter 4.

3.4 Summary and Discussion

In this chapter I have shown how to include effects of both the finite system size and non-zero temperature, or entropy. Both of these effects have been studied individually before, but here a consistent treatment of both effects, for both massless and massive quarks, has been presented. For massless quarks many quantities can be evaluated analytically, while for massive quarks numerical evaluation is necessary. For massless quarks all quantities scale with some power of the bag constant B according to their dimension. This is because in the absence of quark masses the only dimensional parameter in the bag model is the bag constant. The introduction of quark masses break this simple scaling behavior.

The chapter was concluded with a discussion of the phase diagram in the MIT bag model, which was discussed in a qualitative manner in Chapter 1. Effects of finite size was clearly seen in the phase diagram, and this will be further studied in Chapter 4, where a massive strange quark and a hadronic phase are included.

Chapter IV

Quark Matter – Hadronic Matter Equilibrium

In this chapter I present a framework for the inclusion of finite size effects in phase equilibrium calculations. This is a generalization of the work by Lee and Heinz [73], who presented results for the equilibrium between two bulk phases. It should be noted that this work [69] was brought to its natural conclusion by He *et al.* [74]; a point to which I will return at the end of this chapter.

4.1 Scenario

The collision of two heavy nuclei is thought to give rise to a quark-gluon plasma phase if the energy density in the collision becomes sufficiently large. In such a plasma the quarks would be free to roam the entire phase, as a consequence of the asymptotic freedom of quarks predicted by QCD. So far no convincing experimental evidence for this phase has been produced, but there are indications of a very hot, dense, and spatially extended system created during the early stages of the collision. If a quark gluon plasma *is* formed it will expand and cool. When the temperature reaches the transition temperature the system will start to hadronize. If a quark-gluon plasma droplet has a sufficient strangeness content it may cool to form a (meta-) stable strangelet. For the quark-gluon plasma to develop a net amount of strangeness it is necessary that strange quarks are produced in the collision. Strange quarks are only significantly produced in strong interaction processes, since the weak interaction time scale is much too large to play any role. This means that strange quarks are created as part of $s\bar{s}$ -pairs. $s\bar{s}$ production is favored over $u\bar{u}$ and $d\bar{d}$ production because of Pauli blocking of u and d quarks, since the light quark chemical potential is initially much larger than the strange quark chemical potential. Also the mass of the strange quark is believed to be lower at the high temperatures prevailing due to restoration of chiral symmetry. In order to develop a net strangeness the plasma must rid itself of some of the \bar{s} quarks during the hadronization process. Since there is a positive net baryon number, there will be more u and d quarks around to combine with one of the \bar{s} to form a meson with strangeness 1 (K^0, K^+), than there will be \bar{u} and \bar{d} which might combine with an s quark

to form a meson with strangeness -1 (\bar{K}^0, K^-). Thus more \bar{s} would escape the system than s , building up a net negative strangeness. After this process of $s\bar{s}$ separation the total strangeness of the system would be conserved, again since the weak interactions are too slow to ensure flavor equilibrium. This is a very schematic description of how a strangelet might emerge in a heavy ion collision. This scenario for strangelet production in heavy-ion collisions was proposed by Greiner *et al.* [14, 15, 16], and requires a relatively high baryon number density in the plasma; a condition present in the AGS, and to a lesser degree in the SPS. The next generation of colliders, the RHIC and LHC, will obtain much higher energies, resulting in a higher degree of transparency of the colliding nuclei and hence a low baryon number density. A different mechanism is thus needed to form strangelets under such circumstances. It was recently proposed by Spieles *et al.* [75] that fluctuations might be a decisive factor in the formation of strangelets at low baryon number density.

4.2 Description of the Model

4.2.1 The Quark Phase

The quark matter phase is modeled as a collection of non-interacting u, d , and s quarks, their anti-quarks, and gluons in a *spherical* MIT bag. I have assumed massless u and d quarks, and a strange quark with a mass of 150 MeV. Since u and d are degenerate and electromagnetic interactions are ignored there is isospin symmetry, and the two light quark species are characterized by a single chemical potential, μ_q . The s quark has its own chemical potential, μ_s .

The quark phase is thus described by the thermodynamic potential

$$\begin{aligned} \Omega(T, V, \mu_q, \mu_s) = & - \left[\frac{37}{90} \pi^2 T^4 + \mu_q^2 T^2 + \frac{1}{2\pi^2} \mu_q^4 + \Omega_{s\bar{s},V}(T, \mu_s) - B \right] V \\ & + \Omega_{s\bar{s},S}(T, \mu_s) S \\ & + \left[\frac{57}{108} T^2 + \frac{1}{4\pi^2} \mu_q^2 + \Omega_{s\bar{s},C}(T, \mu_s) \right] C. \end{aligned} \quad (4.1)$$

Here the light quarks contribute to the thermodynamic potential with expressions given by Eq. (2.46) and Eq. (2.47), whereas the strange quark contribution must be evaluated numerically.

Instead of working with μ_q and μ_s it is possible to use the chemical potentials μ_B and μ_S associated with the conserved charges baryon number, A , and strangeness, S (not to be confused with \mathcal{S} or \mathcal{S}). The connection between these is

$$\mu_q = \frac{1}{3} \mu_B \quad \mu_s = \frac{1}{3} \mu_B - \mu_S. \quad (4.2)$$

These chemical potentials have a well defined meaning in the hadron phase as well.

The baryon number of the strangelet is given by

$$\begin{aligned} A &= - \left(\frac{\partial \Omega}{\partial \mu_B} \right)_{R,T,\mu_s} \\ &= \frac{1}{3} [(N_{q,V} + N_{s,V})V + N_{s,S}S + (N_{q,C} + N_{s,C})C], \end{aligned} \quad (4.3)$$

where the net number densities of the light quarks are given by Eq. (2.49) and Eq. (2.50).

4.2.2 The Hadronic Phase

The hadronic phase consists of the known hadronic spectrum, as obtained from the summary tables of the Particle Data Group's *Review of Particle Properties* [76] (see also [1]). Interactions are included by means of a hard core repulsion, leading to an excluded volume effect. The longer range attractive part of the potential has been neglected. There are several ways to incorporate excluded volume effects (see *e.g.* Refs. [77, 78], but I use the statistical bootstrap model [79] of Hagedorn and Rafelski, since this allows for a comparison with the results of Lee and Heinz [73].

In this model thermodynamic quantities such as pressure, energy density, and baryon number density are all obtained from the corresponding ideal gas quantities by multiplication with the factor $(1 + \varepsilon^{\text{pt}}/4B)^{-1}$, where "pt" denotes a point particle quantity, and ε and B are the energy density of the hadron gas and the bag constant respectively. The following physical quantities are thus obtained

$$p^{(H)} = \frac{1}{1 + \varepsilon^{\text{pt}}/4B} p^{\text{pt}} \quad (4.4)$$

$$n_B^{(H)} = \frac{1}{1 + \varepsilon^{\text{pt}}/4B} n_B^{\text{pt}}. \quad (4.5)$$

The superscript (H) refers to the hadronic phase. The corresponding point particle expressions are those of an ideal gas, for which the pressure, energy density, and baryon number density, are given by

$$p^{\text{pt}} = \sum_i p_i^{\text{pt}}, \quad p_i^{\text{pt}} = \frac{g_i}{6\pi^2} \int_0^\infty dk \frac{k^4}{\varepsilon_i(k) e^{\beta(\varepsilon_i(k) - \mu_i)} \pm 1} \quad (4.6)$$

$$\varepsilon^{\text{pt}} = \sum_i \varepsilon_i^{\text{pt}}, \quad \varepsilon_i^{\text{pt}} = \frac{g_i}{2\pi^2} \int_0^\infty dk \frac{k^2 \varepsilon_i(k)}{e^{\beta(\varepsilon_i(k) - \mu_i)} \pm 1} \quad (4.7)$$

$$n_B^{\text{pt}} = \sum_i b_i n_i^{\text{pt}}, \quad n_i^{\text{pt}} = \frac{g_i}{2\pi^2} \int_0^\infty dk \frac{k^2}{e^{\beta(\varepsilon_i(k) - \mu_i)} \pm 1}, \quad (4.8)$$

where i runs over the hadronic states. g_i is the degeneracy factor of the species, and b_i is the baryon number, which is ± 1 for baryons/anti-baryons and zero

for mesons. $\epsilon_i(k) = \sqrt{k^2 + m_i^2}$ is the energy of a particle with momentum k and mass m_i . The signs in the denominator of the integrands correspond to Fermi-Dirac and Bose-Einstein statistics.

4.2.3 Equilibrium Criteria

The system consisting of a strangelet and a bulk hadronic phase is considered to be in chemical and thermal equilibrium, so the temperature and the strangeness and baryon chemical potentials are the same in the two phases

$$T^{(Q)} = T^{(H)}, \quad \mu_B^{(Q)} = \mu_B^{(H)}, \quad \mu_S^{(Q)} = \mu_S^{(H)}. \quad (4.9)$$

Minimizing the free energy leads to the pressure equilibrium condition

$$\Omega_V + \frac{2}{R}\Omega_S + \frac{2}{R^2}\Omega_C + p^{(H)} = 0. \quad (4.10)$$

The combined effect of pressure, surface tension, and curvature forces from the quarks are countered by the bag pressure, B , plus the hadronic pressure. In equilibrium the chemical potential for a hadronic species, i , is given by its net light quark and strange quark content $\nu_{q,i}$ and $\nu_{s,i}$ as

$$\mu_i = \nu_{q,i}\mu_q + \nu_{s,i}\mu_s. \quad (4.11)$$

The equilibrium conditions Eq. (4.9) and Eq. (4.10) can then be solved numerically, yielding a set of triplets, (T, μ_q, μ_s) , defining the phase diagram.

4.3 Results

I have solved the above system of equations on a computer for a variety of parameters. Bulk systems as well as finite quark matter phases both at zero and non-zero temperature have been treated in order to check against known limits.

The quark phase is parametrized entirely in terms of the bag constant, B , and the quark masses. In all cases I have used a strange quark mass $m_s = 150$ MeV, while u and d have been assumed massless in all calculations. The bag constant has been varied between $B^{1/4} = 145$ MeV, where u, d matter is marginally stable in the bulk, and $B^{1/4} = 195$ MeV, where u, d, s matter is unstable relative to a gas of Λ 's, at zero temperature.

With the chosen model the hadronic phase is characterized solely in terms of the bag constant and the particle spectrum used. In most cases I have only included the ground state baryons $N, \Lambda, \Sigma, \Xi, \Omega$ and $\Delta(1232)$, while the mesons included are π, K and η . This gives practically identical results compared to the case in which a full spectrum of all resonances below ~ 2000 MeV was used, except for $B^{1/4}$ well in excess of 200 MeV. All the results depicted here are for the limited spectrum (see Table 4.1).

Name	M (MeV)	I	J	g	S	Composition
Baryons						
N	939	1/2	1/2	4	0	$p = uud$ $n = udd$
Λ	1116	0	1/2	2	-1	$\Lambda = uds$
Σ	1194	1	1/2	6	-1	$\Sigma^0 = uds$ $\Sigma^+ = uus$ $\Sigma^- = dds$
Ξ	1317	1/2	1/2	4	-2	$\Xi^0 = uss$ $\Xi^- = dss$
Ω	1672	0	3/2	4	-3	$\Omega^- = sss$
Δ	1232	3/2	3/2	16	0	$\Delta^{++} = uuu$ $\Delta^+ = uud$ $\Delta^0 = udd$ $\Delta^- = ddd$
Mesons						
π	138	1	0	3	0	$\pi^0 = \frac{1}{\sqrt{2}}(u\bar{u} - d\bar{d})$ $\pi^+ = u\bar{d}$ $\pi^- = d\bar{u}$
η	549	0	0	1	0	$\eta = c_1(u\bar{u} + d\bar{d}) + c_2s\bar{s}$
K	496	1/2	0	2	-1	$K^- = s\bar{u}$ $K^0 = s\bar{d}$

Table 4.1: The spectrum of low lying hadrons and hadronic resonances used in the calculations for the hadron gas. For each isospin multiplet with average mass M the isospin I , spin J , statistical weight g , and strangeness S are listed.

The strangeness contents of the system is parametrized by the strangeness fraction, f_s , defined as the ratio of minus the strangeness density to the baryon density

$$f_s \equiv \frac{-n_S}{n_B}. \quad (4.12)$$

4.3.1 The Phase Diagram at $T = 0$

At zero temperature the strange quark thermodynamic potential is given by the analytic expressions in Eqs. (2.51)–(2.52). The integrals occurring in the expressions for the hadronic properties can also be evaluated analytically. There are no non-strange mesons, and no anti-baryons. Solving the equilibrium conditions Eq. (4.9) and Eq. (4.10) gives the phase diagram in the μ_q - μ_s plane as depicted in Fig. 4.1 for a *bulk* quark matter phase. The solid line is the coexistence line, along which quark matter and hadronic matter are in equilibrium. Hadronic matter is the preferred phase inside the region bounded by the coexistence line, while the system is in the quark matter phase outside this region. Baryons are only present at $T = 0$ if the chemical potential μ_i of the species is greater than the mass m_i . This is the case in the region outside the dashed line. Each segment of the line is marked with a symbol denoting the particle species appearing when crossing the line from the inside. When the chemical potential for K^0, K^- becomes equal to the kaon mass, the kaons will undergo a Bose-Einstein condensation. Since this cannot easily be included in the model without a more detailed knowledge of the potential acting between

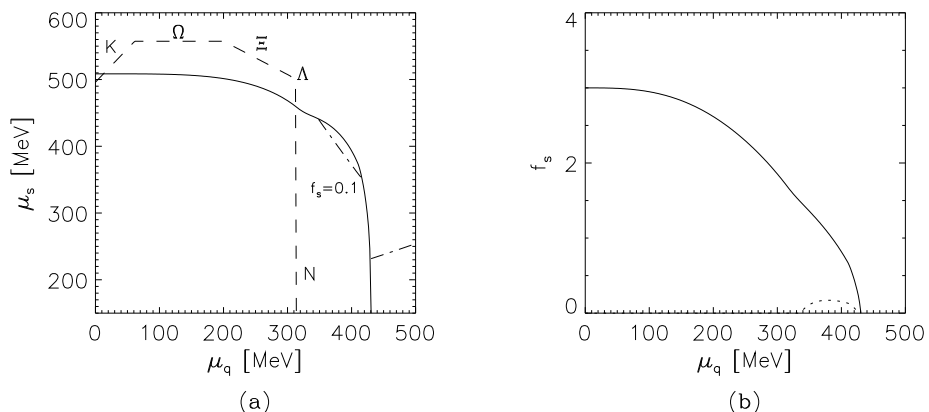


Figure 4.1: (a) Phase diagram for bulk strange quark matter and hadronic matter at $T = 0$. (b) The strangeness fraction in the quark (full line) and hadronic (dotted line) phases as a function of the light quark chemical potential. $B = (190 \text{ MeV})^4$, $m_s = 150 \text{ MeV}$.

the kaons, the region of the phase diagram to the left of the line marked K is not accessible within the present framework. Kaons will be present to the right of this line only at finite temperature, so at zero temperature the region inside the dashed line will be devoid of hadrons. Hadrons may thus be present in the region outside the dashed curve and inside the full curve. Coexistence curves for lower values of B will enclose a smaller region of the phase diagram. At a value of $B^{1/4} \simeq 165 \text{ MeV}$ the “coexistence curve” will lie totally within the dashed curve, since quark matter will then be stable relative to a hadron gas. At the point where the phase coexistence line crosses the line where nucleons first appear there is a visible “kink” due to the fact that nucleons start to contribute to the pressure. The dashed-dotted line represents systems with a total strangeness fraction of 0.1. In the hadronic phase such a system would consist entirely of N ’s and Λ ’s, for the parameter values chosen.

4.3.2 The Phase Diagram for $T \neq 0$

At finite temperature the quark matter phase contains thermal gluons and anti-quarks, while the hadronic phase contains non-strange mesons and anti-baryons. A phase diagram similar to the one in Fig. 4.1 can be constructed for a fixed temperature. The effect of increasing the temperature is that the hadronic phase occupies a smaller region of the phase diagram. This is because there is a large number of massless degrees of freedom in the quark matter phase (g_* defined in Eq. (3.14) has a value of $g_* = 37$ for $\mathcal{N}_q = 2$), whereas the lightest constituent in the hadronic phase is the pion with a mass of $\sim 140 \text{ MeV}$. This means that the pressure increases faster in the quark phase than in the hadronic phase, favoring

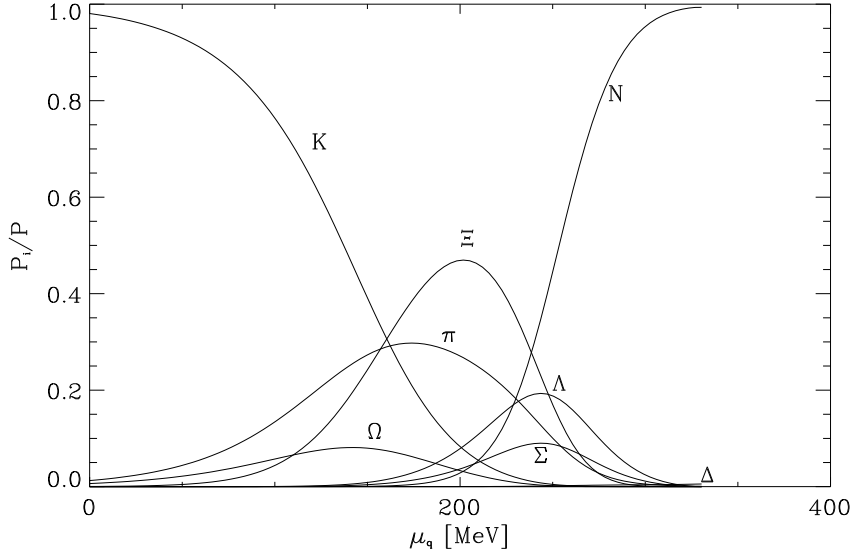


Figure 4.2: The contribution to the hadronic pressure from different hadronic species. $B^{1/4} = 165$ MeV, $T = 40$ MeV, $A = 20$, and $m_s = 150$ MeV.

the former over the latter. From this argument it is also clear that an increase in the bag constant will have the opposite effect, since B effectively contributes to the hadronic pressure.

The relative importance of the different hadronic species can be seen in Fig. 4.2, where the fractional contribution to the total hadron pressure is plotted for all the species listed in Table 4.1. The plot is for values of μ_q and μ_s along the phase coexistence line, which has been parametrized by μ_q in the plot. For low μ_q there is a large strangeness fraction (μ_s is large) and the dominant pressure contribution is from kaons. As μ_q increases other species begin to contribute—mainly the light and/or strangeness rich species, such as the pion and Ξ , while the Ω is somewhat suppressed due to its larger mass. As the system becomes less strange the $S = -1$ baryons Λ and Σ are the main strange contenders. The nucleon dominates at the very highest values of μ_q with the Δ resonance only just visible in this plot. The η -meson's contribution to the pressure is too small to be seen at all.

The quark matter phase benefits from an addition of strange quarks, as opposed to the hadronic phase where the presence of strange hadrons tends to increase the free energy, because of their larger masses. Thus increasing the strangeness fraction will favor the quark phase. This effect is clearly seen in Fig. 4.3, where the phase diagram for a fixed strangeness fraction has been projected onto the n_B - T plane. The solid curves are for a strangeness fraction

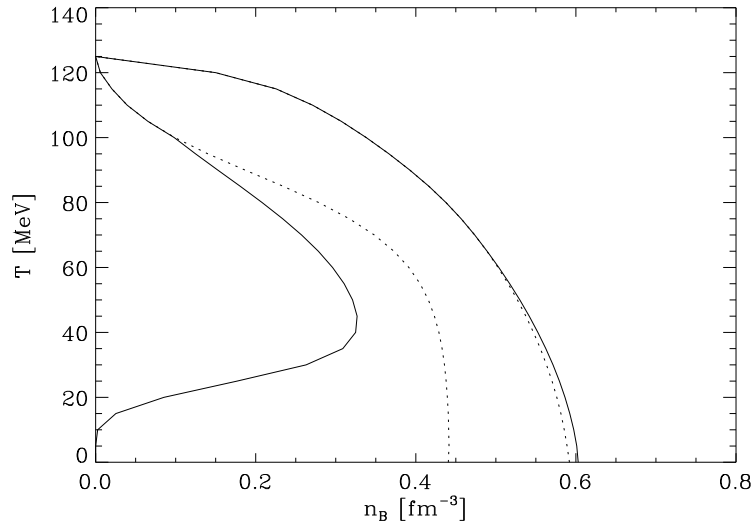


Figure 4.3: Phase diagram for a strangelet with baryon number $A = 20$, and a bulk hadronic phase. The full curve is for a strangeness fraction, $f_s = 0.1$, while the dashed curve is for $f_s = 0.0$. $B^{1/4} = 180$ MeV, $m_q = 0$, $m_s = 150$ MeV.

of 0.1, whereas the dashed curves are for $f_s = 0$. The area between two like curves correspond to a mixed phase. The quark-phase mixed-phase boundary is the curve at high baryon number density, and the other curve is the boundary between the mixed phase and the hadronic phase.

The effect of finite size of the quark matter phase is to destabilize it against the hadronic phase, since the quarks and gluons must now exert a pressure not only balancing the bag pressure B and the hadronic pressure, but also the surface tension and curvature forces of the bag. This effect is seen in Fig. 4.4, where phase diagrams for a bulk quark phase and a quark phase with baryon number $A = 20$ have been superimposed. The most notable difference is that the hadronic phase grows on account of the mixed phase when going from a bulk to a finite quark phase.

4.4 Conclusion and Discussion

In this chapter it has been demonstrated how to include the finite size of the quark phase into phase equilibrium calculations. The effect of varying the various parameters of the model on the equilibrium between the two phases has been discussed, and most of these effects can be understood intuitively by simple arguments.

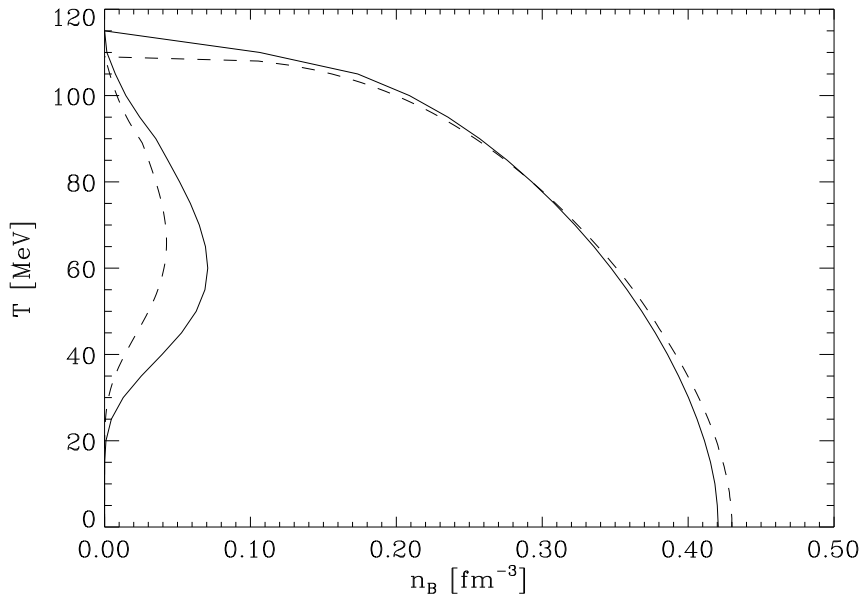


Figure 4.4: Phase diagram for a bulk hadronic phase in equilibrium with a bulk quark phase (dashed line), and a quark phase with baryon number $A = 20$ (full line). $B^{1/4} = 165$ MeV, $m_q = 0$, $m_s = 150$ MeV, $f_s = 0.1$.

There is a shortcoming of the approach to phase equilibrium described in this chapter, *viz.*, that the quark phase is treated as having fixed baryon number, while the hadron phase is considered as being a bulk phase. Without lifting this unnatural constraint and instead fixing the total baryon number of both phases it is not possible to study the phase transition dynamics.

This shortcoming was addressed by He *et al.* [74], who considered an isentropic expansion of the system, as did Lee and Heinz [73] for bulk systems. They found that low B , high f_s , and low specific entropy \mathcal{S}/A favored the production of a strangelet.

Isentropic expansion is only an approximation to the development of the fireball created in a heavy-ion collision, and a more realistic approach could be to solve the rate equations governing the abundances of the hadronic species due to hadronization and reactions among the different species, as was done by Barz, Friman, Knoll, and Schulz [80, 81, 82]. These authors conclude that the distillation of a strangelet is unlikely to happen unless $B^{1/4} \lesssim 150$ MeV.

An approach intermediate between that of Barz *et al.* and that of Lee and Heinz, and He *et al.* was suggested by Greiner and Stöcker [16] who considered a thermodynamic approach to the hadronization, rather than the more com-

plicated rate equation solution of Barz *et al.* Greiner and Stöcker obtain more optimistic estimates of the chance for strangelet distillation than Barz *et al.*, especially at higher initial entropy per baryon.

The inclusion of finite size effects in the models of Barz *et al.* and Greiner and Stöcker would be interesting, and in addition to the work by He *et al.* where the finite baryon number of the system is consistently treated, the inclusion of finite size effects on the hadron phase as well as the quark phase seems a natural next step. This could be done by imposing Dirichlet boundary conditions, and using a multiple reflection expansion density of states for the hadrons.

As mentioned in the beginning of this chapter, Spieles *et al.* [75] recently proposed a scenario for the production of strangelets from an initially almost baryonless plasma, such as is believed to be produced by the next generation of heavy-ion colliders, the RHIC and the LHC. Unfortunately the authors of Ref. [75] disregarded the finite size effects, which have been demonstrated here to be important. Later findings by Spieles *et al.* [83] show that the inclusion of finite size effects makes it practically impossible to produce strangelets assuming the scenario proposed in Ref. [75], except perhaps if shell effects are taken into account.

Chapter V

The Color Singlet Projection

In statistical physics, one is often interested in a description of a system where one or more quantities are conserved overall. The appropriate partition function for such a system is said to be canonical with respect to the conserved quantity (referred to as a conserved charge). It is also possible to construct a grand canonical partition function where the quantity in question is allowed to fluctuate in such a manner that its average value is well defined. A well known example is the conservation of particle number.

When dealing with QCD the situation is somewhat more complicated. Here we want to constrain the system to be overall color singlet. The added complication arises from the fact that the symmetry describing the color interactions is not a simple symmetry, but a higher-dimensional symmetry, *viz.*, $SU(3)$. Demanding that the system be color singlet is thus equivalent to saying that we wish the system to be in a state that transforms according to a particular (unitary irreducible) representation of the symmetry group.

As early as 1936 Bethe [84] calculated the density of states for a compound nucleus of a given total angular momentum. His method was peculiar to the case of $SU(2)$ symmetry, and cannot therefore be generalized to the problem of color singletness. The method used here was developed by Redlich and Turko [85, 86, 87], and it is applicable to any symmetry described by a compact semi-simple Lie group.

5.1 Some Results from Group Theory

In this section I will briefly outline some results from the theory of Lie groups (see *e.g.*, [88, 89, 90, 91]) that will be needed in the following sections. This also serves to introduce the notation used in this chapter. A word of warning: Not all of the results quoted here are valid in general, but I have not always bothered to explicitly list all the necessary assumptions. This is mainly in order not to overburden the reader with “irrelevant” information. As an example of this kind of omission it is implicitly assumed that there exist finite dimensional unitary representations of the group. This is not the case if the group is non-

compact, but as any compact group is also semi-simple, and semi-simple groups are the focus of attention in this chapter it is of no significance for the further applications.

5.1.1 Lie Groups

Let \mathcal{G} denote an n -parameter Lie group with elements U and generators L_i connected through

$$U = e^{i\theta_i L_i}, \quad i = 1, \dots, n \quad (5.1)$$

via the real parameters θ_i . The generators satisfy the commutation relations

$$[L_i, L_j] = iC_{ijk}L_k \quad i = 1, \dots, n \quad (5.2)$$

called the Lie algebra. The constants C_{ijk} are called the structure constants of \mathcal{G} .

A subgroup \mathcal{A} of \mathcal{G} is called invariant if

$$UA_iU^{-1} = A_j \quad U \in \mathcal{G} \quad A_i, A_j \in \mathcal{A}, \quad (5.3)$$

and is called an Abelian invariant subgroup if furthermore

$$[A_i, A_j] = 0 \quad A_i, A_j \in \mathcal{A}. \quad (5.4)$$

A group that does *not* contain an invariant subgroup is called simple, and a group that does not contain an Abelian invariant subgroup is called semi-simple. If a group *does* contain a continuous invariant subgroup it follows that there exists a subalgebra of generators $\{\Lambda_i\}$ satisfying

$$[L_i, \Lambda_j] = iD_{ijk}\Lambda_k. \quad (5.5)$$

Such a subalgebra is called an *ideal*, and a Lie algebra is called simple if it does *not* contain an ideal (other than the null ideal $\{0\}$). If an algebra does not contain an Abelian ideal it is called semi-simple. A semi-simple algebra (or group) can be simple, but the reverse is not true.

The maximal Abelian subalgebra of a Lie algebra is called the Cartan algebra, and the number of generators r in the Cartan algebra is called the *rank* of the group. According to a theorem by Racah [92]—valid for any semi-simple Lie group—there exist exactly r so-called *Casimir operators* C_i that commute with all generators of the group (and therefore also among themselves). Generally the Casimir operators are non-linear functions of the generators.

In the case of $SU(N)$ the number of generators is $n = N^2 - 1$ and the rank is $r = N - 1$.

5.1.2 Representations

A representation Γ of a group \mathcal{G} is a homomorphism of \mathcal{G} into $SL(N)$, the group of linear transformations with determinant 1 of an N -dimensional vector

space. A unitary representation is a homomorphism of \mathcal{G} into $U(N)$, the group of unitary transformations of an N -dimensional vector space. N is called the dimension of the representation. By the very definition of a homomorphism we have

$$\Gamma(U_1 U_2) = \Gamma(U_1) \Gamma(U_2) \quad U_i \in \mathcal{G}. \quad (5.6)$$

If \mathcal{G} and $\Gamma(\mathcal{G})$ are isomorphic, *i.e.* $\Gamma(U_1) \neq \Gamma(U_2)$ if $U_1 \neq U_2$, Γ is said to be *faithful*. It can be shown that every representation is equivalent to a unitary representation (*i.e.*, $\Gamma' = T \Gamma T^{-1}$, where T is a linear transformation, and Γ' is unitary). Thus it is only necessary to consider unitary representations, and in the following all representations will be assumed unitary unless otherwise noted.

Since the group $U(N)$ —to which the elements $\Gamma(U)$ of a unitary representation of \mathcal{G} belongs—is isomorphic to the group of unitary $N \times N$ matrices, a representation Γ establishes a connection between an element U of \mathcal{G} and a matrix $D_{ij}^{(\Gamma)}(U)$.

A (unitary) representation is said to be reducible if there exists a basis of the N -dimensional vector space in which the representative matrices $D_{ij}^{(\Gamma)}(U)$ all have the form

$$D^{(\Gamma)}(U) = \begin{pmatrix} D^{(1)}(U) & 0 \\ 0 & D^{(2)}(U) \end{pmatrix}. \quad (5.7)$$

If the representative matrices of a representation can not be brought into this block diagonal form it is said to be *irreducible*. If the submatrices $D^{(1)}$ and $D^{(2)}$ are themselves reducible, $D^{(\Gamma)}(U)$ can be further reduced. The full reduction of a reducible representation into irreducible ones is written as the direct sum

$$D^{(\Gamma)}(U) = D^{(1)}(U) \oplus D^{(2)}(U) \oplus \dots, \quad (5.8)$$

and the representation is said to be a direct sum of irreducible representations

$$\Gamma = \Gamma^{(1)} \oplus \Gamma^{(2)} \oplus \dots. \quad (5.9)$$

A given irreducible representation $\Gamma^{(i)}$ may appear more than once in the decomposition (5.9).

We may interpret Eq. (5.7) as to say that there are two invariant subspaces of the N -dimensional vector space, under the action of the elements in \mathcal{G} . If $D^{(1)}$ has dimension k the first k basis vectors are said to form a basis of the representation $\Gamma^{(1)}$. The invariant subspace is said to generate a representation, and a vector in the invariant subspace is loosely referred to as a vector in the representation. The irreducible invariant subspaces (those generating the irreducible representations) are called *multiplets*. Because the Casimir operators commute with all generators and therefore with all group elements, the eigenvalues of the Casimir operators are the same for all members of the same multiplet. For a semi-simple Lie group the multiplets are uniquely classified by the eigenvalues of the r Casimir operators.

A character $\chi^{(\Gamma)}(U)$ of a representation Γ is the trace of the representative matrix $D_{ij}^{(\Gamma)}(U)$

$$\chi^{(\Gamma)}(U) = \text{Tr} D_{ij}^{(\Gamma)}(U) = \sum_{i=1}^N D_{ii}^{(\Gamma)}(U), \quad (5.10)$$

which has the property that it is invariant under a change in basis of the N -dimensional vector space. The characters of the irreducible representations satisfy the important orthogonality relation

$$\int d\mu(\{\theta_i\}) \chi^{(m)}(U(\{\theta_i\})) \chi^{(n)}(U(\{\theta_i\}))^* = \delta_{m,n}, \quad (5.11)$$

where $d\mu(\{\theta_i\})$ is the so-called (normalized) Haar measure. It depends only on the parameters $\{\theta_i\}$ corresponding to generators in the Cartan subalgebra.

The representative matrices $D^{(\Gamma)}(U)$ of dimension N are conveniently obtained by the representations of the generators L_i by Hermitian $N \times N$ matrices. Of special importance in gauge theories are the so-called *fundamental* and *adjoint* representations. The fundamental representation is the faithful representation of lowest dimensionality. The adjoint representation is an irreducible representation whose dimension equals the number of generators, and whose matrix elements are given by the structure constants as

$$\lambda_{jk}^{(i)} = -iC_{ijk}. \quad (5.12)$$

The matrices $\frac{1}{2}\sigma$, where σ are the *Pauli matrices*, constitute the fundamental representation of the generators of $SU(2)$.

5.2 The Group Theoretical Projection Method

Consider a system, described by a Hamiltonian \mathcal{H} , that obeys a symmetry described by the group \mathcal{G} . As stated above we assume \mathcal{G} to be a compact semi-simple Lie group. Since \mathcal{G} is a symmetry of the system \mathcal{H} commutes with all the elements of \mathcal{G} and therefore also with the generators, L_i

$$[\mathcal{H}, L_i] = 0 \quad i = 1, \dots, n. \quad (5.13)$$

A maximally commuting set of operators is constituted by \mathcal{H} along with the r generators in the Cartan subalgebra, and r Casimir operators of the group.

The grand canonical partition function for the system is

$$\mathcal{Z}(T, \{\mu_i\}) = \text{Tr} \exp \left[-\beta \left(\mathcal{H} - \sum_{i=1}^r \mu_i Q_i \right) \right], \quad (5.14)$$

where Q_i are representations of the generators in the Cartan algebra (charge operators), and μ_i are the corresponding chemical potentials. The eigenvalues of the operators Q_i are the additive quantum numbers of the system.

In general we can construct a partition function which is canonical with respect to a particular representation Γ of \mathcal{G} , by including only states in the representation Γ . This partition function will be denoted

$$\mathcal{Q}_\Gamma(T) = \text{Tr}_\Gamma e^{-\beta\mathcal{H}} \quad (5.15)$$

The objective of the group theoretical projection method is to obtain \mathcal{Q}_Γ from $\tilde{\mathcal{Z}}$.

Now consider the function $\tilde{\mathcal{Z}}$, defined as

$$\tilde{\mathcal{Z}}(T, \{\gamma_i\}) = \text{Tr} \exp \left[-\beta\mathcal{H} + i \sum_{i=1}^r \gamma_i Q_i \right]. \quad (5.16)$$

It is related to the grand canonical partition function through the Wick rotation $\gamma_i \rightarrow -i\beta\mu_i$. Since a representation of a general group element in \mathcal{G} is

$$D(U) = \exp \left(i \sum_{i=1}^n \theta_i L_i \right), \quad (5.17)$$

where L_i are representations of the generators, $\tilde{\mathcal{Z}}$ may be written

$$\tilde{\mathcal{Z}}(T, \{\gamma_i\}) = \text{Tr} [D(U)e^{-\beta\mathcal{H}}], \quad (5.18)$$

where $D(U)$ is an element in the Cartan subgroup. The representation D is now decomposed into irreducible representations, and the trace is split up into traces over the invariant subspaces corresponding to the irreducible representations (multiplets). Denoting a vector (state) in the multiplet generating the irreducible representation $\Gamma^{(i)}$ by $|\nu_i \xi_i\rangle$ the function $\tilde{\mathcal{Z}}$ is now written

$$\tilde{\mathcal{Z}} = \sum_i \sum_{\nu_i, \xi_i} \langle \nu_i \xi_i | D^{(i)}(U) e^{-\beta\mathcal{H}} | \nu_i \xi_i \rangle. \quad (5.19)$$

The multiplet is characterized by the eigenvalues of the Casimir operators, for which i may be taken as a shorthand notation. States within each multiplet are characterized by the eigenvalues of the Cartan operators denoted by ν , and by any extra quantum numbers ξ needed to uniquely specify the state. Inserting a complete set of states within the i th representation $1 = \sum_{\nu'_i, \xi'_i} |\nu'_i \xi'_i\rangle \langle \nu'_i \xi'_i|$ gives

$$\tilde{\mathcal{Z}} = \sum_i \sum_{\nu_i, \nu'_i} \sum_{\xi_i, \xi'_i} \langle \nu_i \xi_i | D^{(i)}(U) | \nu'_i \xi'_i \rangle \langle \nu'_i \xi'_i | e^{-\beta\mathcal{H}} | \nu_i \xi_i \rangle. \quad (5.20)$$

The Hamiltonian is diagonal in ν , and $D^{(i)}(U)$ is diagonal in ξ since the charge operators act only on the ν part of the state.

$$\begin{aligned} \tilde{\mathcal{Z}} &= \sum_i \sum_{\nu_i, \xi_i} \langle \nu_i \xi_i | D^{(i)}(U) | \nu_i \xi_i \rangle \langle \nu_i \xi_i | e^{-\beta\mathcal{H}} | \nu_i \xi_i \rangle \\ &= \sum_i \sum_{\nu_i} D_{\nu_i \nu_i}^{(i)}(U) \sum_{\xi_i} \langle \nu_i \xi_i | e^{-\beta\mathcal{H}} | \nu_i \xi_i \rangle \\ &= \sum_i \chi^{(i)}(U) \sum_{\xi_i} \langle \nu_i \xi_i | e^{-\beta\mathcal{H}} | \nu_i \xi_i \rangle. \end{aligned} \quad (5.21)$$

Here the definition (5.10) of the character has been used. Since \mathcal{H} is degenerate on each multiplet, it is possible to insert a spurious sum over members in the multiplet

$$\begin{aligned}\tilde{\mathcal{Z}} &= \sum_i \chi^{(i)}(U) \frac{1}{d_i} \sum_{\nu_i} \sum_{\xi_i} \langle \nu_i \xi_i | e^{-\beta \mathcal{H}} | \nu_i \xi_i \rangle \\ &= \sum_i \chi^{(i)}(U) \frac{1}{d_i} \text{Tr}_i e^{-\beta \mathcal{H}} = \sum_i \chi^{(i)}(U) \frac{1}{d_i} \mathcal{Q}_i,\end{aligned}\quad (5.22)$$

where d_i is the dimension of the i th representation. Using the orthogonality of characters (5.11) one readily obtains

$$\mathcal{Q}_j(T) = d_j \int d\mu(\{\theta_i\}) \tilde{\mathcal{Z}}(T, \{\gamma_i\}) \chi^{(j)}(\{\gamma_i\})^* \quad (5.23)$$

This is the formula connecting the grand canonical partition function with the canonical partition function \mathcal{Q}_i . The effect of the integral over the group with the complex conjugate of the character of the j th irreducible representation is to project out from the total trace only that part which is a trace over states in the multiplet generating the j th representation.

5.3 A Simple Example: $U(1)$

As an example of an application of the group theoretical projection method just derived, I will use it to obtain the formula

$$\mathcal{Q}_N(T, V) = \frac{1}{2\pi} \int_{-\pi}^{+\pi} d\lambda e^{i\lambda N} \mathcal{Z}(T, V, iT\lambda), \quad (5.24)$$

where $\mathcal{Q}_N(T, V)$ is the canonical partition function for a system of N particles, and $\mathcal{Z}(T, V, \mu)$ is the grand canonical partition function with chemical potential μ . This expression is the inversion of the very definition of the grand canonical partition function

$$\mathcal{Z}(T, V) = \sum_{N=0}^{\infty} e^{\beta\mu N} \mathcal{Q}_N(T, V). \quad (5.25)$$

In statistical physics texts Eq. (5.24) is usually obtained by inverting the series (5.25) by first performing a Wick rotation and then using Fourier theory (see *e.g.*, [93]), or by introducing a delta function $\delta(N - \bar{N}) = \int \frac{d\lambda}{2\pi} \exp[i\lambda(N - \bar{N})]$ in the density matrix. Here it will follow from the general result of Eq. (5.23) by using $U(1)$ as the symmetry group.

In gauge field theory number conservation arises as a consequence of invariance under phase changes of state vectors of the type

$$\psi'(x) = e^{i\theta(x)N} \psi(x), \quad (5.26)$$

where \mathcal{N} is the number operator satisfying $[\mathcal{H}, \mathcal{N}] = 0$, where \mathcal{H} is the Hamiltonian. This is recognized as a $U(1)$ symmetry, with \mathcal{N} being the sole generator and therefore also both the Casimir operator and the Cartan generator of the group. The irreducible representations are labeled by the eigenvalue N of \mathcal{N} , and since the dimension is 1, they are identical with the characters

$$\chi^{(N)} = D^{(N)} = e^{i\theta(x)N}, \quad (5.27)$$

where

$$\mathcal{N}|N\xi\rangle = N|N\xi\rangle. \quad (5.28)$$

States are labeled by N and ξ , the latter denoting all other quantum numbers of the state. The grand canonical partition function is the unrestricted trace

$$\mathcal{Z} = \text{Tr} e^{-\beta(\mathcal{H}-\mu\mathcal{N})} = \sum_{N\xi} \langle N\xi | e^{-\beta(\mathcal{H}-\mu\mathcal{N})} | N\xi \rangle, \quad (5.29)$$

and the canonical partition function is a trace over states in the representation labeled by N

$$\mathcal{Q}_N = \text{Tr}_N e^{-\beta\mathcal{H}} = \sum_{\xi} \langle N\xi | e^{-\beta\mathcal{H}} | N\xi \rangle. \quad (5.30)$$

The function $\tilde{\mathcal{Z}}$ is given by

$$\tilde{\mathcal{Z}} = \text{Tr} e^{-\beta\mathcal{H}+i\theta\mathcal{N}}. \quad (5.31)$$

Given the Haar measure of $U(1)$, which is $d\mu = d\theta/2\pi$ a direct insertion in Eq. (5.23) gives

$$\begin{aligned} \mathcal{Q}_N &= \frac{1}{2\pi} \int_{-\pi}^{+\pi} d\theta \chi^{(N)}(\theta)^* \tilde{\mathcal{Z}}(\theta) = \frac{1}{2\pi} \int_{-\pi}^{+\pi} d\theta e^{-i\theta N} \tilde{\mathcal{Z}}(\theta) \\ &= \frac{1}{2\pi} \int_{-\pi}^{+\pi} d\theta \text{Tr} e^{-\beta\mathcal{H}+i\theta(\mathcal{N}-N)}, \end{aligned} \quad (5.32)$$

which with the substitution $\lambda = -\theta$ gives

$$\mathcal{Q}_N = \frac{1}{2\pi} \int_{-\pi}^{+\pi} d\lambda e^{i\lambda N} \mathcal{Z}(iT\lambda), \quad (5.33)$$

which is the promised result.

5.4 The Color Singlet Partition Function

After having seen the group theoretical projection method in action in a simple case it is now time to proceed to the actual goal, *viz.*, the calculation of the canonical color singlet partition function of a quark-gluon plasma (or hot strangelet).

5.4.1 Background

Quantum chromodynamics is a Yang-Mills gauge theory based on the $SU(3)$ symmetry group. The Lagrangian density of QCD is invariant under the simultaneous local gauge transformations of quark spinors Ψ and the gluon field tensor $F^{\mu\nu}$ according to

$$\begin{aligned}\Psi(x) &\rightarrow D(x)\Psi(x) \\ F^{\mu\nu}(x) &\rightarrow D(x)F^{\mu\nu}(x)D^{-1}(x)\end{aligned}\tag{5.34}$$

where

$$D(x) = e^{i\theta_i(x)\Lambda_i}\tag{5.35}$$

is the fundamental representation of an element in $SU(3)$, in which the generators are represented by the Gell-Mann matrices $\Lambda_i = \frac{1}{2}\lambda_i$

$$\begin{aligned}\lambda_1 &= \begin{pmatrix} 0 & 1 & 0 \\ 1 & 0 & 0 \\ 0 & 0 & 0 \end{pmatrix} & \lambda_2 &= \begin{pmatrix} 0 & -i & 0 \\ i & 0 & 0 \\ 0 & 0 & 0 \end{pmatrix} & \lambda_3 &= \begin{pmatrix} 1 & 0 & 0 \\ 0 & -1 & 0 \\ 0 & 0 & 0 \end{pmatrix} \\ \lambda_4 &= \begin{pmatrix} 0 & 0 & 1 \\ 0 & 0 & 0 \\ 1 & 0 & 0 \end{pmatrix} & \lambda_5 &= \begin{pmatrix} 0 & 0 & 1 \\ 0 & 0 & 0 \\ 1 & 0 & 0 \end{pmatrix} & \lambda_6 &= \begin{pmatrix} 0 & 0 & 0 \\ 0 & 0 & 1 \\ 0 & 1 & 0 \end{pmatrix} \\ \lambda_7 &= \begin{pmatrix} 0 & 0 & 0 \\ 0 & 0 & -i \\ 0 & i & 0 \end{pmatrix} & \lambda_8 &= \frac{1}{\sqrt{3}} \begin{pmatrix} 1 & 0 & 0 \\ 0 & 1 & 0 \\ 0 & 0 & -2 \end{pmatrix}\end{aligned}\tag{5.36}$$

It is usually more convenient to consider the infinitesimal transformations

$$\begin{aligned}\Psi(x) &\rightarrow \Psi(x) + i\theta_i(x)\Lambda_i\Psi(x) \\ F^{\mu\nu}(x) &\rightarrow F^{\mu\nu}(x) + i[\theta_i(x)\Lambda_i, F^{\mu\nu}(x)]\end{aligned}\tag{5.37}$$

The field tensor is given by the gauge vector potential $A^\mu(x)$ as

$$F^{\mu\nu} = \partial^\mu A^\nu(x) - \partial^\nu A^\mu(x) - ig[A^\mu(x), A^\nu(x)],\tag{5.38}$$

which also introduces the gauge coupling constant g . $A^\mu(x)$ has an index of the adjoint representation

$$A^\mu(x) = A_i^\mu(x)L_i,\tag{5.39}$$

where L_i is the adjoint representation of the generators. Rewriting Eq. (5.37) to display the index of the Lie algebra corresponding to the color degree of freedom gives

$$\begin{aligned}\Psi_a(x) &\rightarrow \Psi_a(x) + i\theta_b(x)(\Lambda_b)_{ac}\Psi_c(x) \\ F_a^{\mu\nu}(x) &\rightarrow F_a^{\mu\nu}(x) - C_{bca}\theta_b(x)F_c^{\mu\nu}(x).\end{aligned}\tag{5.40}$$

Since Λ is the fundamental representation of dimension 3 (usually denoted by $\mathbf{3}$) the quark field color index a can take 3 values, say red, green, and blue. The gluon field tensor is seen to transform according to the adjoint representation given by the structure constants of $SU(3)$. The adjoint representation has dimension 8 and is denoted $\mathbf{8}$. There are thus 8 varieties of gluons. Antiquarks are described by the conjugate spinor $\bar{\Psi}$, which transforms according to the representation $\bar{\mathbf{3}}$ conjugate to $\mathbf{3}$, which has generators $-\frac{1}{2}\lambda_i^*$. These two representations (triplet and anti-triplet) are both fundamental, but they are not equivalent.

A single particle state (in one of the three representations $\mathbf{3}$, $\bar{\mathbf{3}}$, or $\mathbf{8}$) is labeled by the eigenvalues of the Cartan operators, which can be chosen as L_3 and L_8

$$\begin{aligned} L_3 |I_3 Y_8 \xi\rangle &= I_3 |I_3 Y_8 \xi\rangle \\ L_8 |I_3 Y_8 \xi\rangle &= \frac{\sqrt{3}}{2} Y_8 |I_3 Y_8 \xi\rangle, \end{aligned} \tag{5.41}$$

where I_3 is the third component of “strong isospin” and Y_8 is the “strong hypercharge”, in analogy with the nomenclature used in the connection with $SU(3)_{\text{flavor}}$ symmetry. ξ denotes all other quantum numbers that are needed to specify the state. The possible values of I_3 and Y_8 are found by diagonalizing the matrix representations of L_3 and L_8 .

For quarks in the $\mathbf{3}$ representation the pairs of eigenvalues can immediately be read from the Gell-Mann matrices as

$$\begin{aligned} I_3 &= \frac{1}{2}, \quad -\frac{1}{2}, \quad 0 \\ Y_8 &= \frac{1}{3}, \quad \frac{1}{3}, \quad -\frac{2}{3}, \end{aligned} \tag{5.42}$$

and the corresponding states may be labeled by an index $c = r, g, b$. The triplet of quark states in the $\mathbf{3}$ representation is thus $|I_3 Y_8\rangle = |\frac{1}{2}, \frac{1}{3}\rangle_r, |-\frac{1}{2}, \frac{1}{3}\rangle_g, |0, -\frac{2}{3}\rangle_b$.

For antiquarks, the eigenvalues are minus the above, due to the opposite sign on the Gell-Mann matrices in relation to the representative matrices. Antiquark states will be labeled by $c = \bar{r}, \bar{g}, \bar{b}$.

The matrices L_3 and L_8 in the adjoint representation relevant for gluons can be found from the prescription in Eq. (5.12), where the structure constants can be found by calculating commutators of the Gell-Mann matrices. The result of simultaneously diagonalizing the matrices L_3 and L_8 in the adjoint representation is the pairs of eigenvalues

$$\begin{aligned} I_3 &= 0, \quad 0, \quad 1, \quad -1, \quad \frac{1}{2}, \quad -\frac{1}{2}, \quad \frac{1}{2}, \quad -\frac{1}{2} \\ Y_8 &= 0, \quad 0, \quad 0, \quad 0, \quad 1, \quad -1, \quad -1, \quad 1, \end{aligned} \tag{5.43}$$

and the corresponding eigenstates may be labeled by $c = 1, \dots, 8$.

This shows that instead of using the eigenvalues of the two Cartan operators to label states within the irreducible representations it is possible to label them

by a single “color index” c which for quarks and antiquarks has three possible values, and for gluons takes on eight different values. This is just an arbitrary enumeration of substates within each multiplet, with the index taking on as many different values as the dimension of the representation.

The multiplets (and the corresponding unitary irreducible representations) are characterized by the eigenvalues of the two Casimir operators, which like the Hamiltonian are degenerate on a multiplet. For $SU(3)$ it is usual practice [90] to characterize the irreducible representations $D^{(p,q)}$ by two non-negative integers p and q which are given by the maximum values of the eigenvalues of the two Cartan generators within the multiplet as

$$I_3^{(\max)} = \frac{p+q}{2} \quad Y_8^{(\max)} = \frac{p-q}{3}. \quad (5.44)$$

Thus the triplet representation $\mathbf{3}$ is $D^{(1,0)}$, the anti-triplet $\bar{\mathbf{3}}$ is $D^{(0,1)}$, and the octet $\mathbf{8}$ is $D^{(1,1)}$.

5.4.2 The Partition Function

The grand canonical partition function for a system of non-interacting quarks, antiquarks, and gluons taking into account the internal $SU(3)$ symmetry is

$$\mathcal{Z} = \text{Tr} e^{-\beta(\mathcal{H} - \mu_i N_i - \mu_3 L_3 - \mu_8 L_8)}, \quad (5.45)$$

where μ_i ($i = u, d, \dots$) are chemical potentials related to the $U(1)$ symmetries giving rise to conservation of flavor, and μ_3 and μ_8 are the chemical potentials related to the third component of color isospin and color hypercharge respectively. Since only non-interacting systems are considered the Hamiltonian is a sum of single particle Hamiltonians. The partition function therefore factorizes into independent contributions from each species

$$\mathcal{Z} = \prod_i \mathcal{Z}_i. \quad (5.46)$$

A multiparticle state that transforms according to an irreducible representation of $SU(3)$ can in principle be constructed, but this is a complex task. Luckily it is also an unnecessary task, since the trace is independent of the chosen basis. This fact can be used to evaluate the trace in a convenient basis of multiparticle states in which a state of the whole system is a product of states of each species, so that in evaluating \mathcal{Z}_i only substates of the species i are needed.

The grand canonical partition function with Wick rotated chemical potentials is

$$\tilde{\mathcal{Z}} = \text{Tr} e^{-\beta(\mathcal{H} - \mu_i N_i) + i\theta_3 L_3 + i\theta_8 L_8}. \quad (5.47)$$

$\tilde{\mathcal{Z}}$ is used to construct the color singlet canonical partition function by projecting onto the subspace of many-particle states transforming according to the singlet representation $D^{(0,0)}$. The singlet representation has dimension 1, and since it corresponds to $I_3 = 0$ and $Y_8 = 0$ every element is mapped onto the 1×1 unit

matrix, *i.e.* 1. The canonical color singlet partition function is thus given by Eq. (5.23) as

$$\mathcal{Z}_1 = \int d\mu(\theta_3, \theta_8) \tilde{\mathcal{Z}}(\theta_3, \theta_8). \quad (5.48)$$

It is more convenient in the following to use the eigenvalues of I_3 and Y_8 rather than those of L_3 and L_8 , so two parameters ϕ and ψ are introduced by

$$\phi = \theta_3 \quad \psi = \frac{\sqrt{3}}{2}\theta_8, \quad (5.49)$$

so that $\theta_3 L_3 = \phi I_3$ and $\theta_8 L_8 = \psi Y_8$. The Haar measure of $SU(3)$ is most conveniently expressed in terms of yet another parametrization, *viz.*, the parameters corresponding to λ_3 and $\sqrt{3}\lambda_8$, which are

$$\gamma_3 = \frac{1}{2}\phi = \frac{1}{2}\theta_3 \quad \gamma_8 = \frac{1}{3}\psi = \frac{1}{2\sqrt{3}}\theta_8. \quad (5.50)$$

In terms of this set of parameters the Haar measure is [90]

$$d\mu(\gamma_3, \gamma_8) = \frac{8}{3\pi^2} \left[\sin \gamma_3 \sin \frac{1}{2}(3\gamma_8 + \gamma_3) \sin \frac{1}{2}(3\gamma_8 - \gamma_3) \right]^2 d\gamma_3 d\gamma_8, \quad (5.51)$$

where $\gamma_3, \gamma_8 \in [-\pi, \pi]$.

The equations (5.47), (5.48), and (5.51) together give a concise prescription of how to construct the color singlet partition function \mathcal{Z}_1 . The actual calculation of $\tilde{\mathcal{Z}}$ and \mathcal{Z}_1 is the topic of the following sections. In the preceding I have called \mathcal{Z}_1 the canonical color singlet partition function, in order to distinguish it from $\tilde{\mathcal{Z}}(\gamma_3 = 0, \gamma_8 = 0)$, which might be called the grand canonical color singlet partition function, since it represents a system which although color singlet in mean, allows fluctuations with respect to color. On the other hand \mathcal{Z}_1 is still grand canonical with respect to the $U(1)$ symmetries related to the conservation of each quark flavor, *i.e.* it still depends on the chemical potentials μ_i . In order to stress this grand canonical nature of the ensemble, the function \mathcal{Z}_1 will later be referred to as the grand canonical color singlet partition function. Since this is the only color singlet partition function referred to there should be no chance of misunderstanding. All this notational trouble stems from the fact that \mathcal{Z}_1 is really mixed canonical/grand canonical partition function [94].

Quarks

The contribution to $\tilde{\mathcal{Z}}$ from a single quarks species, say q , with chemical potential μ_q is

$$\tilde{\mathcal{Z}}_q = \text{Tr} e^{-\beta(\mathcal{H}_q - \mu_q \mathcal{N}_q) + i\phi \hat{I}_3 + i\psi \hat{Y}_8}, \quad (5.52)$$

where there is *no* summation over q . A single particle state $|\mathbf{k}, \sigma, c\rangle$ is characterized by the quark momentum \mathbf{k} , the helicity $\sigma = \pm \frac{1}{2}$, and its color $c = r, g, b$. The creation operator $a_{\mathbf{k}, \sigma, c}^\dagger$, when acting on the vacuum ket $|0\rangle$, creates the

state $|\mathbf{k}, \sigma, c\rangle$. Multiparticle states $|n\rangle = |n_{\mathbf{k}_1, \sigma_1, c_1}, \dots, n_{\mathbf{k}_l, \sigma_l, c_l}, \dots\rangle$ are constructed by successively applying the creation operators

$$|n\rangle = \prod_i \left(a_{\mathbf{k}_i, \sigma_i, c_i}^\dagger \right)^{n_i} |0\rangle. \quad (5.53)$$

The number of quarks n_i with quantum numbers $\mathbf{k}_i, \sigma_i, c_i$ is either 0 or 1. The anticommutation relations $\{a_{\mathbf{k}_1, \sigma_1, c_1}, a_{\mathbf{k}_2, \sigma_2, c_2}^\dagger\} = \delta_{\mathbf{k}_1 \mathbf{k}_2} \delta_{\sigma_1 \sigma_2} \delta_{c_1 c_2}$ ensures that the resulting state has the correct symmetry. The Hamiltonian, the number operator, and the color isospin and hypercharge operators have the representations

$$\mathcal{H}_q = \sum_{\mathbf{k}, \sigma, c} \epsilon_q(\mathbf{k}) a_{\mathbf{k}, \sigma, c}^\dagger a_{\mathbf{k}, \sigma, c} \quad (5.54)$$

$$\mathcal{N}_q = \sum_{\mathbf{k}, \sigma, c} a_{\mathbf{k}, \sigma, c}^\dagger a_{\mathbf{k}, \sigma, c} \quad (5.55)$$

$$\hat{I}_3 = \sum_{\mathbf{k}, \sigma, c} I_3(c) a_{\mathbf{k}, \sigma, c}^\dagger a_{\mathbf{k}, \sigma, c} \quad (5.56)$$

$$\hat{Y}_8 = \sum_{\mathbf{k}, \sigma, c} Y_8(c) a_{\mathbf{k}, \sigma, c}^\dagger a_{\mathbf{k}, \sigma, c}, \quad (5.57)$$

where $\epsilon_q(\mathbf{k}) = \sqrt{\mathbf{k}^2 + m_q^2}$ is the energy of a quark.

The function $\tilde{\mathcal{Z}}_q$ can now be written

$$\tilde{\mathcal{Z}}_q = \text{Tr} \exp \left(\sum_{\mathbf{k}, \sigma, c} \{-\beta [\epsilon_q(\mathbf{k}) - \mu_q] + i [\phi I_3(c) + \psi Y_8(c)]\} \right). \quad (5.58)$$

The trace is now written as a sum over states in the Fock space of quarks, and the exponential of the sum is written as a product of exponentials, to give

$$\tilde{\mathcal{Z}}_q = \sum_{|n\rangle} \prod_{\mathbf{k}, \sigma, c} \langle n | e^{-\beta [\epsilon_q(\mathbf{k}) - \mu_q] + i [\phi I_3(c) + \psi Y_8(c)]} a_{\mathbf{k}, \sigma, c}^\dagger a_{\mathbf{k}, \sigma, c} | n \rangle. \quad (5.59)$$

Instead of summing over all possible states $|n\rangle$, it is possible to sum over all possible occupation numbers (*i.e.* 0 and 1) in effect interchanging the sum and product

$$\begin{aligned} \tilde{\mathcal{Z}}_q &= \prod_{\mathbf{k}, \sigma, c} \sum_{n_{\mathbf{k}, \sigma, c}=0}^1 e^{-\beta [\epsilon_q(\mathbf{k}) - \mu_q] + i [\phi I_3(c) + \psi Y_8(c)]} n_{\mathbf{k}, \sigma, c} \\ &= \prod_{\mathbf{k}, \sigma, c} \left(1 + e^{-\beta [\epsilon_q(\mathbf{k}) - \mu_q] + i [\phi I_3(c) + \psi Y_8(c)]} \right). \end{aligned} \quad (5.60)$$

It is more convenient to work with the logarithm of this expression

$$\ln \tilde{\mathcal{Z}}_q = 2 \sum_{\mathbf{k}, c} \left(1 + e^{-\beta [\epsilon_q(\mathbf{k}) - \mu_q] + i [\phi I_3(c) + \psi Y_8(c)]} \right), \quad (5.61)$$

where the factor 2 represents the sum over the degenerate spin states $\sigma = \pm \frac{1}{2}$.

Antiquarks

The treatment of antiquarks is very similar to that of quarks. The only difference is that antiquark states transform according to the representation $\bar{\mathbf{3}}$ rather than $\mathbf{3}$ which gives different eigenvalues of \hat{I}_3 and \hat{Y}_8 . The result is therefore almost identical with Eq. (5.61), *viz.*,

$$\ln \tilde{Z}_{\bar{q}} = 2 \sum_{\mathbf{k}, c} \left(1 + e^{-\beta[\epsilon_{\bar{q}}(\mathbf{k}) - \mu_{\bar{q}}] + i[\phi I_3(c) + \psi Y_8(c)]} \right), \quad (5.62)$$

where $c = \bar{r}, \bar{g}, \bar{b}$, instead of r, g, b .

Gluons

Gluons differ from quarks in the respect that they are bosons (massless spin-1 particles) rather than fermions, and again the different transformation properties under the $SU(3)$ transformations also makes a difference relative to quarks.

The Fock space may be built by acting on the vacuum state $|0\rangle$ with creation operators $b_{\mathbf{k}, \lambda, c}^\dagger$ creating a single particle state

$$|\mathbf{k}, \lambda, c\rangle = b_{\mathbf{k}, \lambda, c}^\dagger |0\rangle, \quad (5.63)$$

describing a gluon with momentum \mathbf{k} , helicity $\lambda = \pm 1$, and color index $c = 1, \dots, 8$. The commutation relation

$$[b_{\mathbf{k}, \lambda, c}, b_{\mathbf{k}', \lambda', c'}^\dagger] = \delta_{\mathbf{k}\mathbf{k}'} \delta_{\lambda\lambda'} \delta_{cc'} \quad (5.64)$$

ensures the right symmetry of multiparticle states

$$|n\rangle = |n_{\mathbf{k}_1, \lambda_1, c_1}, \dots, n_{\mathbf{k}_l, \lambda_l, c_l}, \dots\rangle, \quad (5.65)$$

in which each occupation number can take on the values $n_{\mathbf{k}_i, \lambda_i, c_i} = 0, \dots, \infty$.

The number of gluons is not conserved, so gluons have vanishing chemical potential, and since they are massless the dispersion relation is simply $\epsilon(\mathbf{k}) = |\mathbf{k}|$. Taking into account these differences we can immediately write the gluon contribution to \tilde{Z} in the form

$$\tilde{Z}_g = \prod_{\mathbf{k}, \lambda, c} \sum_{n_{\mathbf{k}, \lambda, c}=0}^{\infty} e^{\{-\beta|\mathbf{k}| + i[\phi I_3(c) + \psi Y_8(c)]\} n_{\mathbf{k}, \lambda, c}}. \quad (5.66)$$

Performing the sum, and taking the logarithm gives

$$\ln \tilde{Z}_g = -2 \sum_{\mathbf{k}, c} \left(1 - e^{-\beta|\mathbf{k}| + i[\phi I_3(c) + \psi Y_8(c)]} \right), \quad (5.67)$$

in which the factor two is due to the degeneracy of helicity states.

5.5 Evaluation of the Partition Function

As a first step toward an expression for the color singlet partition function \mathcal{Z}_1 the grand canonical partition function with Wick rotated $SU(3)$ -chemical potentials, $\tilde{\mathcal{Z}}$ needs to be evaluated. In the liquid drop model approach the sums over momentum eigenvalues are approximated by an integral

$$\sum_{\mathbf{k}} \rightarrow \int_0^\infty dk \rho(k), \quad (5.68)$$

where $\rho(k)$ is the density of states in Eq. (2.20), calculated by means of the multiple reflection expansion.

As was the case in section 2.3 there are two limits in which the partition function can be evaluated analytically. The zero temperature limit is not interesting here, since the effect of imposing color singletness disappears in the zero temperature limit.

The other limit in which $\tilde{\mathcal{Z}}$ can be evaluated analytically is the limit of zero quark mass. This means that for a proper inclusion of strange quarks, part of $\tilde{\mathcal{Z}}$ will have to be evaluated numerically. Even for massless quarks the integral over the $SU(3)$ group, as given by the Haar measure Eq. (5.51), has not been solved analytically, but a saddle-point approximation is applicable at high temperature and/or baryon chemical potential. The saddle-point approximation of the color singlet partition function was first calculated by Gorenstein, Lipskikh, Petrov, and Zinovjev [95], including only the volume term in the density of states (it was pointed out by Auberson *et al.* that there was a mistake in the group integration in [95]). Later on Elze and Greiner [96] did a similar calculation including the curvature dependent finite size correction to the density of states. Mustafa [97, 98] has done an equivalent calculation based on the work of Auberson *et al.* [99] and Savatier [100]. Recently Shrauner [101] investigated the effect of color singletness and the use of a continuous density of states instead of a discrete sum, on the thermodynamic treatment of fireballs produced in heavy-ion collisions, but the author does not include terms beyond the volume term in the density of states.

Unfortunately the different derivations mentioned above are not all in agreement. Since the authors do not all treat the exact same situation and do not always give intermediate results, it has not been possible to cross check all of the results, to see where the discrepancies originate. Because of this state of affairs I have done an independent calculation of $\tilde{\mathcal{Z}}$ for massless quarks, antiquarks, and gluons and obtained results in agreement with those of Elze and Greiner [96]. An outline of this calculation will be given in the following sections.

5.5.1 Massless Quarks and Gluons

Performing the substitution in Eq. (5.68), gives integrals of the form

$$\ln \tilde{\mathcal{Z}}_i = \pm 2 \sum_c \int_0^\infty dk \rho_i(k) \ln \left(1 \pm e^{-\beta(k-\mu_i) + i[\phi I_3^{(i)}(c) + \psi Y_8^{(i)}(c)]} \right), \quad (5.69)$$

where the upper sign is for fermions (quarks, antiquarks) and the lower is for bosons (gluons). Inserting the expressions for the multiple reflection expansion density of states given in section 2.3.1, which for massless quarks and antiquarks are

$$\rho(k) = \frac{Vk^2}{2\pi^2} - \frac{C}{24\pi^2}, \quad (5.70)$$

and for gluons

$$\rho(k) = \frac{Vk^2}{2\pi^2} - \frac{C}{6\pi^2}, \quad (5.71)$$

gives integrals of the form

$$\int_0^\infty k^n dk \ln(1 \pm e^{-\beta k + z}), \quad (5.72)$$

with $n = 0, 2$, where $z = \beta\mu_i + i(\phi I_3 + \psi Y_8)$ is a complex number.

For real z it was seen in section 2.3.2 that analytic results could be obtained for the combination $\ln \mathcal{Z}_q + \ln \mathcal{Z}_{\bar{q}}$, provided $\mu_{\bar{q}} = \mu_q$ is assumed. This is also the case here, which rests on the fact that $I_3^{(q)}(c) = -I_3^{(\bar{q})}(\bar{c})$ and $Y_8^{(q)}(c) = -Y_8^{(\bar{q})}(\bar{c})$ so that $z_q(c) = -z_{\bar{q}}(\bar{c})$. For gluons a similar trick is possible, since—as is seen from Eq. (5.43)—the eigenvalues of \hat{I}_3 and \hat{Y}_8 in the $\mathbf{8}$ representation come in pairs of opposite sign.

Hence for both massless quark-antiquark pairs and gluons the integrals can, after a partial integration, be grouped to form integrals of the type

$$\int_0^\infty dk k^n \left(\frac{1}{e^{\beta k - z} \pm 1} + (-1)^{n+1} \frac{1}{e^{\beta k + z} \pm 1} \right) \quad (5.73)$$

with $n = 1$ for the curvature term and $n = 3$ for the volume term.

Using the results in Appendix B for the above integrals, and performing the color sum in Eq. (5.69), I obtain the following results

$$\begin{aligned} \ln \tilde{\mathcal{Z}}_{q\bar{q},V} &\equiv \ln \tilde{\mathcal{Z}}_{q,V} + \ln \tilde{\mathcal{Z}}_{\bar{q},V} \\ &= T^3 \left\{ \frac{7\pi^2}{60} + \frac{1}{4\pi^2} (\beta\mu_q)^4 + \frac{1}{2} (\beta\mu_q)^2 + \frac{1}{\pi^2} \gamma_3^2 \gamma_8^2 + \frac{1}{6\pi^2} (\gamma_3^4 + 9\gamma_8^4) \right. \\ &\quad \left. + \frac{2i}{\pi^2} \beta\mu_q \gamma_8 (\gamma_8^2 - \gamma_3^2) - \left[\frac{1}{3} + \frac{1}{\pi^2} (\beta\mu_q)^2 \right] (\gamma_3^2 + 3\gamma_8^2) \right\} \end{aligned} \quad (5.74)$$

$$\begin{aligned} \ln \tilde{\mathcal{Z}}_{q\bar{q},C} &\equiv \ln \tilde{\mathcal{Z}}_{q,C} + \ln \tilde{\mathcal{Z}}_{\bar{q},C} \\ &= -T \left[\frac{1}{24} + \frac{1}{8\pi^2} (\beta\mu_q)^2 - \frac{1}{12\pi^2} (\gamma_3^2 + 3\gamma_8^2) \right] \end{aligned} \quad (5.75)$$

$$\begin{aligned} \ln \tilde{\mathcal{Z}}_{g,V} &= T^3 \left[\frac{8\pi^2}{45} - 2(\gamma_3^2 + 3\gamma_8^2) + \frac{8}{3\pi} \gamma_3^3 + \frac{18}{\pi} \gamma_8^3 \right. \\ &\quad \left. - \frac{9}{\pi^2} \gamma_3^2 \gamma_8^2 - \frac{3}{2\pi^2} (\gamma_3^4 + 9\gamma_8^4) \right] \end{aligned} \quad (5.76)$$

$$\ln \tilde{Z}_{g,C} = -T \left[\frac{4}{9} - \frac{2}{3\pi}(\gamma_3 + 3\gamma_8) + \frac{1}{\pi^2}(\gamma_3^2 + 3\gamma_8^2) \right] \quad (5.77)$$

To get the color singlet partition function for massless quarks, antiquarks, and gluons in an MIT bag the function \tilde{Z}

$$\tilde{Z} = e^{-\beta BV} \tilde{Z}_g \prod_q \tilde{Z}_{q\bar{q}}, \quad (5.78)$$

has to be integrated over the $SU(3)$ group, using the Haar measure given in Eq. (5.51). The resulting integral is obviously very complicated—even a numerical evaluation is not straightforward.

Fortunately, as has already been mentioned, there is a limit in which an approximate evaluation of Z_1 is applicable, *viz.*, in the limit of high temperature and/or chemical potential.

5.5.2 Saddle-Point Approximation

The idea of the saddle-point method [102] (or the Gaussian approximation), is that an integral of the type

$$\int f(x) e^{-\lambda g(x)} dx \quad (5.79)$$

can be evaluated approximately in the limit of large, positive λ by expanding $g(x)$ to second order around its maximum x_0 , and replacing $f(x)$ by its lowest order expansion (typically $f(x_0)$).

The maximum of $\tilde{Z}(\gamma_3, \gamma_8)$ is at $\gamma_3 = \gamma_8 = 0$, when curvature terms are not included. The linear terms in the gluon curvature contribution will displace the maximum slightly away from this position, but neglecting this small perturbation, and including only terms of second order in γ_3 and γ_8 , the pre-exponential factor is expanded to leading order, and the integration is extended to infinity, giving

$$Z_1 = \frac{1}{6\pi^2} \mathcal{Z} \int_{-\infty}^{\infty} d\gamma_3 \int_{-\infty}^{\infty} d\gamma_8 \gamma_3^2 (\gamma_3^2 - 9\gamma_8^2)^2 e^{-\Lambda(\gamma_3^2 + 3\gamma_8^2)}, \quad (5.80)$$

where \mathcal{Z} is the grand canonical partition function given by the expressions in section 2.3.2, and

$$\Lambda(T, V, C, \mu_q) = VT^3 \left[2 + \frac{\mathcal{N}_q}{3} + \frac{1}{\pi^2} \sum_q \left(\frac{\mu_q}{T} \right)^2 \right] + CT \frac{12 - \mathcal{N}_q}{12\pi^2}, \quad (5.81)$$

where \mathcal{N}_q is the number of massless quarks flavors. The Gaussian integral in Eq. (5.80), is easily reduced to a sum of products of integrals that are given by the gamma function [28]

$$\Gamma(x) = \int_0^{\infty} t^{x-1} e^{-t} dt, \quad (5.82)$$

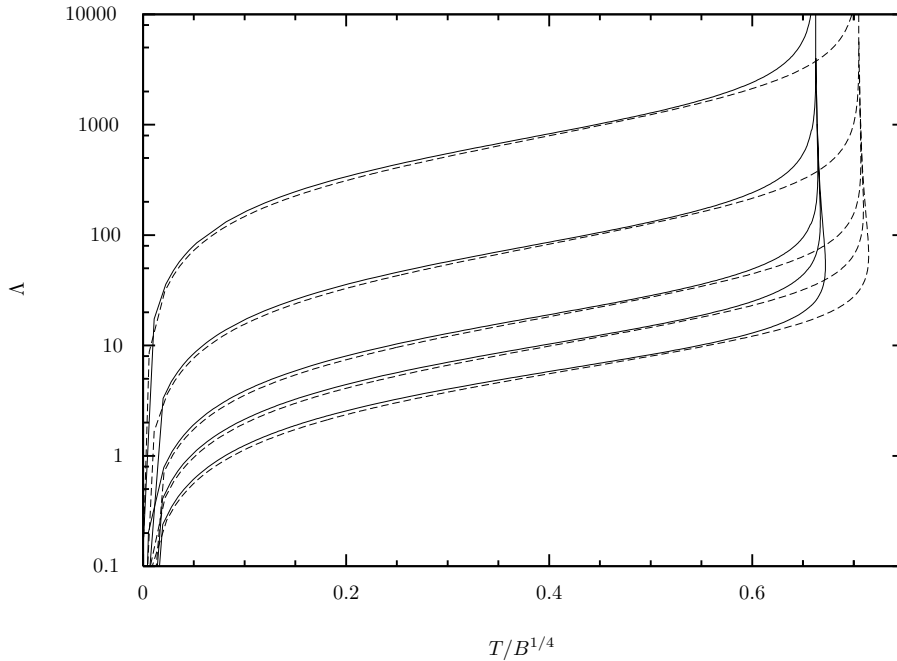


Figure 5.1: Plot of Λ vs. T for different values of the baryon number. From bottom to top: $A = 5, 10, 20, 100, 1000$. Solid lines are for $\mathcal{N}_q = 3$, while dashed lines are for $\mathcal{N}_q = 2$.

yielding

$$\mathcal{Z}_1(T, V, C, \mu_q) = \mathcal{Z}(T, V, C, \mu_q) \frac{1}{2\sqrt{3}\pi} \Lambda^{-4}(T, V, C, \mu_q). \quad (5.83)$$

This is the color singlet partition function in the saddle-point approximation. Each of the functions \mathcal{Z} and Λ is a sum of a volume term and a curvature term, but the resulting \mathcal{Z}_1 does not have this simple form. The result Eq. (5.83) is in agreement with the result obtained by Elze and Greiner [96], but it differs from the results of Gorenstein *et al.* by a factor 9, and from the result of Mustafa [98] by a factor 18, in the former case taking into account only the volume term in the density of states.

It should be noted that this saddle-point approximation can be improved by using the exact location of the maximum, instead of the approximate $\gamma_3 = \gamma_8 = 0$.

When Λ is big ($\Lambda \gg 1$) the saddle-point approximation is good (for quantitative results, see Chapter 6). This corresponds to either high temperature or high chemical potential and moderate to high temperature. The system size also plays a role—entering through V and C in Eq. (5.81)—so the relevant

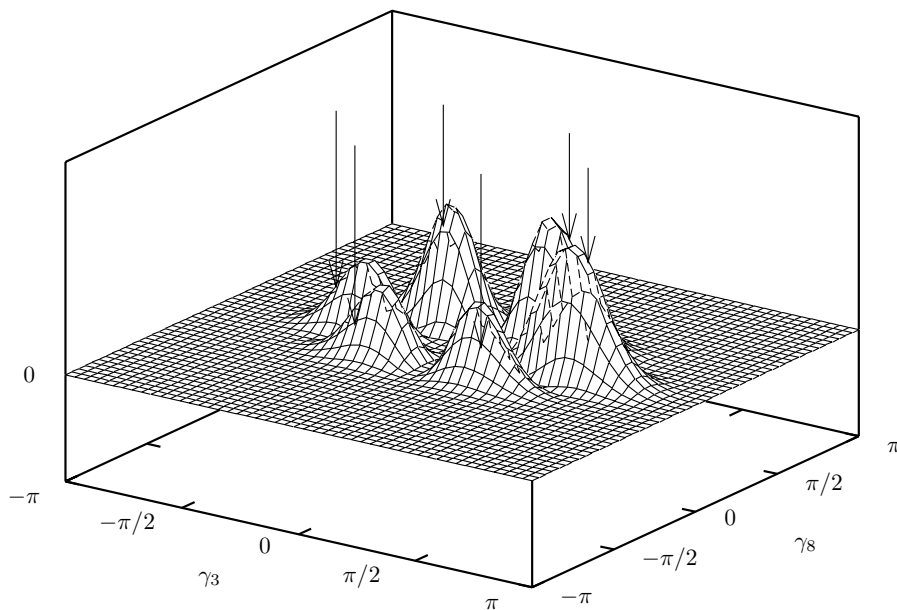


Figure 5.2: The integrand in the $SU(3)$ integration, for massless quarks, in arbitrary units. The parameters chosen are: $T = 45$ MeV, $\mathcal{N}_q = 3$, $\mu = 0$, and $R = 5^{1/3}$ fm, corresponding to $\Lambda \approx 1.49$. Arrows indicate the positions of the maxima as calculated in the saddle-point approximation.

parameters controlling the validity of the saddle-point approximation are RT and $RT(\mu/T)^{2/3}$ for a spherical system with radius R and a typical chemical potential μ . For a baryonless plasma ($\mu = 0$), RT is the only parameter, and for a dense system (cool strangelet) the second parameter is the dominating determinant.

A plot of Λ , calculated along the phase curve, seen in Fig. 3.4, is shown in Fig. 5.1 as a function of temperature, for different values of the baryon number, and for both 2 and 3 massless flavors. Depending on the value of the bag constant and the interpretation of the condition $\Lambda \gg 1$, the validity of the saddle point approximation for given A and T can be learned from this plot.

5.5.3 Numerical Evaluation

For low temperatures and non-zero quark masses it is necessary to evaluate the color singlet partition function numerically. For massive quarks this entails not only a numerical calculation of the integral over the group parameters, but also a numerical calculation of the quark contributions to $\tilde{\mathcal{Z}}$. Hence in the case of massive quarks there are three nested integrations, making for very long computations. Needless to say a lot of time has therefore been spent on

optimizing the integration routines.

One of the important things to take into account, not only in order to speed up execution, but also to improve accuracy is how to evaluate the group integral. It is generally best to start the integrations at, or very near a maximum of the function to be integrated. The function \tilde{Z} has its maximum at $\gamma_3 = \gamma_8 = 0$ (again neglecting the small displacement), where the Haar measure vanishes, thus generating a set of secondary maxima (see Fig. 5.2). The position of these maxima is thus an important prerequisite for the integration. In order to avoid an expensive search for the location of these maxima, the values found in the saddle-point approximation are used. There are six maxima, whose positions in the saddle-point approximation are given by

$$\sqrt{\frac{\Lambda}{3}}(\gamma_3, \gamma_8) = \left(\pm\frac{1}{2}, \pm\frac{1}{2}\right), (\pm 1, 0). \quad (5.84)$$

Figure 5.2 shows the integrand for massless quarks with a particular choice of parameters, and the maxima are seen to lie close to the prediction based on the saddle-point approximation. It is not obvious that this procedure should work as well when including massive quarks, but in fact it does. The integrand itself changes by many orders of magnitude, but the positions of the maxima are almost unchanged.

5.6 Summary and Discussion

The group theoretical projection method has been explained and applied to the construction of a color singlet partition function for a system of non-interacting quarks and gluons. The idea of the projection method is to start with a partition function that takes into account the internal $SU(3)$ symmetry only approximately via chemical potentials corresponding to the conserved charges. Of all the possible color states, those that are color singlets are picked out by a projection onto the color singlet sector.

A $q\bar{q}$ state consisting of a quark in the $\mathbf{3}$ representation and an antiquark in the $\bar{\mathbf{3}}$ representation gives the possible states $\mathbf{3} \otimes \bar{\mathbf{3}} = \mathbf{1} \oplus \mathbf{8}$, where only the singlet state ($\mathbf{1}$) corresponds to a physical meson. Likewise a three quark state gives rise to the multiplets $\mathbf{3} \otimes \mathbf{3} \otimes \mathbf{3} = \mathbf{1} \oplus \mathbf{8} \oplus \mathbf{8} \oplus \mathbf{10}$, where the physical baryon emerges as the color singlet combination, and all the other states remain unobserved.

In the case of flavor $SU(3)$ symmetry all of these combinations are seen, giving rise to the meson octets (*e.g.*, $\pi^+, \pi^0, \pi^-, K^+, K^-, K^0, \bar{K}^0, \eta$) and singlets (*e.g.*, η'), and the baryon singlets (*e.g.*, $\Lambda(1520)$), octets (*e.g.*, $p, n, \Sigma^+, \Sigma^0, \Sigma^-, \Lambda(1690), \Xi^0, \Xi^-$), and decuplets (*e.g.*, $\Delta^{++}, \Delta^+, \Delta^0, \Delta^-, \Sigma^{*+}, \Sigma^{*0}, \Sigma^{*-}, \Xi^{*0}, \Xi^{*-}, \Omega^-$). But the flavor $SU(3)$ symmetry is not exact and members in the same multiplet are not degenerate and mixing between multiplets also take place (*e.g.*, η and η' both contain singlet and octet components).

The non-existence of non-singlets has an analogue in nuclear physics where the deuteron, which is the isospin singlet combination of the nucleon-nucleon

system exists, but the three states in the isospin triplet representation containing the di-neutron and the di-proton do not exist as bound states. The nucleons are members of the fundamental $SU(2)$ doublet generating the representation $\mathbf{2}$. Since $\mathbf{2} \otimes \mathbf{2} = \mathbf{1} \oplus \mathbf{3}$, there are in principle both an isospin singlet and an isospin triplet. The nucleon-nucleon interaction has an isospin dependence which gives the isospin triplet a higher energy than the isospin singlet. The deuteron is only bound by 2.23 MeV, and the difference in energy between the two multiplets is enough to make the isospin 1 triplet of states unbound.

In the case of quarks the difference is even more dramatic—the energy of a quark antiquark pair increases linearly with their separation, making it impossible to break up a meson into a quark and an antiquark. The energy of an isolated quark is literally infinite. Once the energy of the chromoelectric field between two quarks becomes large enough, as the separation grows, new particles will be created. So it is believed that all non-singlet states of QCD have infinite energy, and that therefore they are not observed. Whether the energy is indeed infinite or merely very large does not really matter here. As long as these states are not part of the observable spectrum, they should not be included. The effect of the color singlet projection is exactly to weed out these states in the partition function.

The group theoretical projection method was applied to the simple case of a $U(1)$ symmetry, and the well-known connection between the grand canonical and the canonical partition functions was obtained. The projection method can also be applied to other symmetries, for example the calculation of the partition function (and from that the density of states) for a compound nucleus with fixed isospin.

The color singlet partition function (re-)derived in this chapter is a complicated integral over the $SU(3)$ group manifold, but a saddle-point approximation can be evaluated analytically in the case of massless quarks. For massive quarks there are no other alternatives than a numerical calculation.

Chapter VI

Color Singlet Strangelets

In this chapter I use the results of Chapter 5 to study the effect of the color singlet constraint on the mass of strangelets with non-zero entropy.

Experiments searching for strangelets are presently taking place both at the Brookhaven AGS [12] and at the CERN SPS [13], but so far only upper limits on strangelet production have resulted from these experiments. As a step toward realistic calculations of strangelet yields in heavy-ion collisions it is important to investigate the effect of a hot environment on strangelet properties, most notably strangelet masses. In this chapter I assume that the quark flavors are in equilibrium, so that they are described by a common chemical potential. For some applications it would be more natural to fix the strangeness fraction, as was done in Chapter 4, and use this to relate the chemical potential of the light quarks and that of the strange quark.

6.1 Massless Quarks

Massless quarks are so much easier to deal with than their massive counterparts, that they are a natural first topic of investigation, if for no other reason than to test the results of calculations done for massive quarks. But there are plenty of reasons to study massless quarks in their own right, first because u and d quarks have very low masses, second because massive quarks are not always present, *e.g.*, in the nucleation of quark gluon plasma droplets in ultrarelativistic heavy-ion collisions, or nucleation of quark matter droplets in the centers of neutron stars.

6.1.1 Saddle-Point Approximation

In addition to the constraint of color singletness, there is another, though less important constraint, *viz.*, that the system as a whole should have a fixed momentum [96, 99], which can be included in a way similar to the color singlet constraint. In the saddle-point approximation the two constraints ‘decouple’

[96], each giving rise to a (temperature and chemical potential dependent) correction factor in the resulting partition function

$$\mathcal{Z}_{\mathbf{1},p=0} = \Pi_{\mathbf{1}} \Pi_{p=0} \mathcal{Z} \quad (6.1)$$

where

$$\Pi_{\mathbf{1}} = \frac{1}{2\sqrt{3}\pi} \Lambda^{-4}(T, V, C, \mu_q), \quad (6.2)$$

is the correction due to the color singlet constraint, already calculated, with Λ given by Eq. (5.81), and

$$\begin{aligned} \Pi_{p=0}^{-2/3} &= \pi V T^3 \left\{ \left[\frac{7\mathcal{N}_q}{30} + \sum_q \left(\frac{\mu_q}{\pi T} \right)^2 + \frac{1}{2} \sum_q \left(\frac{\mu_q}{\pi T} \right)^4 \right] + \frac{16}{45} \right\} \\ &- \frac{CT}{\pi} \left\{ \frac{1}{72} \left[\mathcal{N}_q + 3 \sum_q \left(\frac{\mu_q}{\pi T} \right)^2 \right] + \frac{4}{27} \right\}, \end{aligned} \quad (6.3)$$

is the factor arising from the fixed momentum constraint, as given by Elze and Greiner [96], here taken at zero total momentum. \mathcal{N}_q is again the number of massless quark flavors, and terms proportional to \mathcal{N}_q or containing a sum over quark flavors q are due to quark-antiquark pairs, while the remaining terms are gluon contributions. In the following I will assume a common quark chemical potential μ for $\mathcal{N}_q = 3$ massless quark flavors. As is the case for Λ , so is the right hand side of Eq. (6.3) seen to be a sum of volume and curvature terms.

The partition function \mathcal{Z} in Eq. (6.1) is the unprojected grand canonical partition function, given by the expressions in section 2.3.2.

To find the the mass of a spherical strangelet at fixed baryon number A and fixed entropy per baryon \mathcal{S}/A , the equilibrium condition

$$\left(\frac{\partial \Omega}{\partial V} \right)_{T, \mu} = 0, \quad (6.4)$$

has to be solved along with the condition of fixed baryon number

$$-\frac{1}{3} \left(\frac{\partial \Omega}{\partial \mu} \right)_{T, V} = A, \quad (6.5)$$

and the condition of fixed entropy

$$-\frac{1}{A} \left(\frac{\partial \Omega}{\partial T} \right)_{V, \mu} = \frac{\mathcal{S}}{A}. \quad (6.6)$$

In these expressions the thermodynamic potential Ω can be either the unconstrained potential, as in Chapter 3, or it can include either, or both, of the color singlet and fixed (zero) momentum constraints. In the case where both constraints are included Ω is given by

$$\Omega_{\mathbf{1},p=0} = -T \ln \mathcal{Z}_{\mathbf{1},p=0}, \quad (6.7)$$

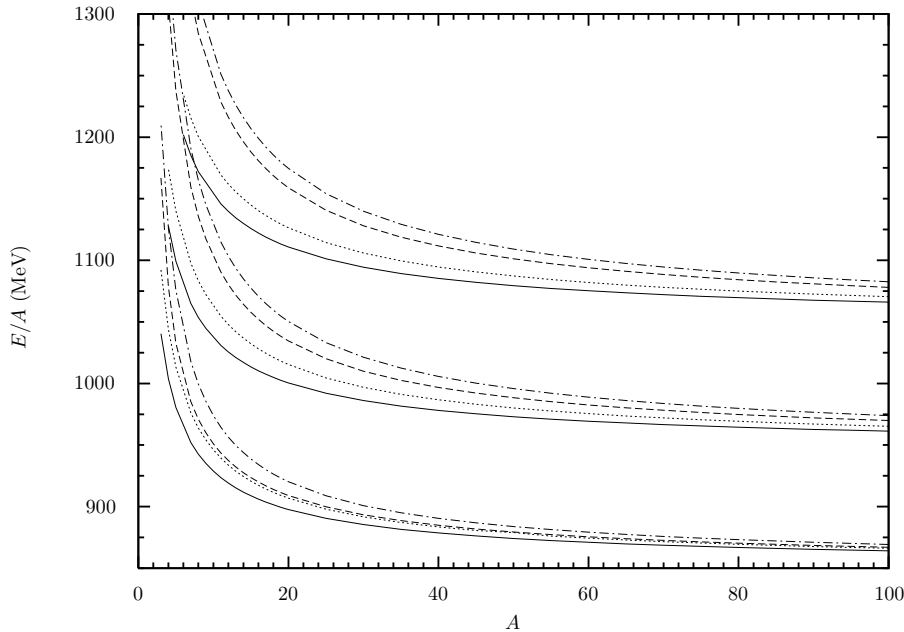


Figure 6.1: The energy per baryon at constant entropy per baryon for $\mathcal{N}_q = 3$ and $B^{1/4} = 145$. The 3 sets of curves are for $S/A = 2, 5,$ and 7 . The solid lines are unconstrained calculations, dotted lines are with the fixed momentum constraint only, dashed lines with the color singlet constraint only, and dotted-dashed lines are with both constraints.

and leaving out one of the constraints corresponds to setting one of Π_1 or $\Pi_{p=0}$ equal to 1. For the spherical system assumed here, the curvature is no longer an independent variable, but is given by $C \equiv 8\pi(3/4\pi)^{1/3}V^{1/3}$.

The result of solving these equations, and calculating the energy per baryon for a range in baryon number, is shown in Fig. 6.1, where dashed curves include the color singlet constraint, but not the fixed momentum constraint, dotted curves include the fixed momentum constraint, but not the color singlet constraint, and dotted-dashed curves include both constraints. The solid curves are results of unconstrained calculations, like the results shown in Fig. 3.3, but for massless quarks.

The particular choice of bag constant, $B^{1/4} = 145$ MeV, corresponds to the most optimistic choice, but results for higher values of B can easily be deduced from Fig. 6.1, since, as is always the case for massless quarks, the energy scales in proportion to $B^{1/4}$.

The effect of both the color singlet constraint and the zero momentum constraint is to increase the energy. The color singlet constraint is seen to be the most significant of the two constraints. The effect of the color singlet constraint

grows with increasing entropy, and decreasing baryon number. In the bulk limit the effect of both constraints disappear, which in the case of the color singlet constraint is due to the fact that the grand canonical ensemble and the canonical ensemble (with respect to color) become equivalent. At zero temperature the effect of the color singlet constraint also disappears, since it is always possible to choose a combination of colors using the lowest lying energy levels which gives a color singlet.

At very low baryon number ($A \leq 0-7$, depending on \mathcal{S}/A) there are no solutions to Eqs. (6.4)–(6.6). This is due to the breakdown of the multiple reflection expansion at very low values of the product of particle momentum and bag radius kR . At kR below the ground state value ($kR \approx 2.04$ for massless quarks; see Table 2.1) the density of states becomes spuriously negative. For low baryon number strangelets this part of the spectrum is weighted relatively more, than at larger baryon number. This is a signal of the breakdown of the multiple reflection expansion, and hence the liquid drop model. This is to be expected since the multiple reflection expansion is an expansion in powers of $(kR)^{-1}$ (see Appendix A).

At low temperature, as already discussed in section 5.5.2, the saddle-point approximation breaks down, so it is necessary to use numerical methods.

6.1.2 Numerical Calculation

In section 5.5.3, I briefly described the numerical evaluation of the color singlet partition function. Apart from the partition function (or equivalently the thermodynamic potential $\Omega = -T \ln \mathcal{Z}$) the derivatives with respect to T , μ , and V are also needed in order to calculate the entropy, baryon number, and pressure, required for solving Eqs. (6.4)–(6.6).

For this the partial derivatives of $\tilde{\mathcal{Z}}$ are needed, so that with

$$\mathcal{Z}(T, V, \mu) = \int_{SU(3)} d\mu(\gamma_3, \gamma_8) \tilde{\mathcal{Z}}(T, V, \mu, \gamma_3, \gamma_8), \quad (6.8)$$

the entropy is given by

$$\begin{aligned} \mathcal{S} &= - \left(\frac{\partial \Omega}{\partial T} \right)_{V, \mu} \\ &= \ln \mathcal{Z} + T \left(\frac{\partial \ln \mathcal{Z}}{\partial T} \right)_{V, \mu} \\ &= \ln \mathcal{Z} + \frac{T}{\mathcal{Z}} \int_{SU(3)} d\mu \tilde{\mathcal{Z}} \left(\frac{\partial \ln \tilde{\mathcal{Z}}}{\partial T} \right)_{V, \mu}. \end{aligned} \quad (6.9)$$

and all other derivatives are evaluated in the same fashion.

The result of such numerical integrations is compared to the saddle-point approximation in Fig. 6.2, where only the color singlet constraint has been taken into account. The agreement is seen to be rather good, although not

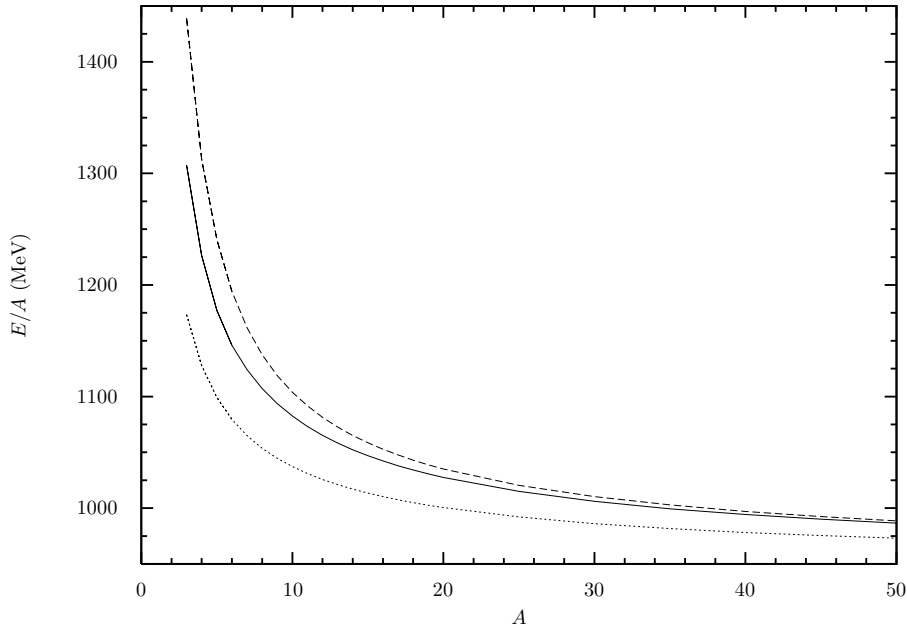


Figure 6.2: The saddle-point approximation (dashed line) compared to an exact numerical calculation (solid line), including only the color singlet constraint. An unconstrained calculation (dotted line) is shown for comparison. The plot is for constant entropy per baryon $S/A = 5$, and $B^{1/4} = 145$ MeV.

as good as reported in Ref. [72], where there was a mistake in the numerical evaluation¹.

The validity of the saddle-point approximation can also be seen in Fig. 6.3, where the relative error of the saddle-point approximation is plotted as a function of RT , where R is the radius of the system. Again only the color singlet constraint has been included. At fixed R and μ the thermodynamic potential has been calculated for a range in T to produce this plot. The bag contribution BV to Ω has been subtracted, since only the particle contributions to Ω are affected by the color singlet constraint.

It was stated in section 5.5.2 that the saddle-point approximation is believed to be good when $RT \gg 1$. Here this statement can now be made more quantitative. At zero chemical potential the saddle-point approximation is good to within 4% for $RT > 2$ and a higher chemical potential improves the approximation. A typical chemical potential for strangelet calculations is around 250 MeV,

¹ The odd terms in γ_3 and γ_8 in $\ln \tilde{Z}$, which appear in the functions S_1^- and S_3^- (see Appendix B) when the chemical potential has a non-zero imaginary part, were not included in the numerical calculation in Ref. [72], which resulted in a better agreement with the saddle-point approximation.

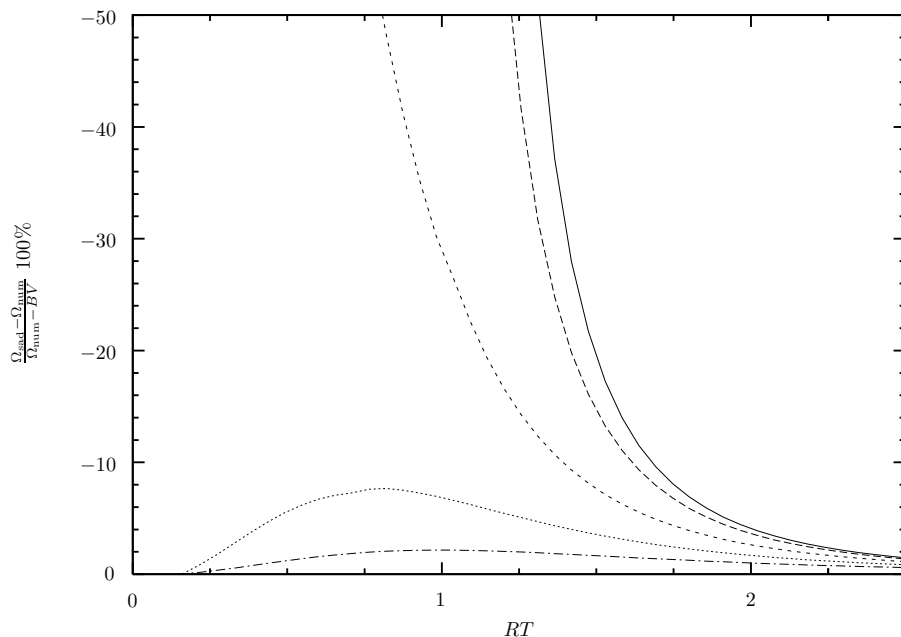


Figure 6.3: The deviation (in %) of the thermodynamic potential, as calculated in the saddle-point approximation, from the exact numerical result, as a function of RT . The bag contribution BV has been subtracted in both potentials. The solid curve is for $\mu = 0$, the long-dashed curve for $\mu = 100$ MeV, the short-dashed curve for $\mu = 200$ MeV, the dotted curve for $\mu = 300$ MeV, and the dotted-dashed curve for $\mu = 400$ MeV.

so as long as RT is sufficiently large, say greater than 1.5, the saddle-point approximation is expected to be reasonably good.

This should be compared with the findings of Elze, Greiner, and Rafelski [103, 104, 96] who state that the saddle point-approximation is good to within 30% at $RT = 1$ and $\mu = 0$, decreasing toward a few percent at $RT = 2$. Their calculation was done without the inclusion of curvature terms, so a better agreement is to be expected.

If the add-on in energy due to the color singlet constraint is 10%, a 5% error in the total energy is more like a 50% error in the energy difference, so one should be careful not to accept too large deviations when looking at differences rather than absolute quantities.

6.2 Massive Quarks

The inclusion of non-zero quark masses in the calculation of strangelet masses at non-zero entropy entails a numerical evaluation of the Fermi-Dirac integrals.

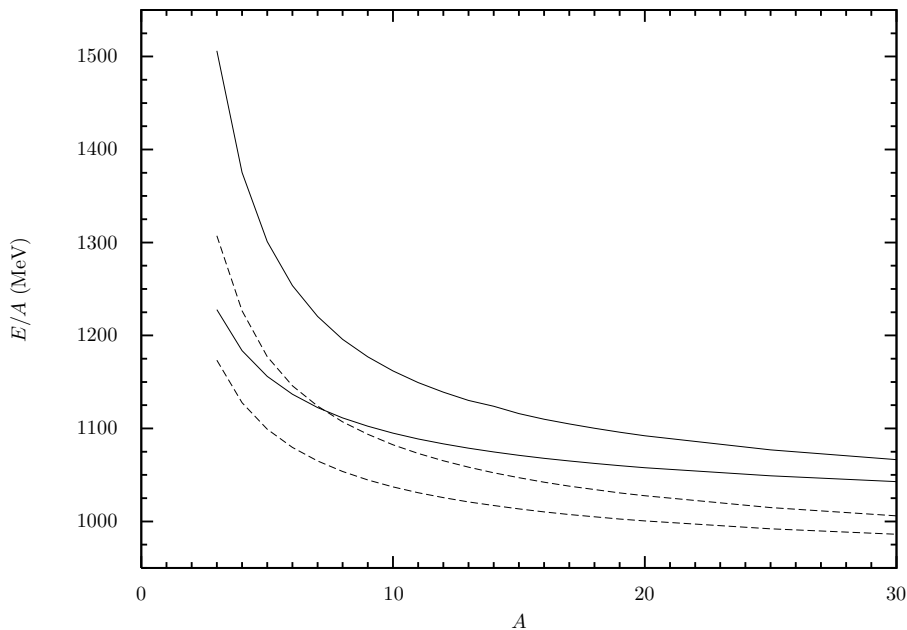


Figure 6.4: The energy per baryon as a function of baryon number, for $S/A = 5$, and $B^{1/4} = 145$ MeV. The solid curves are for a strange-quark mass $m_s = 150$ MeV, while the dashed curves are for a massless strange quark. Upper curves in each set are with the color singlet constraint, while lower curves do not include it.

The u - and d -quark masses are sufficiently small that they may be taken to be zero. The s -quark mass, however, is expected to lie in the range 100–300 MeV, and so a proper treatment should take a non-zero s -quark mass into account. Plots of the energy per baryon as a function of baryon number for different values of the entropy per baryon were shown in Fig. 3.3, for a strange quark mass of 150 MeV.

The numerical evaluation of the energy when the color singlet constraint is taken into account, is in itself a very time consuming. The addition of a non-zero strange quark mass makes it even more so. Therefore I have only performed very few such calculations, for a limited set of different parameters. A plot of the energy per baryon for a strange quark mass $m_s = 150$ MeV, including the color singlet constraint is shown in Fig. 6.4 along with results for the unconstrained case, and a calculation for $m_s = 0$.

The effect of the non-zero strange-quark mass is of course to increase the energy per baryon. This effect is in itself smaller than the mass of the strange quark, which is also seen in Fig. 2.2.

Except at very low A the effect of the color singlet constraint seems to be

relatively independent of the strange quark mass. The calculation for non-zero strange quark mass may not be totally reliable at very low A , though, so a refined calculation could give a more uniform difference.

6.3 Conclusion and Discussion

In this chapter it has been shown that the color singlet constraint, and to a lesser extent the fixed momentum constraint has the effect of increasing strangelet masses, as calculated at fixed entropy per baryon.

The fixed momentum constraint and the color singlet constraint can both be derived in a saddle-point approximation as shown by Elze and Greiner [96]. The saddle-point approximation is generally good at high temperature and chemical potential, but is very sensitive to the size of the system.

The saddle-point approximation is a useful guide for numerical calculations, which have also been performed, although not with the fixed momentum constraint included.

Finally a calculation for a finite strange-quark mass has been presented. At present such calculations are rather time consuming, and further improvement is needed before a systematic study can be performed.

The effect of color singletness on strangelet masses is important in the context of strangelet formation in heavy-ion collisions, and the results of this chapter could be incorporated in a production model, *e.g.* the thermal model by Braun-Munzinger *et al.* [105, 106].

Another obvious application of the results in this chapter is to study the effect of the color singlet constraint on the phase equilibrium between hadronic matter and quark matter, as was done in Chapter 4 without any constraints.

Chapter VII

Color Singlet Suppressed Nucleation

In this chapter the effect of the color singlet constraint on the nucleation rate of quark matter droplets is investigated. The result is a lowering of the nucleation rate relative to the unconstrained case. This has consequences for quark-gluon plasma formation in heavy-ion collisions, and quark matter droplet formation in neutron stars. For the reverse transition, *i.e.*, the quark-hadron phase transition a similar effect may play a role, but it is unclear at present how to properly treat this case.

7.1 Nucleation Rate

The nucleation is assumed to be thermally induced, and the transition to be of first order (it is by construction in the bag model), which means that homogenous nucleation theory [107] is applicable. A common estimate for the nucleation rate \mathcal{R} , within this framework, is given by

$$\mathcal{R} = T^4 e^{-\Delta F/T}, \quad (7.1)$$

where ΔF is the free energy barrier, *i.e.*, the amount of work it takes to produce a droplet of the critical radius. The prefactor T^4 is merely a dimensional estimate. A more refined treatment would include a more realistic choice of prefactor, but in the present case of massless quarks there is no surface term in the free energy, and a derivation of the prefactor when curvature effects rather than surface effects dominate has not been made. In any case the exponential is the dominating factor in the expression for the nucleation rate, so a modification of the prefactor is only expected to have marginal effects.

7.1.1 Free Energy Barrier

For a droplet in chemical equilibrium with the surrounding hadron phase (*i.e.*, with a composition determined by the chemical potential of the hadron phase) the free energy barrier is

$$\Delta F = \Omega + P_{\text{hadron}}V + \sigma_{\text{hadron}}S, \quad (7.2)$$

where Ω is the thermodynamic potential of the quark phase, P_{hadron} is the hadron pressure, σ_{hadron} is the surface tension due to hadrons, and V and S are the volume and surface area of the formed droplet. We will make the seemingly drastic approximation that $P_{\text{hadron}} = \sigma_{\text{hadron}} = 0$. Note, however, that a non-zero pressure or surface tension of the hadronic phase will increase ΔF and thereby lower the nucleation rate. Since it will be demonstrated that the effect of the color singlet constraint is to lower the nucleation rate considerably, the inclusion of the hadronic terms would only strengthen this effect.

An estimate of the effect of the hadron pressure is the pressure of a massless pion gas, with three degrees of freedom, at $\mu = 0$ which is $P_\pi = \pi^2 T^4/30$. The quark-gluon plasma has a number of degrees of freedom given by Eq. (3.14), which for $\mathcal{N}_q = 2$ amounts to $g_* = 37$ giving a pressure $g_* T^4 \pi^2/90$, which is more than 10 times the pion pressure at the same temperature. The pion pressure would add to the bag constant to give an effective bag constant $B[1 + \pi^2/30(T/B^{1/4})^4]$ instead of B . At the critical temperature $T_c \approx 0.7B^{1/4}$ given by Eq. (3.13) this results in a change in $B^{1/4}$ which is less than 2%.

The free energy barrier $\Delta F = \Omega$, for a spherical droplet with two massless quark flavors ($\mathcal{N}_q = 2$), having a common chemical potential μ is shown as a function of radius R in Fig. 7.1 for $T = 170$ MeV, $\mu = 0$ corresponding to about 30 MeV superheating, and for $T = 70$ MeV, $\mu = 400$ MeV corresponding to a superheating of ~ 25 MeV. It is seen that the inclusion of the color singlet constraint results in an increase of the free energy barrier. The critical radii for $\mu = 0$ correspond to values of $RT \approx 1$, which means that the saddle-point approximation cannot be expected to hold (*cf.* the discussion in section 6.1.2). It is clear from Fig. 7.1 that the saddle-point approximation is indeed better for $\mu = 400$ MeV than for $\mu = 0$ MeV even though RT is smaller in the latter case. As mentioned in Chapter 5 this is because another parameter, *viz.*, $RT(\mu/T)^{2/3}$, is also important as a determinant of the validity of the saddle-point approximation. But at higher temperature the critical radius gets smaller (see Fig. 7.2) causing the saddle-point approximation to become less accurate. So it seems that even for large chemical potential it is not safe to use the saddle-point approximation.

This is in contrast to what was claimed in Ref. [108], where the saddle point approximation was used exclusively. A few comments on this seem to be in order. When the calculations in Ref. [108] were done the preliminary numerical calculations indicated that the saddle point approximation was valid for the high temperatures and chemical potentials that were used. As mentioned previously (in the footnote on page 73) there was an error in these calculations, which caused a much better agreement with the saddle-point approximation. The saddle-point approximation *is* valid at high temperature and chemical potential *provided* that the system size is not too small. It is exactly the very small critical radii that bring about the fall of the saddle-point approximation in the present context, despite the favorable values of T and μ . This is clearly seen in Fig. 7.2, where RT is below 1 except very near the critical temperature. In Fig. 7.2 and in the rest of this chapter only results of the numerical calculations

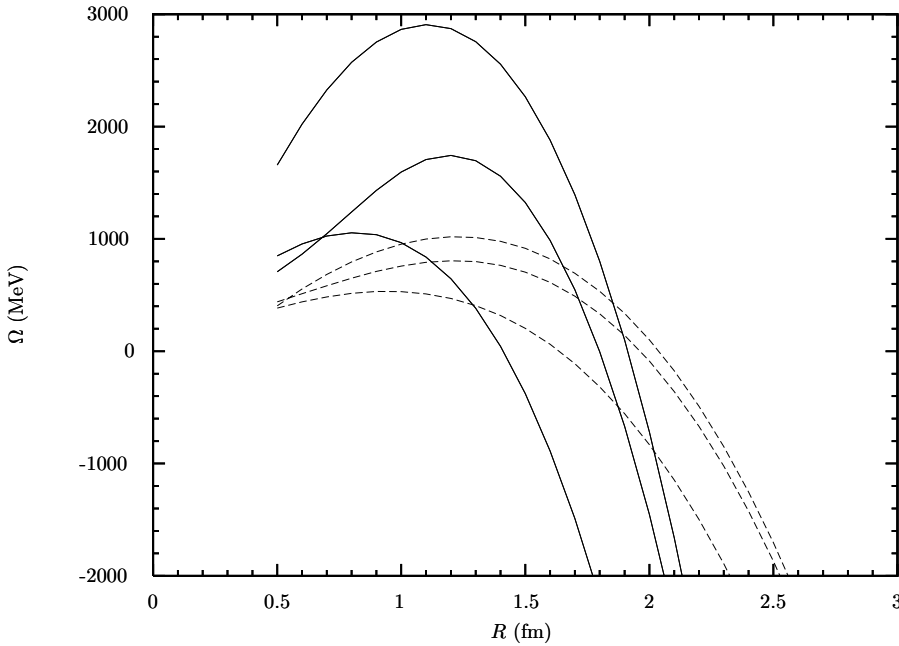


Figure 7.1: The thermodynamic potential Ω as a function of droplet radius R , for $B^{1/4} = 200$ MeV. The solid curves are for $T = 170$ MeV and $\mu = 0$, whereas the dashed curves are for $T = 70$ MeV and $\mu = 400$ MeV. The lower curve in each set is the unconstrained grand potential, the middle curve is the exact numerical calculation including the color singlet constraint, and the upper curve is the saddle-point approximation.

are presented.

In addition to the color singlet constraint the fixed momentum constraint was also taken into account in Ref. [108], but at present this has not been implemented numerically, and so it is left out here. But were it to be included it would result in a further increase in the free energy barrier. As pointed out in Chapter 6 the color singlet constraint is the more decisive of the two, as can also be seen in Ref. [108], which means that the major effect is accounted for.

7.2 Rate Suppression

By finding the maximum in the free energy shown in Fig. 7.1 the critical radius R_c and the barrier height $\Delta F(R_c)$ are found. Inserting the value of $\Delta F(R_c)$ in the expression Eq. (7.1) gives the nucleation rate, which can be rewritten

$$\mathcal{R} \approx 0.2 \text{ fm}^{-3} (10^{-23} \text{ s})^{-1} T_{100}^4 e^{-\Delta F/T}. \quad (7.3)$$

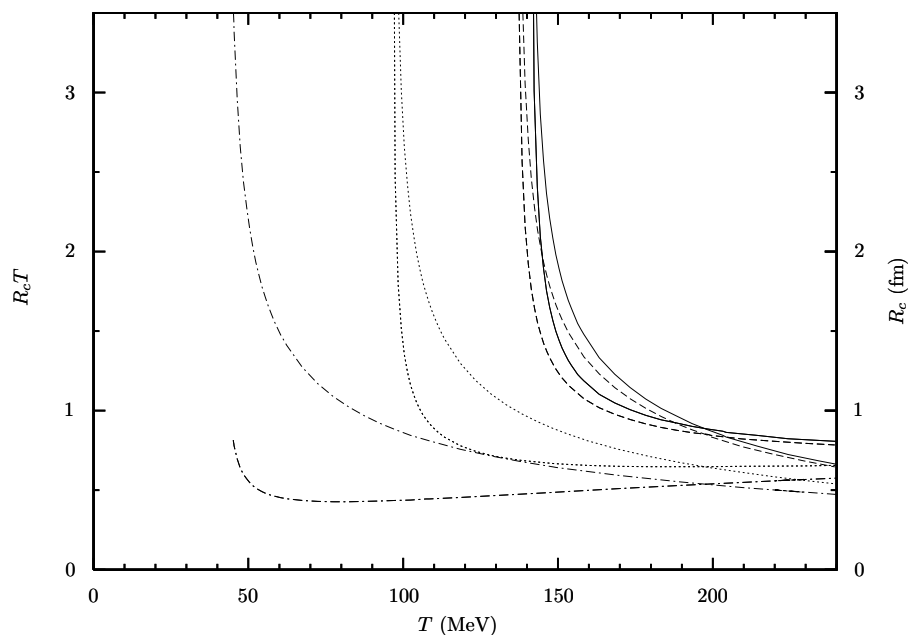


Figure 7.2: The critical radius R_c and the product $R_c T$ as a function of temperature, including the color singlet constraint. Upper (mostly) curves are R_c while (mostly) lower curves are $R_c T$. The solid curves are for $\mu = 0$, the dashed curves for $\mu = 100$ MeV, the dotted curves for $\mu = 300$ MeV, and the dotted-dashed curves for $\mu = 400$ MeV, all for $B^{1/4} = 200$ MeV.

Here T_{100} is the temperature in units of 100 MeV. The nucleation rate is thus given in units of the number of nucleations per fm^3 per 10^{-23} s ($= 3$ fm/c), which is a natural scale in the context of heavy ion collisions.

The nucleation rate is shown in these units in Fig. 7.3, where a considerable suppression of the rate in the constrained case is seen relative to the unconstrained case. At moderate superheating the rate is suppressed by many orders of magnitude, shrinking to 1 order of magnitude only when the superheating exceeds ~ 40 MeV. This clearly seen from Fig. 7.4, where the relative rate, *i.e.*, the rate calculated with the color singlet constraint divided by the rate calculated without the constraint, is plotted as a function of temperature.

Results for other values of the bag constant B can be obtained by scaling the temperature in proportion to $B^{1/4}$ and the nucleation rate in proportion to B . The relative rate, or the suppression factor, shown in Fig. 7.4 is of course unchanged.

The volume and time available in a heavy-ion collision amounts to perhaps $100 \text{ fm}^3 \text{ fm}/c$, so in the case where no constraints are included one thus predicts a fair probability for bubble nucleation at moderate superheating, say 10–20

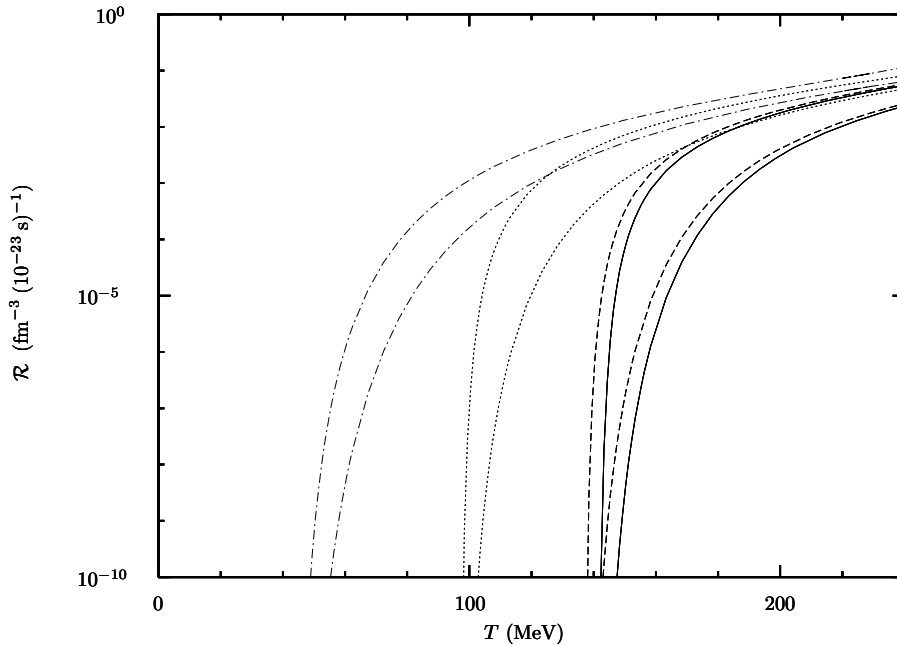


Figure 7.3: The nucleation rate, as a function of temperature, with 2 massless quark flavors, for different values of the chemical potential, and $B^{1/4} = 145$ MeV. Upper curves are without the color singlet constraint, while lower curves include the constraint. Solid curves are for $\mu = 0$, dashed curves for $\mu = 100$ MeV, dotted curves for $\mu = 300$ MeV, and dotted-dashed curves for $\mu = 400$ MeV.

MeV. Conversely, with the color singlet constraint included a superheating of at least double that amount is needed to achieve a similar probability.

7.3 Conclusion and Discussion

It has been demonstrated that in the framework of homogenous nucleation theory, there is a significant suppression of the rate for nucleation of quark-gluon plasma droplets if the formed droplets are subjected to the restriction that they must be color singlets. This conclusion rests on several assumptions that will be discussed below.

First of all the phase transition is assumed to be of first order. This is the case in the bag model, but it could conceivably be second order, as indicated by lattice calculations (at $\mu = 0$). This assumption is not testable until reliable lattice calculations exist, also for $\mu \neq 0$.

The result is of course model dependent. Choosing a different model than

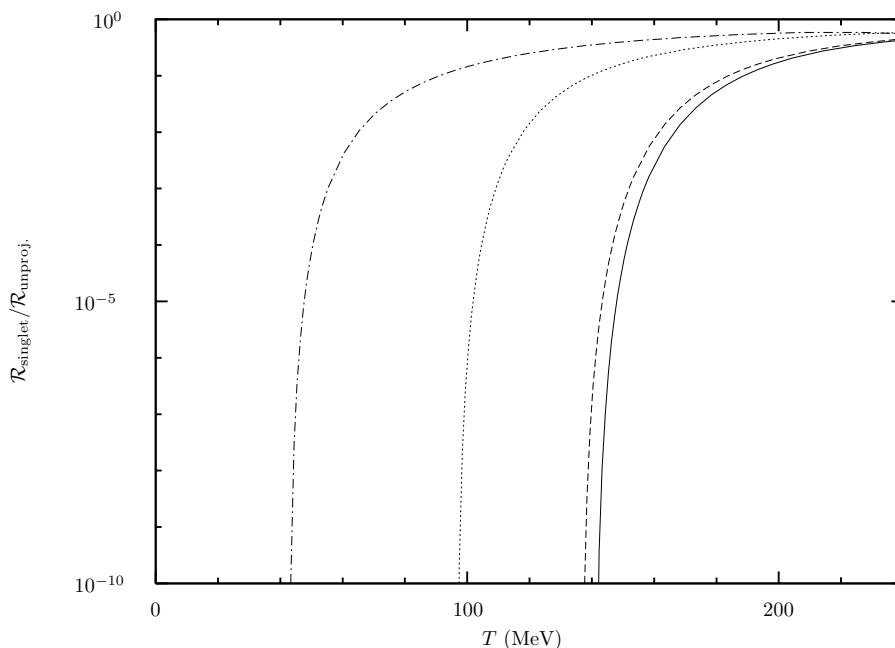


Figure 7.4: The rate suppression factor, as a function of temperature for the same choice of parameters as in Fig. 7.3. Again the curves correspond to (from right to left) $\mu = 0$, $\mu = 100$ MeV, $\mu = 300$ MeV, and $\mu = 400$ MeV.

the bag model, would certainly give different results, but the trend should be the same, as the effect of imposing the color singlet constraint will always be to reduce the effective number of degrees of freedom, and thereby to increase the free energy.

At very high superheating, the critical radius becomes very small which could result in the breakdown of the multiple reflection expansion on which the liquid drop model is based. This can only be tested by a direct comparison of the shell model and the liquid drop model. Shell model calculations at finite temperature have only recently been attempted [71] (see also Ref. [38] for a calculation at $\mu = 0$), and so this has not been checked. But at more moderate superheating, which includes the more realistic temperatures, there should be no problems in using the liquid drop model.

The most serious shortcoming of the present approach is probably that the timescales relevant for a heavy-ion collision are too short for the applicability of a thermodynamic equilibrium approach. Nevertheless this is often used as a first approximation, and even if a thermal nucleation picture is wrong there may still be an effect of the color singlet constraint, which has to be fulfilled regardless of the nucleation mechanism.

In neutron star cores on the other hand, there is ample time for thermodynamic equilibrium to be reached, and so the present approach should not be problematic. A simple model, using a pure neutron gas [109], could be used to estimate the stability of neutron stars with respect to quark matter formation.

So the conclusion remains that a significant suppression of the nucleation rate of quark-gluon plasma droplets in a superheated hadron gas is a direct consequence of the color singlet constraint. Most of the effects left out in this simple treatment, like the pressure of the hadron phase and the fixed momentum constraint will further reduce the nucleation rate.

Chapter VIII

Finale

8.1 Thesis Conclusion and Summary

This thesis has been centered around a few key themes which have been staged differently in individual chapters. These themes are the finite system size, non-zero temperatures, and colorlessness.

The finite size effects were introduced in Chapter 2 by use of the multiple reflection expansion method, explained in Appendix A, and the liquid drop model was compared to the shell model, showing that the multiple reflection expansion approach is valid for strangelets, unless one discusses subjects such as strangelet decay modes which depend on the detailed effects of the shells. The mean effects of the shell structure are well reproduced by the liquid drop model, whose major advantage over the shell model is that many quantities can be evaluated analytically, allowing for more insight into parameter dependences and general trends, as well as making solutions easier. Even in those cases where analytic results are not available, the simpler cases serve as important known limits against which the numerical results can be checked.

The effect of non-zero temperature, was introduced in Chapter 3, where the results were used to calculate strangelet masses and to study the phase diagram of quantum chromodynamics in the bag model at high temperature and baryon density. At finite temperature it is only possible to obtain analytic results for massless quarks, in contrast to the zero temperature case where massive quarks *can* be treated analytically.

In Chapter 4 the phase equilibrium between strange quark matter and a hadron gas was studied with emphasis on the effects of finite size of the quark phase, and a non-zero strangeness fraction. The abundance of strangeness in ultrarelativistic heavy-ion collisions and the mechanism of strangeness separation [14, 15, 16] makes it necessary to study the effect of non-zero strangeness fraction on the phase equilibrium. This was done by Lee and Heinz [73] for bulk phases and generalized by Jensen and Madsen [69] to include the finite size of the quark phase, which is what was described in Chapter 4. This work was extended by He *et al.* [74] to allow the calculation of isentropic expansion

trajectories of the system as a whole.

In Chapter 5 it has been explained how to implement the effect of exact color singletness, using the group theoretical projection method. The color singlet partition function was constructed for a system of non-interacting quarks, antiquarks, and gluons, and the partition function was evaluated in the saddle-point approximation, in the case of massless quarks. The result obtained here was identical with that obtained by Elze and Greiner [96], but other authors have reported different results. The saddle-point approximation is valid at high temperature and chemical potential, but these conditions are not always present, and so a numerical evaluation is necessary. The inclusion of massive quarks cannot be handled in the saddle-point approximation, so this case must always be treated numerically.

In Chapter 6 the effect of the color singlet constraint on strangelet masses was investigated. At fixed entropy per baryon the color singlet constraint has the effect of increasing strangelet masses. The effect is most significant for large entropy and small baryon number, disappearing in the bulk limit as well as at zero temperature. In the saddle-point approximation another effect—demanding fixed, zero momentum—was also included, and though not negligible it was shown to be less important than the color singlet constraint. A thorough discussion of the saddle-point approximation, and a comparison with exact numerical calculations was then performed. It was shown that the saddle-point approximation is generally useful at high temperature and high chemical potential, provided the system size is not excessively small. Finally a calculation including massive quarks was presented, and the effect of the color singlet constraint was seen to be roughly independent of the quark mass. But further refinements and improvements to these $m \neq 0$ calculations need to be done before a large scale investigation of color singlet strangelets can be undertaken.

In Chapter 7 it was demonstrated that the color singlet constraint has the effect of diminishing the rate of quark matter nucleation from a hadronic gas by many orders of magnitude at moderate superheating, only gradually approaching the result obtained without the color singlet constraint included. This suppression of the nucleation rate could have important consequences for the formation of quark gluon plasma droplets in ultrarelativistic heavy-ion collisions, and the nucleation of quark matter droplets in neutron stars.

The approach used relies on some simplifications, like the neglect of the hadron pressure, but this was argued to strengthen the conclusion, and it is therefore not a serious omission. Other assumptions such as the phase transition being of first order, are not readily testable, but must await the outcome of more elaborate lattice gauge calculations.

From the studies presented in these chapters it is learned that all three effects—the effect of finite size, the effect of non-zero temperature, and the effect of exact color singletness—have a destabilizing effect on strange quark matter. This conclusion is *a priory* obvious, and does therefore not come as any surprise. What is important is the magnitude of the effects, and their impact on our chances of ever observing strange quark matter.

The baryon number available in a heavy-ion collision is limited to that of the colliding nuclei (2×207 for Pb on Pb), but a strangelet can only have a small fraction of this number, since most of the baryon number ends up in hadrons. The lower the baryon number the more likely will a strangelet be unstable, unlike nuclei where Coulomb effects give rise to a maximum binding energy near ^{56}Fe . Shell effects, however, play an important stabilizing role for strangelets with a magic number of quarks, such as the $A = 6$ system composed of 6 u quarks, 6 d quarks, and 6 s quarks.

When increasing the temperature, strangelets acquire thermal energy, making them prone to surface evaporation of hadrons. This effect is important in heavy-ion collisions as well as in the early universe. Shell effects become less important at higher temperature, and so this possible stabilizing mechanism is to some degree lost.

In addition to the increase in mass due to thermal energy, the demand of colorlessness also has the effect of increasing the mass of a strangelet with non-zero entropy.

In spite of all these destabilizing effects there is still the chance that cold strange quark matter is stable or metastable, and the production of strangelets in heavy-ion collisions cannot be ruled out. At this point it is relevant again to stress the fact that the MIT bag model can only give a hint at what to expect. The question of the stability of strange quark matter must ultimately be settled experimentally, but model predictions are still important as a guide for experiments.

It seems that the most favorable conditions for strange quark matter is in compact objects such as neutron stars. Here truly bulk systems can exist, and the temperature is low. Even in the case of strange quark matter being unstable, the pressure in the core of a neutron star may be great enough to cause strange quark matter to be the preferred phase of matter.

8.2 Outlook

The results, just summarized, that have been presented in this thesis point toward some possible directions of future research. Some of these prospects have been mentioned in the text, others have not, and so I would like to finish by mentioning some of the topics I find interesting and worthy of further study.

The color singlet constraint is an important addition to the bag model, which otherwise implements the well known confinement feature of QCD. Being able to describe both of these two essential features—confinement and colorlessness—should improve bag model predictions. The color singlet constraint was implemented in the early to mid eighties, but many studies would still benefit from taking this constraint into consideration. With today's more powerful computers, this has become much easier.

One of the places where the effect of the color singlet constraint has not yet been investigated is in phase equilibrium calculations such as those presented in Chapter 4. It will be interesting to see how this changes the phase diagram

and the prospects for forming strangelets in ultrarelativistic heavy-ion collision experiments.

A related area of research is the cosmological quark-hadron phase transition where the effect of color singletness is also expected to play a role. A bubble of hadronic matter nucleating in the supercooled quark matter phase is composed of hadrons that are color singlets. These hadrons materialize from a combination of quarks antiquarks and gluons that must come together to form a color singlet. It is unclear at present how to formulate this, but it is an interesting problem for future research.

The suppression of quark matter formation described in Chapter 7 can be applied to nucleation of quark matter droplets in neutron stars, by a modification of the treatment of Olesen and Madsen [109]. With the present state of the calculations it should be relatively easy to obtain this goal.

It was mentioned in Chapter 5 that the inclusion of the curvature term shifts the location of the maximum in the saddle-point approximation. This means that an improved saddle-point approximation, taking this into account is possible. The feasibility of such an improved approximation has not been undertaken yet, but if it proves not to be beyond analytical evaluation it might greatly improve the saddle-point approximation presented here, and would perhaps obviate the need to do numerical calculations for massless quarks.

Calculations including massive quarks must be done numerically, and results of such calculations were presented in Chapter 6. There is still room for improvement of these calculations, and this work is currently in progress.

Appendix A

The Multiple Reflection Expansion

In the previous chapters I have used an asymptotic expansion of the density of states in powers of $\frac{1}{kR}$, where k is the wavenumber and R is the radius of the system. This appendix describes how such an expansion can be obtained using Green's function methods. The following is a brief exposition of the general formalism used, but a few detailed calculations are presented. The appendix is organized as follows. In section A.1 I relate the density of states to the Green's function. In section A.2 this relation is used to calculate the density of states for a non-interacting free field. Next in section A.3 the multiple reflection expansion for the Green's function is introduced and discussed. Finally in section A.4 a short outline of how to obtain the multiple reflection expansion for the density of states is given. In this appendix a generic 4-vector is denoted $x^\mu = (t, \mathbf{r})$.

A.1 Trace Formula for the Density of States

In this section I derive a formula relating the density of states to the propagator. The propagator in question is that of a non-interacting Dirac field confined to a finite region of space (Ω), obeying appropriate boundary conditions at the surface ($\partial\Omega$). The *form* of the result does not depend on the details of the Hamiltonian or the nature of the boundary conditions, only on the spinor nature of the field, so I will adopt a general notation in which the Dirac equation is written:

$$D\Psi = 0, \tag{A.1}$$

or

$$i\frac{\partial\Psi}{\partial t} = H\Psi, \tag{A.2}$$

where the free particle case corresponds to

$$D = i\gamma^\mu\partial_\mu - m \tag{A.3}$$

$$H = -i\boldsymbol{\alpha} \cdot \nabla + \beta m. \tag{A.4}$$

The particular problem to be solved is that of solving the Dirac equation for a non-interacting quark confined to an MIT-bag. The Dirac equation with boundary condition in this case is:

$$\begin{aligned} (i\gamma_\mu\partial_\mu - m)\Psi(x) &= 0 & \mathbf{r} \in \Omega \\ in_\mu\gamma^\mu\Psi(x) &= \Psi(x) & \mathbf{r} \in \partial\Omega \end{aligned} \quad (\text{A.5})$$

where \mathbf{n} is the outward normal to $\partial\Omega$ at \mathbf{r} . The second boundary condition in Eq. (2.2) has been omitted since it corresponds to pressure equilibrium, which is taken into account when minimizing the free energy. In the rest of this section an accompanying boundary condition is always assumed when I refer to the field equation. The propagator or Green's function, $S(x, x')$, for the Dirac equation is defined through

$$DS(x, x') = \delta(x - x'), \quad (\text{A.6})$$

which in terms of the Hamiltonian is

$$\left(i\frac{\partial}{\partial t} - H\right)S(x, x') = \gamma^0\delta(x - x'). \quad (\text{A.7})$$

The time independent Green's function is obtained as the Fourier transform, with respect to time, of the time dependent Green's function defined above.

$$S(x, x') = \int_{-\infty}^{\infty} \frac{d\omega}{2\pi} S(\mathbf{r}, \mathbf{r}', \omega) e^{-i\omega t} \quad (\text{A.8})$$

$$S(\mathbf{r}, \mathbf{r}', \omega) = \int_{-\infty}^{\infty} dt S(x, x') e^{i\omega t}, \quad (\text{A.9})$$

where $t = x_0 - x'_0$. Inserting this in the previous equation gives

$$(\omega - H)S(\mathbf{r}, \mathbf{r}', \omega) = \gamma^0\delta(\mathbf{r} - \mathbf{r}'). \quad (\text{A.10})$$

Denote the eigenfunctions of H by $\Psi_n(\mathbf{r})$ and the corresponding eigenvalues E_n , here assumed to be discrete. (The generalization to a continuous spectrum is straightforward). Then the eigenvalue equation is

$$H\Psi_n(\mathbf{r}) = E_n\Psi_n(\mathbf{r}). \quad (\text{A.11})$$

The eigenfunctions are assumed to constitute a complete set:

$$\sum_n \Psi_n(\mathbf{r})\Psi_n^\dagger(\mathbf{r}') = \delta(\mathbf{r} - \mathbf{r}'). \quad (\text{A.12})$$

Without loss of generality we can assume them to be orthonormal as well, thus satisfying

$$\int_\Omega d^3\mathbf{r} \Psi_n^\dagger(\mathbf{r})\Psi_m(\mathbf{r}) = \delta_{n,m}. \quad (\text{A.13})$$

The orthonormality relation can also be written as

$$\int_{\Omega} d^3\mathbf{r} \operatorname{Tr} (\Psi_n(\mathbf{r})\Psi_m^\dagger(\mathbf{r})) = \delta_{n,m}. \quad (\text{A.14})$$

Using the eigenvalue equation (A.11) and the completeness relation (A.12) in the equation (A.10) for the time independent Green's function gives

$$S(\mathbf{r}, \mathbf{r}', \omega) = \sum_n \frac{\Psi_n(\mathbf{r})\Psi_n^\dagger(\mathbf{r}')}{\omega - E_n} \gamma^0. \quad (\text{A.15})$$

Since H is Hermitian, the eigenvalues are real, and $S(\mathbf{r}, \mathbf{r}', \omega)$ is observed to have its poles distributed along the real ω -axis. Taking the trace and integrating over Ω with $\mathbf{r}' = \mathbf{r}$ (using Eq. (A.14)) yields

$$\int_{\Omega} d^3\mathbf{r} \operatorname{Tr} (S(\mathbf{r}, \mathbf{r}, \omega)\gamma^0) = \sum_n \frac{1}{\omega - E_n}. \quad (\text{A.16})$$

Now the identity

$$\lim_{\varepsilon \rightarrow 0_+} \frac{1}{x \pm i\varepsilon} = \mathcal{P} \frac{1}{x} \mp i\pi\delta(x)$$

is applied, giving the result

$$\int_{\Omega} d^3\mathbf{r} \operatorname{Tr} (S(\mathbf{r}, \mathbf{r}, \omega \pm i\varepsilon)\gamma^0) = \sum_n \left(\mathcal{P} \frac{1}{\omega - E_n} \mp i\pi\delta(\omega - E_n) \right). \quad (\text{A.17})$$

\mathcal{P} denotes the Cauchy principal value. Here and in the following the limit $\varepsilon \rightarrow 0_+$ is implicitly assumed. The density of states $\rho(\omega) = \sum_n \delta(\omega - E_n)$ is thus given by

$$\rho(\omega) = \mp \frac{1}{\pi} \operatorname{Im} \int_{\Omega} d^3\mathbf{r} \operatorname{Tr} [S(\mathbf{r}, \mathbf{r}, \omega \pm i\varepsilon)\gamma^0]. \quad (\text{A.18})$$

Since the integration is actually a trace operation performed on the spatial "indices" of S we can compactify the notation a little, by introducing the trace operation

$$\operatorname{tr} \mathbf{A} = \int d^3\mathbf{r} \operatorname{Tr} \mathbf{A}(\mathbf{r}, \mathbf{r}) = \int d^3\mathbf{r} \sum_{\mu} A_{\mu\mu}(\mathbf{r}, \mathbf{r}). \quad (\text{A.19})$$

The final result is then

$$\rho(\omega) = \mp \frac{1}{\pi} \operatorname{Im} \operatorname{tr} S(\omega \pm i\varepsilon)\gamma^0. \quad (\text{A.20})$$

A.2 Density of States for a Free Field

The simplest possible case that we can apply the method of the previous section to is that of a free field. The density of states could be obtained from simple arguments (waves in a box) in this case, but it is instructive and reassuring that the more formal approach yields the same result. In the case of a free field the Green's function can be obtained directly from the field equation, since there is no boundary condition. The basic definition of the Green's function is

$$(i\gamma^\mu \partial_\mu - m) S^{(0)}(x - x') = \delta(x - x'). \quad (\text{A.21})$$

Introducing the Fourier transform as

$$\begin{aligned} S^{(0)}(x) &= \int \frac{d^4 p}{(2\pi)^4} S^{(0)}(p) e^{-ip \cdot x} \\ S^{(0)}(p) &= \int d^4 x S^{(0)}(x) e^{ip \cdot x}, \end{aligned} \quad (\text{A.22})$$

we get the field equation in momentum space

$$(\gamma^\mu p_\mu - m) S^{(0)}(p) = 1 \quad (\text{A.23})$$

Thus $S^{(0)}(p)$ is the inverse matrix of the ‘‘Dirac operator’’ in momentum space. From the algebra satisfied by the gamma matrices it is easily shown that

$$(\not{p} - m)(\not{p} + m) = p^2 - m^2,$$

which gives the following form of the free space propagator

$$S^{(0)}(p) = \frac{\not{p} + m}{p^2 - m^2}. \quad (\text{A.24})$$

The Green's function in configuration space is thus

$$S^{(0)}(x - x') = \int \frac{d^4 p}{(2\pi)^4} e^{-ip \cdot (x - x')} \frac{\not{p} + m}{p^2 - m^2}. \quad (\text{A.25})$$

It is useful to compare this to the Green's function for a free scalar field. The field equation, in this case, is the Klein–Gordon equation and the Green's function, $\Delta^{(0)}(x - x')$, is defined by

$$(\square + m^2) \Delta^{(0)}(x - x') = -\delta(x - x'). \quad (\text{A.26})$$

Note the minus sign on the right hand side, which has been introduced for convenience. In analogy to the spinor case we take the Fourier transform, to obtain the momentum space representation

$$\begin{aligned} \Delta^{(0)}(k) &= \frac{1}{k^2 - m^2} \\ \Delta^{(0)}(x) &= \int \frac{d^4 k}{(2\pi)^4} e^{-k \cdot x} \frac{1}{k^2 - m^2}. \end{aligned} \quad (\text{A.27})$$

Comparing this with the spinor result, we see that the two Green's functions are connected as

$$\begin{aligned} S^{(0)}(p) &= (\not{p} + m)\Delta^{(0)}(p) \\ S^{(0)}(x - x') &= (i\not{\partial} + m)\Delta^{(0)}(x - x'). \end{aligned} \quad (\text{A.28})$$

This is a convenient way of obtaining the propagator for the free Dirac field. In order to find the density of states we need to know the time independent Green's function. This was previously defined as the Fourier transform with respect to time of the time dependent Green's function. In the scalar case this gives

$$\begin{aligned} \Delta^{(0)}(\mathbf{r} - \mathbf{r}', \omega) &= \int_{-\infty}^{\infty} dt \Delta^{(0)}(x - x') e^{i\omega t} \\ &= \int_{-\infty}^{\infty} dt \int \frac{d^4 k}{(2\pi)^4} e^{i\mathbf{k}\cdot(\mathbf{r}-\mathbf{r}')} e^{it(\omega-k_0)} \frac{1}{k^2 - m^2} \\ &= \int \frac{d^3 \mathbf{k}}{(2\pi)^3} e^{i\mathbf{k}\cdot(\mathbf{r}-\mathbf{r}')} \frac{1}{\omega^2 - \mathbf{k}^2 - m^2} \end{aligned} \quad (\text{A.29})$$

Since the integrand has poles for $\mathbf{k}^2 = \omega^2 - m^2$, which lie on the path of integration for real ω , the integral is not well defined. It is however uniquely specified by the imaginary part added to the energy in the trace formula for the density of states. Using the upper sign in Eq. (A.20) the pole is pushed into the upper k -plane, and the integral can be evaluated by closing the contour of integration along an infinite semi circle. The result is

$$\Delta^{(0)}(\mathbf{r} - \mathbf{r}', \omega + i\varepsilon) = \frac{e^{ik|\mathbf{r}-\mathbf{r}'|}}{4\pi|\mathbf{r} - \mathbf{r}'|}, \quad (\text{A.30})$$

where $k = \sqrt{\omega^2 - m^2 + i\varepsilon}$, is the square root with positive imaginary part. The above result immediately gives the corresponding result in the spinor case

$$\begin{aligned} S^{(0)}(\mathbf{r} - \mathbf{r}', \omega + i\varepsilon) &= (\gamma^0 \omega + i\boldsymbol{\gamma} \cdot \nabla + m) \Delta^{(0)}(\mathbf{r} - \mathbf{r}', \omega + i\varepsilon) \\ &= \left(\gamma^0 \omega - i\boldsymbol{\gamma} \cdot (\mathbf{r} - \mathbf{r}') \frac{ik|\mathbf{r} - \mathbf{r}'| - 1}{|\mathbf{r} - \mathbf{r}'|^2} + m \right) \Delta^{(0)}(\mathbf{r} - \mathbf{r}', \omega + i\varepsilon) \end{aligned} \quad (\text{A.31})$$

Multiplying by γ^0 and taking the trace—using $\text{Tr} \gamma^\mu \gamma^\nu = 4\eta^{\mu\nu}$, where $\eta^{\mu\nu} = \text{diag}(1, -1, -1, -1)$ is the Minkowski metric—gives the result

$$\text{Tr} S^{(0)}(\mathbf{r} - \mathbf{r}', \omega + i\varepsilon) \gamma^0 = 4\omega \Delta^{(0)}(\mathbf{r} - \mathbf{r}', \omega + i\varepsilon) \quad (\text{A.32})$$

The density of states is then

$$\rho(\omega) = \frac{1}{\pi} \int_{\Omega} d^3 \mathbf{r} \lim_{\mathbf{r}' \rightarrow \mathbf{r}} \text{Im} \text{Tr} S^{(0)}(\mathbf{r} - \mathbf{r}', \omega + i\varepsilon) \gamma^0$$

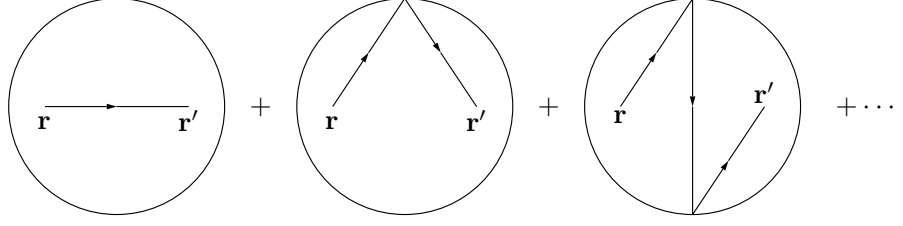


Figure A.1: The first three terms in the multiple reflection expansion for the propagator.

$$\begin{aligned}
&= \frac{1}{\pi} \int_{\Omega} d^3\mathbf{r} \lim_{\mathbf{r}' \rightarrow \mathbf{r}} 4\omega \frac{e^{-\text{Im } k|\mathbf{r}-\mathbf{r}'|} \sin \text{Re } k|\mathbf{r}-\mathbf{r}'|}{4\pi|\mathbf{r}-\mathbf{r}'|} \\
&= \int_{\Omega} d^3\mathbf{r} \frac{4\omega \text{Re } k}{4\pi^2} = V \frac{4\omega\sqrt{\omega^2 - m^2}}{4\pi^2}. \tag{A.33}
\end{aligned}$$

To obtain the density of states in terms of the momentum of the fermion the substitution $\omega \rightarrow k$ is performed

$$\rho(\omega)d\omega = \rho(\omega(k)) \frac{k}{\omega} dk = 2 \frac{Vk^2}{2\pi^2} dk. \tag{A.34}$$

This expression is the desired result. The factor two taken out in front represents the degeneracy of spin states for a non-interacting field.

A.3 Expansion of the Green's function

The basic idea of the multiple reflection expansion, is that the propagation of a particle in Ω can occur either directly (as described by the free space propagator), or via one or more reflections at the surface. Schematically the propagator can be written as in Fig. A.1, where each line represents a free space propagator. The multiple reflection expansion for the time independent Green's function has the following form

$$\begin{aligned}
S(\mathbf{r}, \mathbf{r}') &= S^{(0)}(\mathbf{r}, \mathbf{r}') + \oint_{\partial\Omega} d\sigma_{\alpha} S^{(0)}(\mathbf{r}, \boldsymbol{\alpha}) K(\boldsymbol{\alpha}) S^{(0)}(\boldsymbol{\alpha}, \mathbf{r}') \\
&+ \oint_{\partial\Omega} d\sigma_{\alpha} d\sigma_{\beta} S^{(0)}(\mathbf{r}, \boldsymbol{\alpha}) K(\boldsymbol{\alpha}) S^{(0)}(\boldsymbol{\alpha}, \boldsymbol{\beta}) K(\boldsymbol{\beta}) S^{(0)}(\boldsymbol{\beta}, \mathbf{r}') \\
&+ \dots \tag{A.35}
\end{aligned}$$

Here K is a reflection kernel describing the “interaction” with the surface due to the confining boundary conditions. In the following I will denote spatial vectors in Ω by bold face Roman symbols (e.g. \mathbf{r}, \mathbf{r}'), and spatial vectors on

$\partial\Omega$ by boldface Greek letters ($\boldsymbol{\alpha}, \boldsymbol{\beta}, \boldsymbol{\gamma}, \dots$). The multiple reflection expansion was first studied by Balian and Bloch [33, 35]. They considered a scalar field with different boundary conditions, and later also a vector field in a cavity with conducting walls. The multiple reflection expansion for scalar, spinor and vector fields with the boundary conditions of the MIT bag was treated by Hansson and Jaffe [24, 110] and later also Jaffe and Vintro [111]. The following derivation of the multiple reflection expansion follows [24, 110], but the results are generalized to a massive spinor field. For a static bag, the differential equation and boundary condition satisfied by the time independent Green's function are

$$\begin{aligned} (\gamma^0\omega + i\boldsymbol{\gamma} \cdot \nabla - m) S(\mathbf{r}, \mathbf{r}', \omega) &= \delta(\mathbf{r} - \mathbf{r}') & \mathbf{r}, \mathbf{r}' &\in \Omega \\ (i\boldsymbol{\gamma} \cdot \mathbf{n}_\alpha + 1) S(\boldsymbol{\alpha}, \mathbf{r}, \omega) &= 0 & \boldsymbol{\alpha} &\in \partial\Omega \end{aligned} \quad (\text{A.36})$$

The problem of solving the above equations, can be transformed into an integral equation for $S(\mathbf{r}, \mathbf{r}', \omega)$. This is a well known technique in potential theory. For the classical Dirichlet and Neumann Problems the integral equations can be derived directly from the differential equation and boundary condition, using Green's theorem (Gauss' law in 3 dimensions) for converting a volume integral into a surface integral [112]. Because of the more complicated nature of the problem at hand a direct derivation is not so simple. Therefore the solution will be arrived at by an analogy with electrostatics. The Green's function is split up into a free space part, and a boundary term

$$S(\mathbf{r}, \mathbf{r}') = S^{(0)}(\mathbf{r}, \mathbf{r}') + \tilde{S}(\mathbf{r}, \mathbf{r}'). \quad (\text{A.37})$$

I have chosen to suppress the ω -variable in the above expression, and will continue to do so in the following. The idea is now to write the surface term as a kind of potential arising from a surface distribution at the boundary

$$\tilde{S}(\mathbf{r}, \mathbf{r}') = \oint_{\partial\Omega} d\sigma_\alpha S^{(0)}(\mathbf{r}, \boldsymbol{\alpha}) \eta(\boldsymbol{\alpha}, \mathbf{r}'). \quad (\text{A.38})$$

In electrostatics the potential arising from a surface distribution, ς , of charges (a so called simple layer) is given by [113]

$$\varphi(\mathbf{r}) = \int_{\partial\Omega} \frac{\varsigma(\boldsymbol{\alpha})}{4\pi|\mathbf{r} - \boldsymbol{\alpha}|} d\sigma_\alpha. \quad (\text{A.39})$$

This potential has the well known property that it is continuous across $\partial\Omega$, whereas the electric field has a discontinuous normal component, the discontinuity being proportional to the surface charge density

$$-\mathbf{n} \cdot \nabla\varphi|_{(+)} + \mathbf{n} \cdot \nabla\varphi|_{(-)} = \varsigma, \quad (\text{A.40})$$

where \mathbf{n} is the normal to $\partial\Omega$, and the indices $+$ and $-$ denote the limiting values when approaching the surface from the inside and outside respectively. (In this case $\partial\Omega$ need not be the boundary of a finite region of space, so the "outside"

is defined as the side to which the normal points). This result can be obtained from Eq. (A.39), or by a direct application of Gauss' law. The potential due to a surface distribution of dipoles (a dipole layer) has the form [113]

$$\varphi(\mathbf{r}) = \int_{\partial\Omega} D(\boldsymbol{\alpha}) \mathbf{n}_\alpha \cdot \nabla_\alpha \frac{1}{4\pi|\mathbf{r} - \boldsymbol{\alpha}|} d\sigma_\alpha, \quad (\text{A.41})$$

where $D(\boldsymbol{\alpha})$ is the dipole density. Unlike a simple layer, a dipole layer causes a discontinuity in the potential itself

$$\varphi_{(-)}(\boldsymbol{\alpha}) - \varphi_{(+)}(\boldsymbol{\alpha}) = D(\boldsymbol{\alpha}). \quad (\text{A.42})$$

Here $\varphi_{(+)}(\boldsymbol{\alpha})$ is the limiting value of the potential when approaching the surface from the inside, and $\varphi_{(-)}(\boldsymbol{\alpha})$ from the outside. Substituting the Green's function for the Laplace equation with the scalar Green's function gives quite analogous results. Thus the potential generated by a simple layer is continuous in the scalar case, while its normal derivative is discontinuous at the surface. The gradient in the connection A.28 between the spinor and scalar Green's functions generates a dipole layer, causing the potential of a "simple" spinor layer to be discontinuous. In addition to not being simple in the sense that it produces a discontinuity it may also have a matrix structure, complicating things further. The discontinuity is found by a detailed analysis to be

$$\tilde{S}_{(+)}(\boldsymbol{\beta}, \mathbf{r}') - \tilde{S}(\boldsymbol{\beta}, \mathbf{r}') = -\frac{i}{2} \boldsymbol{\gamma} \cdot \mathbf{n}_\beta \eta(\boldsymbol{\beta}, \mathbf{r}'). \quad (\text{A.43})$$

The factor 1/2 comes from the fact that the discontinuity is from the inside to a point *on* the boundary. If the boundary had been crossed it would produce double the above amount. However, since we wish to describe quarks confined to a bag, crossing the boundary is not allowed. The "source", η , is to be determined by the boundary condition to be satisfied by $S(\boldsymbol{\alpha}, \mathbf{r})$. As the free space part of the Green's function is obviously continuous across $\partial\Omega$ the total Green's function has the same discontinuity as the boundary term

$$S_{(+)}(\boldsymbol{\alpha}, \mathbf{r}) = S(\boldsymbol{\alpha}, \mathbf{r}) - \frac{i}{2} \boldsymbol{\gamma} \cdot \mathbf{n}_\alpha \eta(\boldsymbol{\alpha}, \mathbf{r}). \quad (\text{A.44})$$

Since $S(\mathbf{r}, \mathbf{r}')$ is continuous within Ω it is the limit of $S(\mathbf{r}, \mathbf{r}')$ as $\mathbf{r} \rightarrow \boldsymbol{\alpha}$ from the inside that is required to fulfill the boundary condition.

$$\begin{aligned} (i\boldsymbol{\gamma} \cdot \mathbf{n}_\alpha + 1) S_{(+)}(\boldsymbol{\alpha}, \mathbf{r}) &= 0 \\ \Downarrow \\ 0 &= (i\boldsymbol{\gamma} \cdot \mathbf{n}_\alpha + 1) S(\boldsymbol{\alpha}, \mathbf{r}) - (i\boldsymbol{\gamma} \cdot \mathbf{n}_\alpha + 1) \frac{i}{2} \boldsymbol{\gamma} \cdot \mathbf{n}_\alpha \eta(\boldsymbol{\alpha}, \mathbf{r}) \\ &= (1 + i\boldsymbol{\gamma} \cdot \mathbf{n}_\alpha) S(\boldsymbol{\alpha}, \mathbf{r}) - \frac{1}{2} (1 + i\boldsymbol{\gamma} \cdot \mathbf{n}_\alpha) \eta(\boldsymbol{\alpha}, \mathbf{r}). \end{aligned} \quad (\text{A.45})$$

The factor multiplying η is the projection operator,

$$P_\alpha = \frac{1}{2} (1 + i\boldsymbol{\gamma} \cdot \mathbf{n}_\alpha), \quad (\text{A.46})$$

which satisfies $P_\alpha^2 = P_\alpha$. With this notation the equation for η is

$$\begin{aligned} P_\alpha \eta(\boldsymbol{\alpha}, \mathbf{r}) &= 2P_\alpha S(\boldsymbol{\alpha}, \mathbf{r}) \\ &= 2P_\alpha S^{(0)}(\boldsymbol{\alpha}, \mathbf{r}) + 2 \oint_{\partial\Omega} d\sigma_\beta P_\alpha S^{(0)}(\boldsymbol{\alpha}, \boldsymbol{\beta}) \eta(\boldsymbol{\beta}, \mathbf{r}). \end{aligned} \quad (\text{A.47})$$

This is an integral equation for η , involving only the known free space Green's function $S^{(0)}$. Technically an equation of this form is known as a Fredholm equation of the second kind. Hansson and Jaffe show that the form

$$\eta(\boldsymbol{\alpha}, \mathbf{r}) = P_\alpha \mu(\boldsymbol{\alpha}, \mathbf{r}), \quad (\text{A.48})$$

is a possible solution, and then proceed to iterate the equation for η , giving

$$\begin{aligned} \eta(\boldsymbol{\alpha}, \mathbf{r}) &= 2P_\alpha S^{(0)}(\boldsymbol{\alpha}, \mathbf{r}) + 2^2 \oint_{\partial\Omega} d\sigma_\beta P_\alpha S^{(0)}(\boldsymbol{\alpha}, \boldsymbol{\beta}) \\ &+ 2^3 \oint_{\partial\Omega} d\sigma_\beta d\sigma_\gamma P_\alpha S^{(0)}(\boldsymbol{\alpha}, \boldsymbol{\beta}) P_\beta S^{(0)}(\boldsymbol{\beta}, \boldsymbol{\gamma}) P_\gamma S^{(0)}(\boldsymbol{\gamma}, \mathbf{r}) \\ &+ \dots \end{aligned} \quad (\text{A.49})$$

Inserting this in Eq. (A.38) gives the multiple reflection expansion for the Green's function as

$$\begin{aligned} S(\mathbf{r}, \mathbf{r}') &= S^{(0)}(\mathbf{r}, \mathbf{r}') + 2 \oint_{\partial\Omega} d\sigma_\alpha S^{(0)}(\mathbf{r}, \boldsymbol{\alpha}) P_\alpha S^{(0)}(\boldsymbol{\alpha}, \mathbf{r}') \\ &+ 2^2 \oint_{\partial\Omega} d\sigma_\alpha d\sigma_\beta S^{(0)}(\mathbf{r}, \boldsymbol{\alpha}) P_\alpha S^{(0)}(\boldsymbol{\alpha}, \boldsymbol{\beta}) P_\beta S^{(0)}(\boldsymbol{\beta}, \mathbf{r}') \\ &+ \dots, \end{aligned} \quad (\text{A.50})$$

which is the result advertised in the beginning of this section. It is not clear, however, that this expansion is suited for the purpose of doing a perturbation calculation. Such an approach demands that the successive terms become rapidly smaller. This is only the case if the integral kernel $P_\alpha S^{(0)}(\boldsymbol{\alpha}, \boldsymbol{\beta})$ is sufficiently small. The multiple reflection expansion is not unique, for example Hansson and Jaffe show that it may equally well be written

$$\begin{aligned} S(\mathbf{r}, \mathbf{r}') &= S^{(0)}(\mathbf{r}, \mathbf{r}') + 2 \oint_{\partial\Omega} d\sigma_\alpha S^{(0)}(\mathbf{r}, \boldsymbol{\alpha}) S^{(0)}(\boldsymbol{\alpha}, \mathbf{r}') \\ &+ 2^2 \oint_{\partial\Omega} d\sigma_\alpha d\sigma_\beta S^{(0)}(\mathbf{r}, \boldsymbol{\alpha}) S^{(0)}(\boldsymbol{\alpha}, \boldsymbol{\beta}) S^{(0)}(\boldsymbol{\beta}, \mathbf{r}') \\ &+ \dots \end{aligned} \quad (\text{A.51})$$

The two expansions do not correspond term by term, which means that the notion of the n th reflection is not well defined. This should not concern us too much, since we are looking for a geometrical expansion of the density of states. Each term in this expansion may receive contributions from several reflection terms yielding a result independent of the particular form of the expansion used. The expansion should thus be chosen in such a way as to make the calculations as easy as possible.

A.4 Expansion of the Density of States

Using the trace formula, (A.20), and the general form of the multiple reflection expansion for the Green's function, (A.35), yields the following expansion for the density of states

$$\begin{aligned}
 \rho(\omega) &= \mp \frac{1}{\pi} \text{Im tr } S^{(0)}(\omega \pm i\varepsilon) \gamma^0 \\
 &\mp \frac{1}{\pi} \int_{\Omega} d^3 \mathbf{r} \oint_{\partial\Omega} d\sigma_{\alpha} \lim_{\mathbf{r}' \rightarrow \mathbf{r}} \text{Im } S^{(0)}(\mathbf{r}, \boldsymbol{\alpha}, \omega \pm i\varepsilon) K(\boldsymbol{\alpha}) S^{(0)}(\boldsymbol{\alpha}, \mathbf{r}', \omega \pm i\varepsilon) \gamma^0 \\
 &+ \dots
 \end{aligned} \tag{A.52}$$

The first term was shown in section A.2 to give the volume contribution to the density of states. In order to obtain the geometrical expansion Eq. (2.20), terms proportional to the surface area $\oint_{\partial\Omega} d\sigma$ and the extrinsic curvature $\oint_{\partial\Omega} d\sigma (1/R_1 + 1/R_2)$ must be extracted from the above expansion. For a specific choice of the reflection kernel, $K(\boldsymbol{\alpha})$, this involves the following steps. The integrals over $\partial\Omega$ are evaluated in a series of approximations, where the lowest corresponds to approximating $\partial\Omega$ with a plane surface (its tangent plane), in the next a second order surface, and so on, at each point $\boldsymbol{\alpha}, \boldsymbol{\beta}, \dots$. This gives corrections of increasing order in the principal radii of curvature. Within each approximation the terms of Eq. (A.52) contributing to a given order $\oint_{\partial\Omega} (1/R_1 + 1/R_2)^n d\sigma$, $n = 0, 1, \dots$ should be identified and summed. Finally the integral expressions must be evaluated, i.e. the Im and tr operations must be performed. This gives an expansion of the form Eq. (2.20).

Appendix B

Fermi-Dirac and Bose-Einstein Integrals

In this appendix I give some results for a special class of the Fermi-Dirac and Bose-Einstein integrals (massless particles), that are used throughout this thesis. The work by Elze [114] for the case of complex chemical potential needed in Chapter 5, is reproduced in some detail, since it has not been published.

B.1 Fermions

I have performed calculations of the Fermi integrals

$$I_n^+(\eta) \equiv \int_0^\infty dx \frac{x^n}{e^{x-\eta} + 1}, \quad (\text{B.1})$$

for both positive and negative values of η and the results agree with those of Dingle [40] and Elze [114]. My own calculation is rather lengthy, and if only the combination

$$S_n^+(\eta) \equiv I_n^+(\eta) + (-1)^{n+1} I_n^+(-\eta), \quad (\text{B.2})$$

is needed (as is indeed the case here) the elegant derivation due to Elze [114] is much to be preferred. The form of the result is slightly different, and my own result as well as that of Dingle [40] is

$$S_n^+(\eta) = 2 \sum_{k=0}^{\lfloor \frac{n+1}{2} \rfloor} \frac{n! \zeta(2k)}{(n+1-2k)!} (1 - 2^{1-2k}) \eta^{n+1-2k}, \quad (\text{B.3})$$

where $\zeta(x)$ is the Riemann zeta function [28], and $\lfloor x \rfloor$ is the floor of x , *i.e.*, the largest integer smaller than or equal to x . The first few polynomials are

$$S_0^+(\eta) = \eta \quad (\text{B.4})$$

$$S_1^+(\eta) = \frac{\pi^2}{6} + \frac{1}{2}\eta^2 \quad (\text{B.5})$$

$$S_2^+(\eta) = \frac{\pi^2}{3}\eta + \frac{1}{3}\eta^3 \quad (\text{B.6})$$

$$S_3^+(\eta) = \frac{7\pi^4}{60} + \frac{\pi^2}{2}\eta^2 + \frac{1}{4}\eta^4 \quad (\text{B.7})$$

B.2 Bosons

For the Bose integral

$$I_n^-(\eta) \equiv \int_0^\infty dx \frac{x^n}{e^{x-\eta} - 1}, \quad (\text{B.8})$$

the results of Dingle [115] can be used to evaluate the combination

$$S_n^-(\eta) \equiv I_n^-(\eta) + (-1)^{n+1} I_n^-(-\eta), \quad (\text{B.9})$$

which gives

$$S_n^-(\eta) = 2 \sum_{k=0}^{\lfloor \frac{n+1}{2} \rfloor} \frac{n! \zeta(2k)}{(n+1-2k)!} \eta^{n+1-2k}. \quad (\text{B.10})$$

The first few polynomials are

$$S_0^-(\eta) = -\eta \quad (\text{B.11})$$

$$S_1^-(\eta) = \frac{\pi^2}{3} - \frac{1}{2}\eta^2 \quad (\text{B.12})$$

$$S_2^-(\eta) = \frac{2\pi^2}{3}\eta - \frac{1}{3}\eta^3 \quad (\text{B.13})$$

$$S_3^-(\eta) = \frac{2\pi^4}{15} + \pi^2\eta^2 - \frac{1}{4}\eta^4 \quad (\text{B.14})$$

The Fermi and Bose results can be combined to the expression

$$S_n^\pm(\eta) = 2 \sum_{k=0}^{\lfloor \frac{n+1}{2} \rfloor} \frac{n! \zeta(2k)}{(n+1-2k)!} [1 - (1 \pm 1)2^{-2k}] \eta^{n+1-2k} \quad (\text{B.15})$$

B.3 Complex Chemical Potential

In this section I will reproduce a derivation of the integrals

$$S_n^\pm(z) \equiv \int_0^\infty dx x^n \left(\frac{1}{e^{x-z} \pm 1} + (-1)^{n+1} \frac{1}{e^{x+z} \pm 1} \right), \quad n = 0, 1, 2, \dots \quad (\text{B.16})$$

with complex z , which is due to Elze [114].

The integrals are periodic in z along the imaginary axis

$$S_n^\pm(z + 2m\pi i) = S_n^\pm(z), \quad m \in \mathbb{Z}, \quad (\text{B.17})$$

with period 2π . The Fermi and Bose cases are connected through

$$S_n^-(z) = S_n^+(z + (2m+1)\pi i), \quad m \in \mathbb{Z}. \quad (\text{B.18})$$

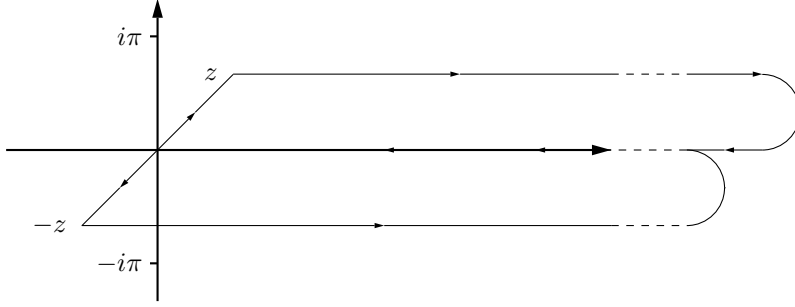


Figure B.1: The contours used to evaluate the integrals in Eq. (B.20).

Thus the result for bosons can be obtained from that for fermions, so from now on consider just the integral $S_n^+(z)$, with z lying in the strip

$$-\pi < \text{Im } z < \pi. \quad (\text{B.19})$$

If z is in another strip the result can be found by using the periodicity. Note that the poles of the integrand are distributed along the two axes $\text{Re } x = \pm \text{Re } z$, with period 2π .

The substitution $y = x \pm z$ is performed shifting the integration into the complex plane,

$$S_n^+(z) = \int_{-z}^{\infty-z} dy \frac{(y+z)^n}{e^y+1} + (-1)^{n+1} \int_z^{\infty+z} dy \frac{(y-z)^n}{e^y+1}, \quad (\text{B.20})$$

and shifting the poles onto the imaginary axis.

The integration contours are closed as shown in Fig. B.1, and an application of Cauchy's theorem on the resulting integrals, after doing a binomial expansion of the factors $(y \pm z)^n$, gives

$$S_n^+(z) = \frac{z^{n+1}}{n+1} + \sum_{k=0}^n \binom{n}{k} z^k [1 + (-1)^{n+k+1}] (1 - 2^{-n+k}) \Gamma(n-k+1) \zeta(n-k+1), \quad (\text{B.21})$$

where the integral representation [28]

$$\zeta(t) = \frac{1}{(1-2^{1-t})\Gamma(t)} \int_0^\infty dx \frac{x^{t-1}}{e^x+1}, \quad (\text{B.22})$$

of the Riemann zeta function has been used. $\Gamma(z)$ is the gamma function [28].

Elze expresses this result in terms of Bernoulli polynomials, but note that the first term can be included in the sum as the $(n+1)$ th term, since $\zeta(0) = 1/2$.

Using the identity $\Gamma(n+1) = n!$ the result of Elze can be rewritten

$$S_n^+(z) = \sum_{k=0}^{n+1} \frac{n!}{k!} z^k [1 + (-1)^{n+1+k}] (1 - 2^{k-n}) \zeta(n-k+1). \quad (\text{B.23})$$

It may not be obvious that this result is identical to Eq. (B.3), but an evaluation of the low order polynomials using the above expression, gives results identical to Eqs. (B.4)–(B.7), for real z .

The Bose integral $S_n^-(z)$, as evaluated here, is defined in the strip $0 < \text{Im } z < 2\pi$, and therefore, as pointed out by Elze [114, 116], the expression cannot be extended to the real axis. The reason for this is that for $\text{Im } z = 0$ there is a pole on the contour of integration, resulting in an ill-defined integral.

In the strip $0 < \text{Im } z < 2\pi$ the polynomials of lowest order are

$$S_0^-(z) = i\pi - z, \quad (\text{B.24})$$

$$S_1^-(z) = \frac{\pi^2}{3} + i\pi z - \frac{1}{2}z^2, \quad (\text{B.25})$$

$$S_2^-(z) = \frac{2\pi^2}{3}z + i\pi z^2 - \frac{1}{3}z^3, \quad (\text{B.26})$$

$$S_3^-(z) = \frac{2\pi^4}{15} + \pi^2 z^2 + i\pi z^3 - \frac{1}{4}z^4. \quad (\text{B.27})$$

Comparing this to Eqs. (B.11)–(B.14) shows that there are extra terms relative to the result of Dingle [115] valid on the real axis.

As mentioned above, Elze relates $S_n^\pm(z)$ to Bernoulli polynomials $B_n(x)$ [28]. His result is

$$\begin{aligned} S_n^+(z) &= \frac{(2\pi i)^{n+1}}{n+1} B_{n+1}\left(\frac{\pi - iz}{2\pi}\right) & \text{Im } z \in (-\pi, \pi) \\ S_n^-(z) &= -\frac{(2\pi i)^{n+1}}{n+1} B_{n+1}\left(\frac{-iz}{2\pi}\right) & \text{Im } z \in (0, 2\pi). \end{aligned} \quad (\text{B.28})$$

Appendix C

The SHELL Program

This appendix contains a short Fortran90 program that implements the shell model calculation of the energy for a spherical strangelet at zero temperature. In addition to the routines shown here, the program has to be linked against the routines `solver`, `minimizer`, and `sphbes`, used for root finding, function minimization, and the calculation of spherical Bessel functions respectively. Such routines are part of any good repository of numerical techniques (see *e.g.* Ref. [117]).

C.1 The Main Loop

The main routine of the program is merely a loop over baryon number `A`. For every `A`, the minimum energy is found and the result is written to standard output.

```
Program shell
  implicit none
  integer, parameter :: STDOUT = 6
  integer, parameter :: MaxA=100
  integer A
  real E
  real, external :: MinimumEnergy

  Do A=1,MaxA
    E = MinimumEnergy(A)
    write(STDOUT,*) A, E/real(A)
  End Do
End ! Program shell
```

C.2 Minimizing the Energy

The function `MinimumEnergy` calculates the minimum energy of a strangelet with baryon number `A` by varying the radius. For a fixed radius `R` the function `Energy` calculates the energy for a strangelet of optimal composition. This is

done in the routine `Find_composition` by trying the various possible distributions of quarks among the available flavors.

C.2.1 MinimumEnergy

This routine finds the minimum energy as a function of radius `R` for a given baryon number `A`. The number of levels included in the calculation is determined by the chemical potentials. These are found from a liquid drop calculation in the function 'Energy'. We still need a maximum number of allowable levels `MaxLevels` to dimension the arrays in the other routines.

```
Real Function MinimumEnergy(A)
  implicit none
  integer, intent(in) :: A

  real Rmin, R_guess, R1, R2, R3
  real, parameter :: acc=1.E-3
  real, parameter :: MeVfm = 197.3      ! conversion factor
  real, external :: Energy, minimizer
  integer MaxLevels

  MaxLevels = 51 !must be odd!

!   Make a guess for initial bracketing triplet
  R_guess = real(A)**(1/3.) / MeVfm
  R1 = R_guess / 5.
  R2 = R_guess
  R3 = R_guess * 5.
  MinimumEnergy = minimizer(R1, R2, R3, Energy, acc, Rmin, &
                           A, MaxLevels)
End ! MinimumEnergy
```

C.2.2 Energy

This routine calculates the energy of a strangelet of optimal composition. It calls `Find_levels` to get the eigenvalue spectrum, which is then used by the routine `Find_composition` to deduce the distribution of quarks among flavors. The energy due to the bag constant is also added here.

In order to get an estimate of how many levels it is necessary to include in the calculation, the chemical potential is found from a liquid drop model calculation in the routine `Find_chempot`.

```
Real Function Energy(R, A, MaxLevels)
  implicit none
  real, intent(in) :: R
  integer, intent(in) :: A, MaxLevels

  real, parameter :: BBag = 145.**4
  real, parameter :: PI = 3.141592654
  integer, parameter :: Nflavor = 3
  real, dimension(Nflavor, MaxLevels) :: energies
  integer, dimension(Nflavor, MaxLevels) :: degen
```



```

integer, dimension(Nflavor)      :: NumLevels
real, dimension(1:3), parameter  :: mass = (/ 0.0, 0.0, 150.0 /)
real, dimension(1:3)            :: chemical
real E

call Find_chempot(R, A, mass, chemical, Nflavor);
call Find_levels(R, mass, chemical, energies, degen, &
  Nflavor, MaxLevels, NumLevels)
call Find_composition(A, E, energies, degen, Nflavor, &
  MaxLevels, NumLevels)

Energy = E + 4./3.*PI*R**3 * BBag
End ! Energy

```

C.2.3 Find_chempot

A liquid drop model calculation of the chemical potential μ , assuming only one flavor is done here, using the expressions in Chapter 2. The precision is given by `tol`. This is used in `Get_eigenvalues` to find all single particle energies less than the chemical potential.

```

Subroutine Find_chempot(R, A, mass, chemical, Nflavor)
  implicit none
  real,          intent(in)  :: R
  integer,       intent(in)  :: A, Nflavor
  real, dimension(1:3),      intent(in)  :: mass
  real, dimension(1:3),      intent(out) :: chemical

  real, external  :: solver, Number
  real, parameter :: tol = 1.E-3
  real            :: m, mu, mumin, mumax
  integer         :: i

  Do i = 1, Nflavor
    mumin = mass(i) ! Lower bound mu = m
    mumax = 1500.   ! Upper bound on mu_i (in MeV)
    m = mass(i)
    mu = solver(Number, mumin, mumax, tol, A, m, R)
    ! I add 30% to the found value, since this is only an estimate.
    chemical(i) = 1.3 * mu
  End Do
End ! Find_chempot

```

C.2.4 Number

The function `Number` is solved for the chemical potential μ that satisfies the condition that the total baryon number of the system is $A = \frac{1}{3}\text{Number}$, where `Number` is given in terms of volume, surface, and curvature number densities (Eq. (2.49), Eq. (2.50), and Eqs. (2.54)–(2.56)) obtained from the liquid drop model. If the quark mass is less than `eps` the expressions for massless quarks are used.

```

Real Function Number(mu, A, mass, R)
  implicit none
  real,          intent(in) :: mu, mass, R

```

```

integer,      intent(in) :: A

real, parameter      :: PI = 3.141592654, eps = 1.E-3
real               :: V, S, C, NV, NS, NC, x

V = 4./3.*PI*R**3
S = 4.*PI*R**2
C = 8.*PI*R
If (mass < eps) Then
  NV = mu**3/PI**2
  NS = 0.0
  NC = -4.*mu/PI**2
Else
  x = mu/mass
  NV = mass**3/PI**2 * (x**2-1)**(3./2.)
  NS = -3.*mass**2/4./PI * ( 0.5*(x**2-1)    &
    - 1/PI*( x**2*atan(sqrt(x**2-1))    &
    - sqrt(x**2-1) ) )
  NC = 3.*mass/8./PI**2 * (-0.5*PI*(x**2-1) &
    + 1/3.*sqrt(x**2-1)    &
    + x**2 * atan(sqrt(x**2-1)) )
End If
Number = NV*V + NS*S + NC*C - 3*A
End ! Number

```

C.3 The Optimal Composition

C.3.1 Find_composition

This routine finds the composition of a strangelet, *i.e.*, the distribution of quarks among the levels, that minimizes the total energy, subject to the constraint that the baryon number equals A . On return `levels` and `deg` have been sorted (by `Sort_levels`) in ascending order. This procedure is not as difficult as it looks. The idea is to try all possible combinations of flavors $n_1 + n_2 + n_3 = 3A$, and for each flavor fill the levels from the bottom up. Allowing for from 1 to 3 flavors makes this look more complicated than it really is.

```

Subroutine Find_composition(A, E, levels, deg, Nflavor, &
                          MaxLevels, NumLevels)

  implicit none
  integer,intent(in) :: A, Nflavor, MaxLevels
  real,               intent(out) :: E
  real, dimension(Nflavor, MaxLevels), intent(inout) :: levels
  integer,dimension(Nflavor, MaxLevels), intent(inout) :: deg
  integer,dimension(Nflavor),           intent(in)    :: NumLevels

  real, parameter :: HUGE = 1.E30
  integer n1, n2, n3, cur_lev, n_cur_lev, cur_flg, n_cur_flg
  real E_min, E1
  external Sort_levels

!   Sort the energy levels according to energy, in ascending
!   order, and rearrange the 'deg' array to reflect this.
  call Sort_levels(levels, deg, Nflavor, MaxLevels, NumLevels)

```

```

! Now find the optimal composition of the strangelet.
E_min = HUGE
If (Nflavor == 1) Then
  n1 = 3*A
  E = 0.0
  cur_lev = 1;  n_cur_lev = 0
  cur_fla = 1;  n_cur_fla = 0
q11: Do
  If (n_cur_fla == n1) Exit q11
  E = E + levels(cur_fla,cur_lev)
  n_cur_fla = n_cur_fla + 1
  n_cur_lev = n_cur_lev + 1
  If (n_cur_lev == deg(cur_fla,cur_lev)) Then
    cur_lev = cur_lev + 1
    n_cur_lev = 0
  End If
End Do q11
E_min = E
Else
  Do n1 = 0,3*A
  E = 0.0
  cur_lev = 1;  n_cur_lev = 0
  cur_fla = 1;  n_cur_fla = 0
q12: Do
  If (n_cur_fla == n1) Exit q12
  E = E + levels(cur_fla,cur_lev)
  n_cur_fla = n_cur_fla + 1
  n_cur_lev = n_cur_lev + 1
  If (n_cur_lev == deg(cur_fla,cur_lev)) Then
    cur_lev = cur_lev + 1
    n_cur_lev = 0
  End If
End Do q12
  If (Nflavor == 2) Then
    n2 = 3*A-n1
    cur_lev = 1;  n_cur_lev = 0
    cur_fla = 2;  n_cur_fla = 0
q21: Do
  If (n_cur_fla == n2) Exit q21
  E = E + levels(cur_fla,cur_lev)
  n_cur_fla = n_cur_fla + 1
  n_cur_lev = n_cur_lev + 1
  If (n_cur_lev == deg(cur_fla,cur_lev)) Then
    cur_lev = cur_lev + 1
    n_cur_lev = 0
  End If
End Do q21
  If (E < E_min)  E_min = E
Else
  E1 = E
  Do n2 = 0,3*A-n1
  E = E1
  cur_lev = 1;  n_cur_lev = 0
  cur_fla = 2;  n_cur_fla = 0
q22: Do

```

```

        If (n_cur_fla == n2) Exit q22
        E = E + levels(cur_fla,cur_lev)
        n_cur_fla = n_cur_fla + 1
        n_cur_lev = n_cur_lev + 1
        If (n_cur_lev == deg(cur_fla,cur_lev)) Then
            cur_lev = cur_lev + 1
            n_cur_lev = 0
        End If
    End Do q22
    n3 = 3*A-n1-n2
    cur_lev = 1; n_cur_lev = 0
    cur_fla = 3; n_cur_fla = 0
q3:    Do
        If (n_cur_fla == n3) Exit q3
        E = E + levels(cur_fla,cur_lev)
        n_cur_fla = n_cur_fla + 1
        n_cur_lev = n_cur_lev + 1
        If (n_cur_lev == deg(cur_fla,cur_lev)) Then
            cur_lev = cur_lev + 1
            n_cur_lev = 0
        End If
    End Do q3
    If (E < E_min) E_min = E
End Do ! n2
End If
End Do ! n1
End If
E = E_min
End ! Find_composition

```

C.3.2 Sort_levels

This subroutine performs a comb sort [118], on the array `levels`, sorting it in ascending order, and rearranges the array `deg` accordingly.

```

Subroutine Sort_levels(levels, deg, Nflavor, MaxLevels, &
                    NumLevels)
    implicit none
    integer,intent(in) :: Nflavor, MaxLevels
    real, dimension(Nflavor, MaxLevels), intent(inout) :: levels
    integer,dimension(Nflavor, MaxLevels), intent(inout) :: deg
    integer,dimension(Nflavor), intent(in) :: NumLevels

    real, parameter :: SHRINK = 1.3
    integer q, switches, i_hold, i, j, top, gap
    real r_hold

    Do q = 1, Nflavor
        gap = NumLevels(q)
loop: Do
        gap = int(real(gap)/SHRINK)
        Select Case (gap)
        Case (0)
            gap = 1
        Case (9:10)
            gap = 11

```

```

      Case Default
        gap = gap
      End Select
      switches = 0
      top = NumLevels(q) - gap
      Do i=1,top
        j = i + gap
        If (levels(q,i) > levels(q,j)) Then
          r_hold = levels(q,i)
          levels(q,i) = levels(q,j)
          levels(q,j) = r_hold
          i_hold = deg(q,i)
          deg(q,i) = deg(q,j)
          deg(q,j) = i_hold
          switches = switches + 1
        End If
      End Do
      If ( (switches == 0) .AND. (gap == 1) ) Exit loop
    End Do loop
  End Do
End ! Sort_levels

```

C.4 The Eigenvalues

C.4.1 Find_levels

This routine does the quantum number book-keeping, while leaving the actual calculation of single particle levels to the routine `Get_levels`.

```

Subroutine Find_levels(R, mass, chem, levels, degen, &
                    Nflavor, Maxlevels, NumLevels)
  implicit none
  real,          intent(in)  :: R
  real,    dimension(1:3), intent(in)  :: mass, chem
  integer, intent(in)        :: Nflavor, MaxLevels
  real,    dimension(Nflavor, MaxLevels), intent(out) :: levels
  integer, dimension(Nflavor, MaxLevels), intent(out) :: degen
  integer, dimension(Nflavor),          intent(out)  :: NumLevels

  integer, parameter :: STDERR = 0
  integer l, lmax, kappa, q, nu, numax
  real, dimension(MaxLevels) :: eps
  external Get_eigenvalue

!   lmax is the number of l-values that it takes to accomodate
!   the number of quarks of a single flavor that can fill
!   MaxLevels levels if only the nu=1 levels are used. This gives
!   an upper limit to l.

!   The maximum number of l values (MaxLevels is odd)
  lmax = (MaxLevels - 1)/2

  Do q = 1, Nflavor      ! Loop over quark flavors
!   Initialize NumLevels to zero
    NumLevels(q) = 0

```

```

!      First of all the ground state (l=0, j=1/2, kappa=-1) is
!      found. It has degeneracy 3*(2j+1) = 6
kappa = -1
!      Here we find all eps < mu_q
call Get_eigenvalues(eps, chem(q), mass(q), kappa, &
                    numax, R, MaxLevels)
If (numax == 0) Exit
Do nu=1,numax
  NumLevels(q) = NumLevels(q) + 1
  levels(q,NumLevels(q)) = eps(nu)
  degen(q,NumLevels(q)) = 6
End Do
! Now for the remaining levels
Do l = 1, lmax ! Loop over orbital angular momentum
  kappa = 1 ! First possible value of kappa (j=l-1/2)
  call Get_eigenvalues(eps, chem(q), mass(q), kappa, &
                    numax, R, MaxLevels)
  If (numax == 0) Exit
  Do nu=1,numax
    NumLevels(q) = NumLevels(q) + 1
    levels(q,NumLevels(q)) = eps(nu)
    degen(q,NumLevels(q)) = 6*l
  End Do
  kappa = -(l+1) !Second possible value of kappa (j=l+1/2)
  call Get_eigenvalues(eps, chem(q), mass(q), kappa, &
                    numax, R, MaxLevels)
  If (numax == 0) Exit
  Do nu=1,numax
    NumLevels(q) = NumLevels(q) + 1
    levels(q,NumLevels(q)) = eps(nu)
    degen(q,NumLevels(q)) = 6*(l+1)
  End Do
End Do
If (NumLevels(q) >= MaxLevels) Then
  Write(STDERR,*) 'MaxLevels exceeded in "Find_levels"'
  Exit
End If
End Do
End ! Find_levels

```

C.4.2 Get_eigenvalues

For a fixed value of `kappa` the routine `Get_eigenvalues` finds `numax` roots of the Dirac equation, with precision `eps`, so that the `numax` roots have energies less than the chemical potential `mu`. It returns the energies `eps` and `numax`.

```

Subroutine Get_eigenvalues(eps, mu, mass, kappa, numax, &
                          R, MaxLevels)
  implicit none
  integer,          intent (in) :: MaxLevels
  real, dimension(MaxLevels), intent(out) :: eps
  real,            intent (in) :: mu, mass
  integer,         intent (in) :: kappa
  integer,         intent(out) :: numax
  real,            intent (in) :: R

```

```

real, parameter :: acc = 1.E-3
real, parameter :: dx = 0.1
real x, xmin, xmax, fx, fxmin, energy
real, external :: Dirac, solver
integer nu

! Search for an xvalue for which Dirac(x) changes sign and
! use that as xmax. The first root (nu = 1) is x=2.04..
! for kappa = -1.
x = 1.0
Do nu=1,MaxLevels
  xmin = x + dx
  fxmin = Dirac(xmin, kappa, mass, R)
  x = xmin + dx
  Do
    fx = Dirac(x, kappa, mass, R)
    If (fx*fxmin > 0.0) Then
      xmin = x
      x = x + dx
    Else
      xmax = x
      Exit
    End If
  End Do

! Now find the root between xmin and xmax
x = solver(Dirac, xmin, xmax, acc, kappa, mass, R)
energy = sqrt( (x/R)**2 + mass**2 )
if (energy > mu) Exit
eps(nu) = energy
End Do
numax = nu-1 ! The last radial quantum number
End ! Get_eigenvalues

```

C.4.3 Dirac

The equation $\text{Dirac} = 0$ is the Dirac equation for a single quark with quantum number κ in an MIT bag of radius R . It has several solutions corresponding to different values of the radial quantum number.

```

Real Function Dirac(x, kappa, mass, R)
  implicit none
  real, intent (in) :: x, mass, R
  integer, intent (in) :: kappa

  real mR
  integer kap1
  real, external :: fxx

  mR = mass*R
  kap1 = kappa - 1
  Dirac = fxx(kappa, x) &
    + x * fxx(kap1, x) / (sqrt(x**2+mR**2) + mR)
End ! Dirac

```

C.4.4 f_{kx}

The function f_{kx} ($f_{\kappa}(x)$ defined in Eq. (2.12)) occurs in *Dirac* and it is given in terms of spherical Bessel functions.

```
Real Function fkx(k,x)
  implicit none
  integer, intent(in) :: k
  real,    intent(in) :: x

  external sphbes ! Spherical Bessel function of integer order
  real sj, sy, sjp, syp
  integer k2

  If (k >= 0) Then
    call sphbes(k, x, sj, sy, sjp, syp)
    fkx = sj
  Else
    k2 = -(k+1)
    call sphbes(k2, x, sj, sy, sjp, syp)
    fkx = (-1)**(k+1) * sj
  End If
End ! fkx
```


Bibliography

- [1] Particle Data Group, Phys. Rev. D **54**, PART 1, 1 (1996).
- [2] A. R. Bodmer, Phys. Rev. D **4**, 1601 (1971).
- [3] S. A. Chin and A. K. Kerman, Phys. Rev. Lett. **43**, 1292 (1979).
- [4] H. Terazawa, INS-Rep. 336, Institute for Nuclear Study, University of Tokyo, Midori-cho, Tanashi, Tokyo 188 (unpublished).
- [5] E. Witten, Phys. Rev. D **30**, 272 (1984).
- [6] *Strange Quark Matter in Physics and Astrophysics*, edited by J. Madsen and P. Haensel (Nucl. Phys. B (Proc. Suppl.), **24B**, 1991).
- [7] E. Farhi and R. L. Jaffe, Phys. Rev. D **30**, 2379 (1984).
- [8] F. R. Brown *et al.*, Phys. Rev. Lett. **65**, 2491 (1990).
- [9] C. Alcock and E. Farhi, Phys. Rev. D **32**, 1273 (1985).
- [10] J. Madsen, H. Heiselberg, and K. Riisager, Phys. Rev. D **34**, 2947 (1986).
- [11] K. Sumiyoshi and T. Kajino, in *Strange Quark Matter in Physics and Astrophysics*, edited by J. Madsen and P. Haensel (Nucl. Phys. B (Proc. Suppl.), **24B**, 1991), pp. 80–83. See Ref. [6].
- [12] D. Beavis *et al.*, Phys. Rev. Lett. **75**, 3078 (1995).
- [13] G. Appelquist *et al.*, Phys. Rev. Lett. **76**, 3907 (1996).
- [14] C. Greiner, P. Koch, and H. Stöcker, Phys. Rev. Lett. **58**, 1825 (1987).
- [15] C. Greiner, D.-H. Rischke, H. Stöcker, and P. Koch, Phys. Rev. D **38**, 2797 (1988).
- [16] C. Greiner and H. Stöcker, Phys. Rev. D **44**, 3517 (1991).
- [17] S. A. Shapiro and S. A. Teukolsky, *Black Holes, White Dwarfs, and Neutron Stars* (John Wiley & Sons, New York, NY, 1983).

- [18] C. Alcock, in *Strange Quark Matter in Physics and Astrophysics*, edited by J. Madsen and P. Haensel (Nucl. Phys. B (Proc. Suppl.), **24B**, 1991), pp. 93–102. See Ref. [6].
- [19] M. Weigel and F. Weber, *Bild der Wissenschaft* **8**, 48 (1994), in German.
- [20] J. Madsen, *Phys. Rev. Lett.* **61**, 2909 (1988).
- [21] J. Madsen, in *Physics and Astrophysics of Quark-Gluon Plasma*, edited by B. Sinha, Y. P. Viyogi, and S. Raha (World Scientific, Singapore, 1994), pp. 186–205.
- [22] A. Chodos *et al.*, *Phys. Rev. D* **9**, 3471 (1974).
- [23] K. Johnson, *Acta Physica Polonica* **B6**, 865 (1975).
- [24] T. H. Hansson and R. L. Jaffe, *Phys. Rev. D* **28**, 882 (1983).
- [25] C. Itzykson and J.-B. Zuber, *Quantum Field Theory* (McGraw-Hill, New York, NY, 1985).
- [26] D. Flamm and F. Schöberl, *Introduction to the quark model of elementary particles* (Gordon and Breach, New York, NY, 1982).
- [27] J. Madsen, in *Strangeness and Quark Matter*, edited by G. Vassiliadis, A. D. Panagiotou, S. Kumar, and J. Madsen (World Scientific, Singapore, 1995), pp. 191–205. See Ref. [119].
- [28] M. Abramowitz and I. Stegun, *Handbook of Mathematical Functions* (Dover Publications Inc., New York, NY, 1965).
- [29] J. D. Bjorken and S. D. Drell, *Relativistic Quantum Mechanics* (McGraw-Hill, New York, NY, 1964).
- [30] D. Vasak, W. Greiner, and L. Neise, *Phys. Rev. C* **34**, 1307 (1986).
- [31] E. P. Gilson and R. L. Jaffe, *Phys. Rev. Lett.* **71**, 332 (1993).
- [32] J. Madsen, *Phys. Rev. D* **50**, 3328 (1994).
- [33] R. Balian and C. Bloch, *Ann. Phys.* **60**, 401 (1970).
- [34] R. Balian and C. Bloch, *Ann. Phys.* **64**, 271 (1970).
- [35] R. Balian and C. Bloch, *Ann. Phys.* **84**, 559 (1974), erratum.
- [36] M. S. Berger and R. L. Jaffe, *Phys. Rev. C* **35**, 213 (1987).
- [37] M. S. Berger and R. L. Jaffe, *Phys. Rev. C* **44**, 566 (1991), erratum.
- [38] I. Mardor and B. Svetitsky, *Phys. Rev. D* **44**, 878 (1991).

- [39] P. Rhodes, Proc. Roy. Soc. A **204**, 396 (1951).
- [40] R. B. Dingle, Appl. Sci. Res. **B 6**, 225 (1957).
- [41] I. S. Gradshteyn and I. M. Ryzhik, *Table of Integrals, Series, and Products* (Academic Press, New York, NY, 1965).
- [42] J. Madsen, Phys. Rev. Lett. **70**, 391 (1993).
- [43] J. Madsen, Phys. Rev. D **47**, 5156 (1993).
- [44] J. Madsen, in *Strangeness in Hadronic Matter*, Vol. 340 of *AIP Conf. Proc.*, edited by J. Rafelski (AIP, New York, NY, 1995), pp. 32–45.
- [45] A. Chodos, R. L. Jaffe, K. Johnson, and C. B. Thorn, Phys. Rev. D **10**, 2599 (1974).
- [46] R. Friedberg and T. D. Lee, Phys. Rev. D **15**, 1694 (1977).
- [47] P. Gnädig, P. Hasenfratz, J. Kuti, and A. S. Szalay, Phys. Lett. B **64**, 62 (1976).
- [48] T. H. R. Skyrme, Nucl. Phys. **31**, 556 (1962).
- [49] T. H. R. Skyrme, Proc. Roy. Soc. **260**, 127 (1991).
- [50] G. E. Brown and M. Rho, Phys. Lett. B **82**, 177 (1979).
- [51] L. Sathpathy, P. K. Sahu, and V. S. U. Maheswari, Phys. Rev. D **49**, 4642 (1994).
- [52] M. Iwasaki and T. Iwado, Phys. Lett. B **350**, 163 (1995).
- [53] M. Iwasaki and T. Iwado, Prog. Theor. Phys. **94**, 1073 (1995).
- [54] D. Bailin and A. Love, Nucl. Phys. B **190**, 175 (1981).
- [55] D. Bailin and A. Love, Nucl. Phys. B **205**, 119 (1982).
- [56] M. D. Francia, Phys. Rev. D **50**, 2908 (1994).
- [57] K. Kajantie, L. Kärkkäinen, and K. Rummukainen, Phys. Lett. B **286**, 125 (1992).
- [58] S. Huang, J. Potvin, and C. Rebbi, Int. Journ. Mod. Phys. **3**, 931 (1992).
- [59] G. Baym and S. Chin, Phys. Lett. **62B**, 241 (1976).
- [60] B. Freedman and L. McLerran, Phys. Rev. D **16**, 1130 (1977).
- [61] B. Freedman and L. McLerran, Phys. Rev. D **17**, 1109 (1978).
- [62] V. Baluni, Phys. Lett. **72B**, 381 (1978).

- [63] V. Baluni, Phys. Rev. D **17**, 1978 (1978).
- [64] A. Goyal and J. D. Anand, in *Strange Quark Matter in Physics and Astrophysics*, edited by J. Madsen and P. Haensel (Nucl. Phys. B (Proc. Suppl.), **24B**, 1991), pp. 18–22. See Ref. [6].
- [65] M. Ishii and R. Tamagaki, Prog. Theor. Phys. **89**, 657 (1993).
- [66] M. Ishii and R. Tamagaki, Prog. Theor. Phys. **87**, 969 (1992).
- [67] M. Ishii, R. Tamagaki, and A. Tohsaki, Prog. Theor. Phys. **92**, 111 (1994).
- [68] M. G. Mustafa and A. Ansari, Z. Phys. C **57**, 51 (1993).
- [69] D. M. Jensen and J. Madsen, in *Strangeness and Quark Matter*, edited by G. Vassiliadis, A. D. Panagiotou, S. Kumar, and J. Madsen (World Scientific, Singapore, 1995), pp. 220–229. See Ref. [119].
- [70] Y. B. He, C. S. Gao, X. Q. Li, and W. Q. Chao, Phys. Rev. C **53**, 1903 (1996).
- [71] M. G. Mustafa and A. Ansari, Phys. Rev. D **53**, 5136 (1996).
- [72] D. M. Jensen and J. Madsen, Phys. Rev. D **53**, R4719 (1996).
- [73] K. S. Lee and U. Heinz, Phys. Rev. D **47**, 2068 (1993).
- [74] Y. B. He, W. Q. Chao, C. S. Gao, and X. Q. Li, Phys. Rev. C **54**, 857 (1996).
- [75] C. Spieles *et al.*, Phys. Rev. Lett. **76**, 1776 (1996).
- [76] Particle Data Group, Phys. Rev. D **45**, S1 (1992).
- [77] J. Cleymans, M. I. Gorenstein, J. Stålnacke, and E. Suhonen, Physica Scripta **48**, 277 (1993).
- [78] D. H. Rischke, M. I. Gorenstein, H. Stöcker, and W. Greiner, Z. Phys. C **51**, 485 (1991).
- [79] R. Hagedorn and J. Rafelski, in *Statistical Mechanics of Quarks and Hadrons*, edited by H. Satz (North Holland Publishing Company, Amsterdam, NL, 1981), pp. 237–272. See Ref. [120].
- [80] H. W. Barz, B. L. Friman, J. Knoll, and H. Schulz, Nuc. Phys. **A484**, 661 (1988).
- [81] H. W. Barz, B. L. Friman, J. Knoll, and H. Schulz, Phys. Lett. B **242**, 328 (1990).

- [82] H. W. Barz, B. L. Friman, J. Knoll, and H. Schulz, in *Strange Quark Matter in Physics and Astrophysics*, edited by J. Madsen and P. Haensel (Nucl. Phys. B (Proc. Suppl.), **24B**, 1991), pp. 211–220. See Ref. [6].
- [83] C. Spieles *et al.*, in *Proceedings of the International Conference: Structure of Vacuum and Elementary Matter, March 10-16, 1996, Wilderness/George, South Africa* (World Scientific Publ. Co., Singapore, 1996), (To be published; also available at <http://xxx.lanl.gov/abs/nucl-th/9606027>).
- [84] H. A. Bethe, Phys. Rev. **50**, 332 (1936).
- [85] K. Redlich and L. Turko, Z. Physik **C5**, 201 (1980).
- [86] K. Redlich and L. Turko, in *Statistical Mechanics of Quarks and Hadrons*, edited by H. Satz (North Holland Publishing Company, Amsterdam, NL, 1981), pp. 303–318. See Ref. [120].
- [87] L. Turko, Physics Letters **104B**, 153 (1981).
- [88] H. F. Jones, *Groups, Representations and Physics* (Adam Hilger, Bristol, UK, 1990).
- [89] K. Huang, *Quarks, Leptons and Gauge Fields*, 2nd ed. (World Scientific Publishing Co. Pte. Ltd., Singapore, 1992).
- [90] W. Greiner and B. Müller, *Quantum Mechanics, Symmetries*, Vol. 2 of *Theoretical Physics* (Springer-Verlag, Berlin, D, 1989).
- [91] V. Borchsenius, *Forelæsningsnoter til Teorien for Grupper og Grupperrepræsentationer* (Matematisk Institut, Aarhus Universitet, Århus, DK, 1982), in Danish.
- [92] G. Racah, *Group theory and spectroscopy: Notes by Eugen Merzbacher and David Park* (The Institute for Advanced Study, Princeton, NJ, 1951).
- [93] W. Greiner, L. Neise, and H. Stöcker, *Thermodynamics and Statistical Mechanics* (Springer-Verlag, New York, NY, 1995).
- [94] H.-Th. Elze and W. Greiner, Phys. Rev. A **33**, 1879 (1986).
- [95] M. I. Gorenstein, S. I. Lipskikh, V. K. Petrov, and G. M. Zinovjev, Phys. Lett. **123B**, 437 (1983).
- [96] H.-Th. Elze and W. Greiner, Physics Letters **B 179**, 385 (1986).
- [97] M. G. Mustafa, Phys. Rev. D **49**, 4634 (1992).
- [98] M. G. Mustafa, Phys. Lett. B **318**, 517 (1993).

- [99] G. Auberson, L. Epele, G. Mahoux, and F. R. A. Simão, *J. Math. Phys.* **27**, 1658 (1986).
- [100] F. Savatier, *J. Math. Phys.* **32**, 2243 (1991).
- [101] J. E. Shrauner, *J. Phys. G* **22**, 243 (1996).
- [102] J. Mathews and R. L. Walker, *Mathematical Methods of Physics*, 2nd ed. (Addison-Wesley, Redwood City, CA, 1970).
- [103] H.-Th. Elze, W. Greiner, and J. Rafelski, *Physics Letters* **124B**, 515 (1983).
- [104] H.-Th. Elze, W. Greiner, and J. Rafelski, *Z. Phys. C* **24**, 361 (1984).
- [105] P. Braun-Munzinger, J. Stachel, J. P. Wessels, and N. Xu, *Phys. Lett. B* **344**, 43 (1995).
- [106] P. Braun-Munzinger, J. Stachel, J. P. Wessels, and N. Xu, *Phys. Lett. B* **365**, 1 (1996).
- [107] L. D. Landau and E. M. Lifshitz, *Statistical Physics, Part 1*, Vol. 5 of *Course of Theoretical Physics*, 3rd ed. (Pergamon, New York, NY, 1980).
- [108] J. Madsen, D. M. Jensen, and M. B. Christiansen, *Phys. Rev. C* **53**, 1883 (1996).
- [109] M. L. Olesen and J. Madsen, *Phys. Rev. D* **49**, 2698 (1994).
- [110] T. H. Hansson and R. L. Jaffe, *Ann. Phys.* **151**, 204 (1983).
- [111] R. L. Jaffe and L. C. Vintro, *Ann. Phys.* **162**, 312 (1984).
- [112] I. Stakgold, *Boundary Value Problems of Mathematical Physics* (Macmillan, New York, NY, 1968).
- [113] J. D. Jackson, *Classical Electrodynamics*, 2nd ed. (Wiley, New York, NY, 1962).
- [114] H.-Th. Elze, LBL preprint 21560, Lawrence Berkeley Laboratory, University of California, Berkeley, CA (unpublished).
- [115] R. B. Dingle, *Appl. Sci. Res.* **B 6**, 240 (1957).
- [116] H.-Th. Elze, private communication.
- [117] W. H. Press, S. A. Teukolsky, W. T. Vetterling, and B. P. Flannery, *Numerical Recipes*, 2nd ed. (Cambridge University Press, Cambridge, UK, 1992).
- [118] S. Lacey and R. Box, *BYTE* **16**, 315 (1991).

- [119] *Strangeness and Quark Matter*, edited by G. Vassiliadis, A. D. Panagiotou, S. Kumar, and J. Madsen (World Scientific, Singapore, 1995).
- [120] *Statistical Mechanics of Quarks and Hadrons*, edited by H. Satz (North Holland Publishing Company, Amsterdam, NL, 1981).

Index

- adjoint representation
 - and gluons, 57
 - gauge potential, 56
- asymptotic freedom, 39
- bag constant, 12
- Bernoulli polynomials, 101
- Bessel function, 14, 103, 112
- big bang, 6, 9
- Bose-Einstein condensation, 43
- boundary conditions
 - effect on density of states, 17
 - of MIT bag model, 12–13, 26
 - periodic, 16
- Cartan algebra, 50
- Cartan operator, 52, 53, 57
- Casimir operator, 50, 52
 - and multiplets, 51
- center of mass energy, 28
- character, 52
 - orthogonality of, 52
- charge operators, 52
- chiral symmetry
 - breaking of, 27
 - restoration of, 39
- Clifford algebra, 12
- collapsed nuclei, 3
- color singlet constraint, 69
- confinement, 11, 87
- conserved charge, 49
- cosmic rays, 8–9
- Coulomb energy, 28
- critical temperature, 36
- curvature
 - extrinsic, 18
 - Gaussian, 18
- dark matter, 6
- decay modes, 28
- deconfinement, 37
- density of states, 16–20
 - for a free field, 92–94
 - for gluons, 19
 - for quarks, 18–19
 - trace formula, 89–91
- Dirac equation, 89
 - for quark in MIT bag, 12, 90
 - numerical solution, 110, 111
 - radial, 14
- direct sum, 51
- energy
 - differential of, 22
- energy momentum tensor, 13
- equilibrium criteria, 42
- excluded volume effect, 41
- fine-structure constant, 28
- finite size corrections, 17–19
- finite size effects, 22, 36
- fixed momentum constraint, 69–70
- Fredholm equation, 97
- free energy, 22
 - barrier, 77–79
- gamma function, 64, 101
- Gaussian approximation, *see* saddle-point approximation
- Gell-Mann matrices, 56
- gravitational radiation, 8
- Green's function
 - for Dirac equation, 90–93
 - for Klein-Gordon equation, 92
 - for quark in MIT bag, 95–97

- Green's theorem, 95
- Haar measure, 52, 62, 64
 - of $SU(3)$, 59
 - of $U(1)$, 55
- heavy-ion collision, 6–7, 31, 39
- helicity
 - for gluons, 61
 - for quarks, 59
- homomorphism, 50
- ideal, 50
- invariant subgroup, 50
- irreducible representation, 51
- isomorphism, 51
- Kepler limit, 8
- Lagrangian
 - for MIT bag model, 12
- Laplace equation, 96
- lattice gauge calculations, 5, 27, 86
- Lie algebra, 50
- Lie group, 49
- liquid drop model, 16–26, 62
 - at finite temperature, 31–37
 - compared to shell model, 19–20
- magic numbers, 16, 87
- mass formula, 25–26
 - finite temperature, 32–35
- Minkowski metric, iv, 12, 93
- MIT bag model, 11–13
 - Lagrangian, 12
- multiple reflection expansion, 17, 62, 89–98
 - breakdown of, 72
 - of the density of states, 18, 98
 - of the Green's function, 94–97
 - validity, 18
- multiplet, 51
- neutron star, 9, 83, 88
- nucleation rate, 77
 - suppression of, 79–81
- nucleosynthesis, 6
- orthogonality
 - of characters, 52
- orthonormality
 - of spinors, 90
- partition function, 20–25
 - grand canonical, 21
- Pauli matrices, 14
 - as representations of $SU(2)$, 52
- perturbation theory, 11, 12, 28
- perturbative vacuum, 11
- phase diagram, 4–5, 35–37, 43–48
- propagator, *see* Green's function
- QCD, 49, 56
- quark current, 13
- quark star, *see* strange star
- quark-gluon plasma, 5, 7, 31, 37, 39, 77
- quark-hadron phase transition
 - cosmological, 6, 88
- rank, 50
 - of $SU(N)$, 50
- representation, 49–52
 - adjoint, 52
 - fundamental, 52
 - irreducible, 51
 - unitary, 51
- Riemann zeta function, 99, 101
- saddle-point approximation, 62, 64–66, 69–72
 - validity of, 65, 72–74, 78–79
- shell effects, 16, 29, 48, 87
- shell model, 14–16, 103–112
 - at finite temperature, 31
 - compared to liquid drop model, 19–20, 26
- simple group, 50
- simple Lie algebra, 50
- stability
 - of strange quark matter, 4, 28–29
- statistical bootstrap model, 41
- strange star, 7–9

- strangelet, 4
 - creation in heavy-ion coll., 7, 39, 69, 76
- strangeness
 - chemical potential, 40, 42
 - distillation of, 39
- strangeness fraction, 43, 45
- strangeness separation, 40, 85
- structure constants, 50
 - and adjoint representation, 52
- $SU(3)$, 11, 49, 56
 - of flavor, 57, 67
- $SU(N)$, 50
- superconductivity, 27
- supernova, 8, 9

- thermodynamic potential, 21–24
 - for gluons, 22
 - for massless quarks, 23
 - for quarks, 23–24
 - zero temperature, 23
- transparency, 40

- weak interaction, 25
- Wick rotation, 58

- Yang-Mills theory, 56
- Yang–Mills theory, 11

- zero-point energy, 28